SYNAPTIC PROTEIN EXPRESSION IN DEVELOPING AUDITORY BRAINSTEM

EARLY POSTNATAL EXPRESSION OF PROTEINS ASSOCIATED WITH INHIBITORY SYNAPSES IN THE AUDITORY BRAINSTEM

By ALAN COOPER, B.Sc.

A Thesis Submitted to the School of Graduate Studies

in Partial Fulfillment of the Requirements for the

Degree of Doctorate of Philosophy

McMaster University

DOCTORATE OF PHILOSOPHY (2014)

NEUROSCIENCE

MCMASTER UNIVERSITY

HAMILTON, ON

TITLE: Early postnatal expression of proteins associated with inhibitory synapses in the auditory brainstem

AUTHOR: Alan P. Cooper, B.Sc. (McMaster University)

SUPERVISOR: Dr. Deda C. Gillespie

NUMBER OF PAGES: xii, 194.

ABSTRACT

The lateral superior olive (LSO) is a binaural nucleus that is critical for azimuthal sound localization. Bipolar principal cells of the LSO compute interaural level differences (ILDs) by comparing converging excitatory and inhibitory inputs driven by either ear. More specifically, this computation relies on integrating excitatory inputs from the ipsilateral cochlear nucleus with inhibitory, GABA/glycinergic inputs from the medial nucleus of the trapezoid body (MNTB), which are driven by sound originating at the contralateral ear. In order to reliably compute ILDs, the converging inputs must represent sounds of the same frequency. This specificity emerges during the first few weeks of postnatal life in rats as a result of functional and anatomical refinement. Interestingly, significant refinement of this auditory circuit occurs in the absence auditory experience. We focused on changes in the subcellular location of MNTB inputs and the expression of vesicular proteins before hearing onset.

The subcellular distribution of inputs onto a neuron heavily influences synaptic integration and the mature distribution likely emerges during a period of circuit refinement. Little is known about how the inputs are distributed onto LSO principal cells and how the mature distribution is achieved. We studied the distribution of inhibitory inputs onto LSO neurons and found that significant re-distribution occurs before hearing onset. The mechanisms underlying the refinement of the inhibitory MNTB projection are not well understood but could be related to the transient co-transmission of the excitatory neurotransmitter

glutamate. We studied the expression of vesicular proteins that may regulate the release of GABA/glycine and glutamate at the immature MNTB terminal. We found that MNTB terminals transiently express two Ca^{++} sensors, which may be associated with the different release properties for GABA/glycine and glutamate. Lastly, we asked one specific example of what controls the expression and sorting of vesicular proteins at the immature MNTB terminal.

ACKNOWLEDGEMENTS

I would like to thank my supervisor Dr. Deda Gillespie. Deda has guided me through each of my projects and was faithfully committed to my academic development. Deda always leaves her door open for scientific discussions and her enthusiasm is inspirational. I would like to thank Dr. Daniel Goldreich and Dr. Roger Jacobs for serving on my supervisory committee. They provided me with valuable input and time during my period as a graduate student. I would like to thank all members of the Gillespie lab. I would especially like to thank Dr. Dan Case and Dr. Javier Alamilla for their help in the lab and Hugo Wang for his help with analysis.

I am very grateful to all the family and friends who supported during my time as a graduate student. My parents and brothers were always willing to help me through the difficult times and recognize my successes.

TABLE OF CONTENTS

LISTS OF FIGURES AND TABLES

Chapter 1

Chapter 2

LIST OF ALL ABBREVIATIONS AND SYMBOLS

ATP	adenosine triphosphate
AVCN	anteroventral cochlear nucleus
Ca^{++}	calcium
GABA	gamma-aminobutyric acid
IHC	inner hair cell
ILD	interaural level difference
IR	immunoreactivity
ITD	interaural time difference
LNTB	lateral nucleus of the trapezoid body
LSO	lateral superior olive
LTD	long term depression
LTP	long term potentiation
MNTB	medial nucleus of the trapezoid body
MSO	medial superior olive
NMDA(R)	n-methyl-d-aspartate receptor
P11	postnatal day 11 (etc.)
SOC	superior olivary complex
SPN	superior paraolivary nucleus
Syt	synaptotagmin
VGLUT	vesicular glutamate transporter
VIAAT	vesicular inhibitory amino acid transporter

DECLARATION OF ACADEMIC ACHIEVEMENT

For Chapter 2, I designed the experiments with Dr. Deda Gillespie, I performed the experiments with Dr. Javier Alamilla, I analyzed the data, Adam Bleckert provided custom written scripts to calculate puncta density along dendrites, and I wrote the manuscript.

For Chapter 3, I designed the experiments with Dr. Deda Gillespie, I performed the experiments, I analyzed the data, and I wrote the manuscript with Dr. Deda Gillespie.

For Chapter 4, I designed the experiments with Dr. Deda Gillespie, I performed the experiments, Dr. Dan Case and Dr. Javier Alamilla genotyped the mice, I analyzed the data, and I wrote the manuscript.

Chapter 3 was published in *The Journal of Comparative Neurology* in 2011.

Chapter 1: General Introduction

Section 1: Azimuthal sound localization in auditory brainstem

Reliably locating the source of a sound is a critical function of the auditory system. Sound localization ability is ultimately tested in predator-prey relationships, where locating the member of another species is crucial for survival. Sound localization also plays a role in human communication by helping us orient to relevant events and attend to a specific stimulus in a noisy environment. Sound localization abilities improve with experience (Hoffman et al, 1998) and this improvement may be supported by changes to the underlying sound localization circuitry in the central auditory system. Interestingly, the sound localization circuitry begins to mature before the onset of hearing, almost as if the auditory system is preparing to compute environmental stimuli before sound can be transduced. Here I will focus on the events that change before hearing onset in a region of the brain where sound localization is first computed, the auditory brainstem.

The auditory system does not organize space the same way the visual and somatosensory systems organize space. The visual system, for example, can organize spatial information based on the topographic organization of the visual receptors in the retina. This topographically organized map of visual space is then maintained throughout the central visual system. Auditory space, on the other hand, does not have a direct physical projection onto the cochlea. Instead

of sound stimuli being organized by their spatial coordinates, the cochleae organize stimuli based on frequency. The inner hair cells (IHCs) of the cochlea vibrate in response to specific sound frequencies, and the frequency to which they respond to depends on their position along the basilar membrane. Inner hair cells at the apex of the cochlea respond to low frequencies whereas IHCs at the base of the cochlea respond to high frequencies (Von Bekesy, 1956. The spatial organization of frequency coding, known as tonotopy, is maintained at the IHC-spiral ganglion synapse and throughout the central auditory system. Precise tonotopic organization of auditory inputs is required for the central auditory system to compare stimuli of the same sound source. The location of a sound source in azimuthal (horizontal) space is determined centrally by neurons that compare properties of frequency-matched binaural inputs. Binaural sound localization is first computed in the auditory brainstem, the region of the brain that contains circuits relevant to this thesis. Sound sources are also located using spectral cues, but spectral cues will not be discussed here.

Section 1.1: Auditory brainstem circuitry

Auditory information enters the central nervous system along the auditory nerve. Type I auditory nerve fibers synapse in the three subdivisions of the cochlear nucleus. A single auditory nerve fiber bifurcates before entering the cochlear nuclear complex; the descending branch terminates in the posteroventral cochlear nucleus (PVCN) and dorsal cochlear nucleus (DCN)

whereas the ascending branch terminates in the anteroventral cochlear nucleus (AVCN) (Webster, 1991). The AVCN is involved in azimuthal sound localization and this subdivision of the cochlear nucleus is relevant to this thesis. The AVCN is predominantly populated by bushy cells, which receive excitatory inputs from auditory nerve fibers at the highly reliable axo-somatic endbulb of Held synapse.

Bushy cells project to a group of brainstem nuclei that make up the superior olivary complex (SOC, for review on circuitry and sound localization see Grothe et al, 2010). The SOC is recognized as the first site of binaural integration and is involved in locating sounds along the horizontal plane (azimuthal sound localization). The major nuclei in the mammalian SOC include the medial superior olive (MSO), the lateral superior olive (LSO), and the medial nucleus of the trapezoid body (MNTB). The MSO is involved in detecting interaural time differences (ITDs) for low-frequency sounds and the LSO is involved in detecting interaural level differences (ILDs) for high-frequency sounds**.** Despite these differences, the MSO and LSO have a lot in common and because more is known about the MSO in both the mature and immature nervous system, I will be making comparisons between the developing MSO and LSO throughout this thesis.

The MSO detects ITDs by comparing the arrival times of the excitatory inputs from bushy cells in each cochlear nucleus (Goldberg and Brown, 1969, Cant and Casseday, 1986, Yin and Yang, 1990). Principal bipolar cells of the MSO, which make up nearly all the cells in the MSO, have a laterally projecting

dendritic tree which receives inputs from the ipsilateral AVCN and a medially projecting dendritic tree which receives inputs from the contralateral AVCN (Cant and Casseday, 1986, Fig. 1). The converging excitatory inputs must be tonotopically matched to compare a sound from the same source. MSO cells also receive inhibitory, glycinergic inputs from the lateral nucleus of the trapezoid body (LNTB) and the MNTB that target the soma and proximal dendrites (Kuwabara and Zook ,1992, Kapfer et al, 2002, not shown in Fig. 1). It has been suggested that well-timed inhibition at the soma is essential for precise ITD computation in mammals, though the role of inhibition remains intensely debated (Brand et al, 2002, Grothe et al 2010).

The LSO is involved in detecting ILDs (Boudreau and Tsuchitani, 1968). The ILD results from the head reflecting sound energy, creating a sound shadow. Because of this sound shadow, the sound level is lower at the ear opposite to the sound source. High-frequency sounds are more likely to be reflected than low-frequency sounds therefore high-frequency sounds are more likely to produce an ILD. The LSO is a binaural nucleus and if the sound is louder at the right ear, for example, the cells of the right LSO will have a higher firing rate than cells of the left LSO. Bipolar principal cells in the LSO are excited by sound from the ipsilateral ear and inhibited by sound from the contralateral ear. The excitation comes from glutamatergic inputs from bushy cells in the ipsilateral AVCN (Cant and Casseday, 1986, Wu and Kelly, 1992, Fig.1). The inhibition comes indirectly from the contralateral AVCN through the MNTB. Bushy cells from the

contralateral AVCN terminate on neurons of the ipsilateral MNTB at the high fidelity calyx of Held synapse (Smith et al, 1991). MNTB neurons then provide glycinergic input to LSO principal cells (Moore and Caspary, 1983, Bledsoe et al, 1990). The converging inputs must be tonotopically aligned as ILDs are computed in a frequency-dependent manner (Boudreau and Tsuchitani, 1968). There is no apparent left-right input organization onto LSO bipolar principal cells, unlike the ear-specific organization of excitatory inputs in MSO where inputs from the left ear are relayed via the cochlear nucleus to the dendrites projecting to the left and inputs from the right ear are relayed through the cochlear nucleus to the dendrites projecting to the right (Fig. 1). Knowing the subcellular location of inputs to LSO bipolar principal cells will be a major advance and help us understand how the converging inputs are integrated.

LSO bipolar principal cells project to nuclei further along the central auditory system, notably the nuclei of the lateral lemniscus and the inferior colliculus. These nuclei are also involved in sound localization but they will not be discussed here.

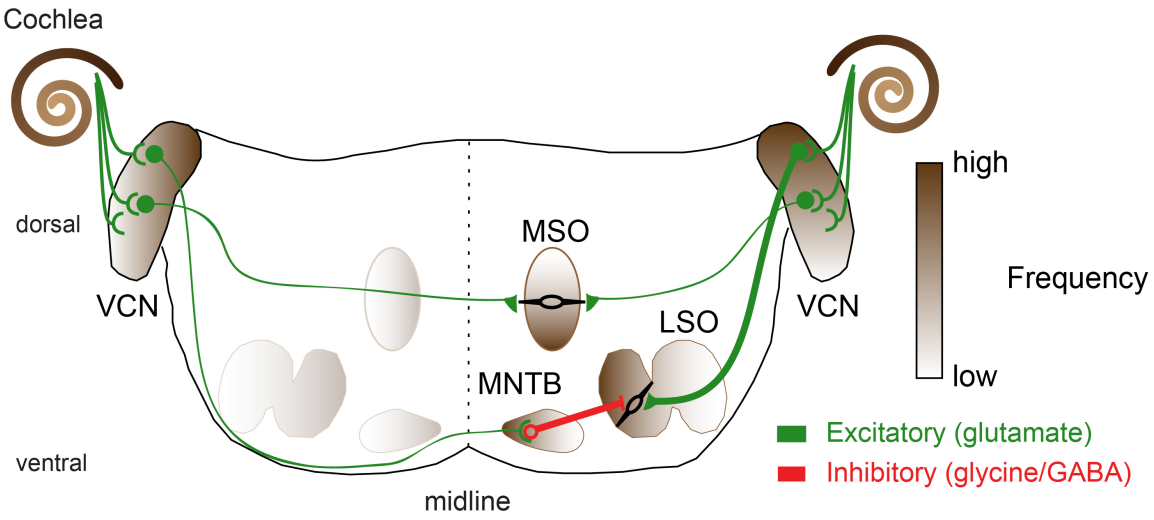

Figure 1. Coronal brainstem slice, showing glutamatergic (green) and glycinergic/ GABAergic (red) inputs to the superior olivary complex (SOC). The brainstem is bilaterally symmetric; for clarity, the relevant circuitry for only one side is illustrated here. Principal neurons in the lateral superior olive (LSO) receive an excitatory projection from bushy cells in the ipsilateral anteroventral cochlear nucleus (AVCN) and an inhibitory projection from the medial nucleus of the trapezoid body (MNTB), which is driven by an excitatory input from bushy cells in the contralateral AVCN. Principal cells in the medial superior olive (MSO) receive bilateral excitatory inputs from bushy cells in each AVCN. Principal cells in the MSO also receive inhibitory inputs from the MNTB and lateral nucleus of the trapezoid body (LNTB) (not shown).

Section 1.2: Refinement in the Lateral Superior Olive

Neural circuits rely on precise, topographically organized synaptic connections in order to properly function. This organization develops early in life during a period of refinement and this refinement nearly always requires molecular guidance cues and patterned neural activity. In the LSO, molecular guidance cues and patterned neural activity are required for circuit refinement and, according to the current working model in the field, this refinement occurs in three phases. I will outline these phases here and provide more details in the following paragraphs. First, molecular guidance cues direct axons to approximately the right location in the target nuclei. Second, patterned neural activity results in the strengthening of certain synapses and weakening of other synapses. These changes can be measured electrophysiologically and are known as functional refinement. Third, the activity-dependent physiological changes are followed by structural changes to the circuit, which can be measured anatomically. The current working model in the field stresses that axon path finding, functional refinement, and anatomical refinement occur as three separate processes. However, work in this thesis challenges the idea that functional and anatomical refinement are temporally distinct events. Below, I will discuss the evidence for the current working model, with a focus on the physiological and anatomical processes. I will also explain why a re-examination of the working model is needed.

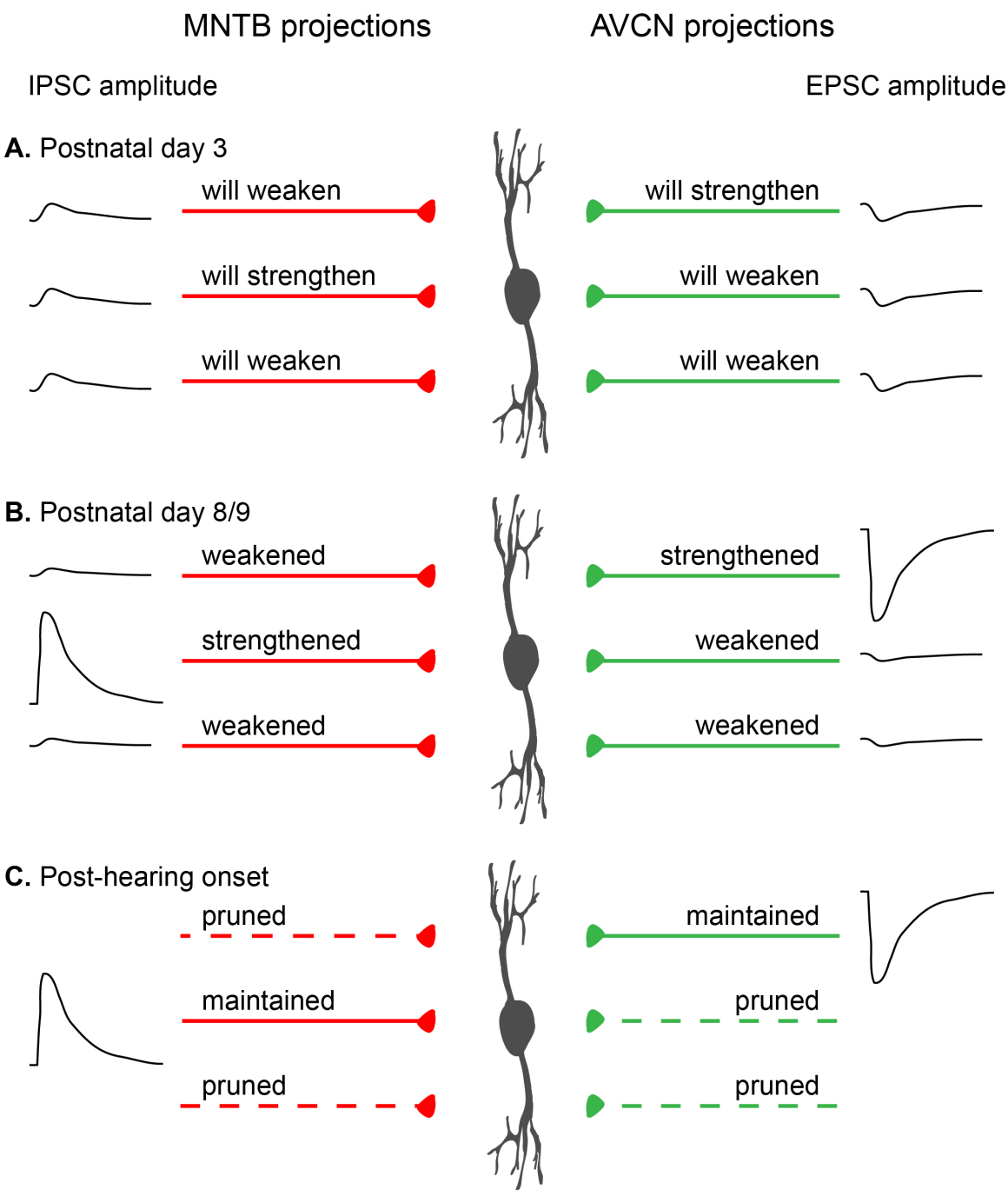

Figure 2. A schematic of functional refinement, and resulting anatomical refinement, of MNTB and AVCN inputs to the LSO. (Based on Kim and

Kandler, 2003, Case et al, 2011). **A.** Shortly after birth (postnatal day 3), LSO neurons receive many weak inputs from the MNTB and the AVCN. **B.** By P8/P9, certain inputs from the MNTB and AVCN strengthen, as indicated by an increase in the amplitude of the inhibitory postsynaptic current (IPSC) and excitatory postsynaptic current (EPSC). Concurrently, other inputs weaken, as indicated by a decrease in the amplitude of the PSC. **C.** Functional refinement is followed by anatomical refinement. The strengthened inputs persist whereas the weakened inputs are pruned. This schematic does not intend to suggest the ratio of fibers that strengthen or weaken, nor does it intend to suggest the subcellular locations to which the maintained axons project.

First, axons innervate the LSO at embryonic day 18 (E18), 4 days before birth in rats (Kandler and Friauf, 1993). The axons are likely guided through the expression of molecular guidance cues (Cramer, 2005) and the connections in the embryonic animal are capable of supporting synaptic transmission (Kandler and Friauf, 1995). The axons are, however, structurally unrefined and project outside of their final target zone within the nucleus.

Next, comes a period of refinement when functional connections become tonotopically sharpened. This is achieved through strengthening of certain connections and elimination of others. Functional refinement has been demonstrated for both MNTB and AVCN inputs to the LSO. In the MNTB-LSO

pathway, the strength of a single input increases 12-fold between postnatal day 3 (P3) and P8/9 (Kim and Kandler, 2003, Fig. 2). This increase in strength is accompanied by a 75% decrease in the area of the MNTB that elicits a response from an LSO neuron (Kim and Kandler, 2003). The excitatory AVCN-LSO inputs undergo functional refinement during this same time period (Case et al, 2011). The number of inputs from the AVCN to single LSO neurons drops between postnatal day 3 (P3) and P8, and the strength of single inputs increases 5-fold during this time (Fig. 2). Interestingly, functional refinement occurs in the absence of acoustically driven activity, as the onset of hearing occurs approximately at P12 in rodents. If functional refinement is activity-dependent, then there must be internally generated neural activity that can drive these processes before hearing onset. The origin and role of spontaneous activity in the auditory system is discussed in the following section (Section 1.3).

Structural reorganization commonly follows functional changes in the nervous system (Antonini and Stryker, 1993, Colman et al, 1997). A third qualitatively distinct process of refinement in the SOC is anatomical refinement. In the LSO, there is a period when MNTB-LSO axonal arbors increase in length and complexity, followed anatomical refinement of the arbor (Sanes and Siverls, 1991, Fig. 3). Between P2 and P13, MNTB-LSO projections become more complex, longer, and occupy regions of the LSO that are outside the final innervation zone. Around the time of hearing onset (P13), MNTB axons continue to grow in complexity and increase in length, but there are fewer axons projecting

outside the final innervation zone. Between P13 and P18-25, axons appear more refined and their growth has stabilized. By P18-P25, MNTB axons occupy a smaller proportion of the LSO than they did at younger ages. There is also a decrease in the spread and number of MNTB boutons compared to P13. Together, these observations suggest that anatomical refinement occurs after hearing onset (Sanes and Siverls, 1991, Fig. 3). Anatomical refinement of the AVCN-LSO has not been studied but based on the findings that functional refinement of the AVCN-LSO and MNTB-LSO occurs on the same timeline, one might expect the anatomical refinement between the two pathways to be similar as well.

Morphological changes in MNTB-LSO projections are matched with morphological changes in the dendritic fields of LSO neurons. Between P13 and P21, the number of dendritic branchpoints and the width of the dendritic arbor of LSO principal cells decrease significantly in the high-frequency region of the gerbil LSO (Sanes et al, 1992a). Interestingly, if the inputs to the LSO are manipulated by cochlear removal or pharmacological silencing, then the MNTB-LSO axonal projections and the dendritic fields of LSO neurons are significantly less refined (Sanes et al, 1992b, Sanes and Chokshi, 1992, Sanes and Takacs, 1993). Therefore, anatomical refinement in LSO circuitry is activity-dependent.

Based on the above studies, the current working model in the field suggests that anatomical refinement in the LSO occurs after hearing onset and relies on acoustically-driven activity, as seen in the MSO (Kapfer et al, 2002, Werthat et al,

2008). This is consistent with the idea that anatomical refinement follows functional refinement (complete by P8/9) at some delay. However, many of the experiments upon which this working model is built do not directly address the question of when anatomical refinement begins. In the case of MNTB-LSO projections, the spread of axonal boutons in the LSO was not measured before P12/P13; therefore it is unclear when the decrease in spread begins (Sanes and Siverls, 1991). Similarly, Sanes and colleagues studied developmental refinement of dendritic arbors of LSO cells starting at P10; therefore any morphological changes before then would not be observed (Sanes et al, 1992a). Moreover, technical issues surrounding Golgi staining, which was used to label LSO neurons, may have compromised these studies (Sanes et al, 1992a). Since the time these studies were performed, advancements have been made methods for labeling dendritic arbors of single neurons. A more recent study labeled LSO cells by intracellular injection and quantified arbor morphology from P4 onwards (Rietzel and Friauf, 1998). Rietzel and Friauf (1998) found that reductions in the number of primary dendrites, dendritic endpoints, and dendritic appendages begins before hearing onset. The finding that anatomical refinement of dendritic arbors of LSO principal cells begins before hearing onset contradicts the current working model in the field and prompts us to look more closely at refinement in the SOC. In this thesis, we challenge the working model of circuit refinement in the field by asking new questions about whether or not anatomical refinement requires acoustical experience.

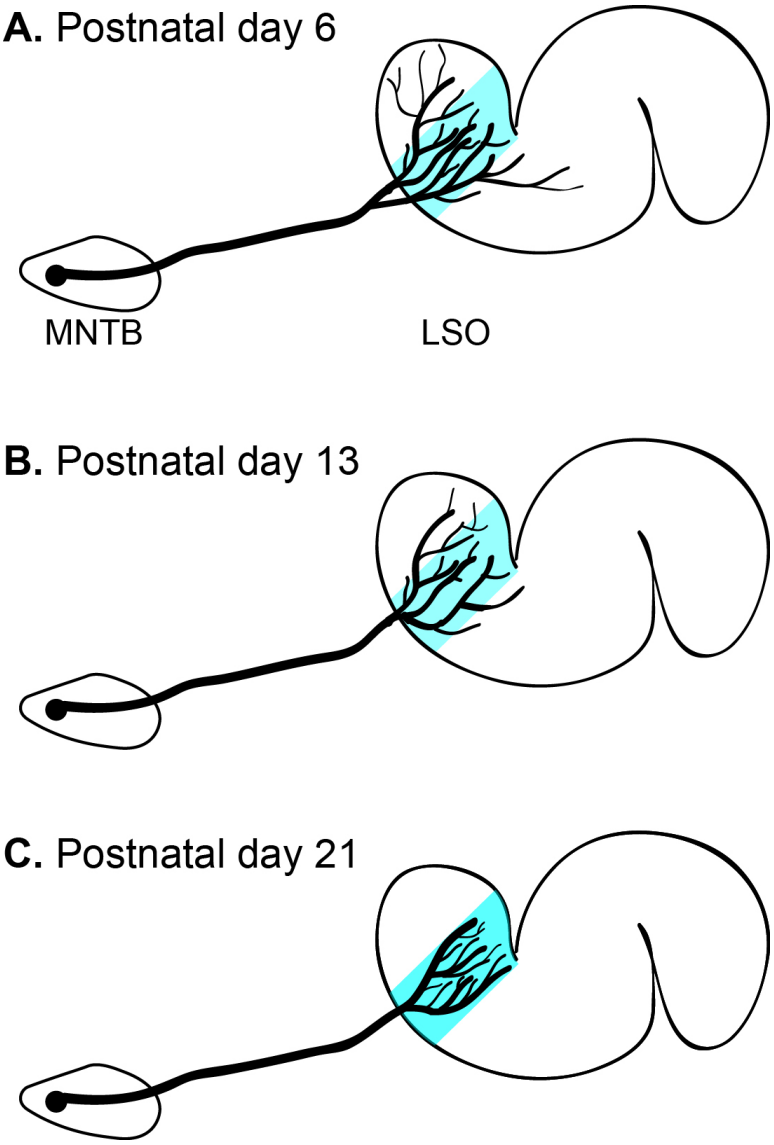

Figure 3. A schematic of anatomical refinement of MNTB-LSO projections during the first three postnatal weeks in rodent (based on work in gerbil, Sanes and Siverls, 1991). The schematic shows a principal cell from the MNTB projecting to the medial limb of the LSO. In blue is the region of the LSO that the axonal arbor will occupy following anatomical refinement. **A.**

Before hearing onset (P6-9), MNTB axons are found in approximately the correct location in the LSO. However, MNTB axons project outside of the final innervation zone and occupy a large area in the LSO relative to the size of the nucleus. At this age, axons are growing in length and increasing in branch number. **B.** After hearing onset (P13), MNTB projections still occupy a region outside their final innervation zone, though these aberrant projections are not as noticeable compared to earlier ages. Axons continue to grow in length and branch number. **C.** By the end of the third postnatal week, MNTB projections innervate their principal zone in the LSO and occupy a smaller area in the LSO (proportional to nuclear size) than at younger ages. Axon growth has stabilized and the arbors are less complex than at younger. This schematic does not incorporate the growing size of the LSO.

Refinement in the LSO is clearly an early postnatal event that is thought to result in mature circuitry by the third or fourth postnatal week. Much of this refinement occurs before hearing onset, which raises the questions; what is the source of the activity and how does refinement occur? Below I will discuss the origin of spontaneous activity in the mammalian auditory system and possible mechanisms for refinement at the immature MNTB-LSO synapse.

Section 1.3: What drives refinement before hearing onset?

Sensory systems develop through a combination of molecular guidance cues and activity-dependent plasticity (Tessier-Lavigne and Goodman, 1996, Katz and Shatz, 1996). This activity can be sensory driven, or before sensory information can be transduced, the activity can be generated spontaneously within a sensory organ (Galli and Maffei, 1988, Meister et al, 1991). Visual system development relies on patterned bursts of spontaneously activity generated in the retina to refine projections to thalamus (Penn et al, 1998). Refinement in the developing auditory system can be prevented by cochlear removal, suggesting that spontaneous activity generated in the cochlea plays a crucial role in the development of the auditory system. Moreover, spontaneous bursts of activity *are* present in the developing avian auditory system (Lippe, 1994). Details on the mechanisms that create spontaneous activity in the mammalian cochlea have recently been discovered and characterized (Tritsch et al, 2007). The spontaneous activity originates from Kolliker's organ, a transient structure in the cochlea that is composed of support cells located next to inner hair cells. Supporting cells in Kolliker's organ spontaneously contract and release adenosine triphosphate (ATP). ATP release from supporting cells depolarizes IHCs and if the IHC is sufficiently depolarized, the IHC will generate Ca^{++} spikes. The Ca^{++} spikes lead to glutamate release from IHCs onto spiral ganglion neurons. Suprathreshold activity in spiral ganglion neurons results in action potentials in the auditory nerve. The ATP-dependent bursting activity in the

cochlea begins around P3 and lasts until the onset of hearing (Tritsch and Bergles, 2010). *In vivo* recordings in the spiral ganglion and MNTB show that the bursts propagate into the SOC, and it has been suggested that this patterned activity could influence plasticity in the developing auditory system (Tritsch et al, 2010).

The period when patterned bursts of spontaneous activity are relayed into the auditory brainstem encompasses the period of functional refinement in the MNTB-LSO pathway and AVCN-MNTB pathway (P3-P8). The mechanisms that drive the refinement are not well understood. Activity-dependent plasticity is understood to underlie the strengthening and weakening of synapses and can exist in many forms including long-term potentiation (LTP), long-term-depression (LTD), and homeostatic plasticity (Citri and Malenka, 2008). There are several examples of LTD in the MNTB-LSO pathway (Kotak and Sanes, 2000, Kotak et al, 2001, Kotak and Sanes, 2002, Chang et al 2003), but to date there have been no published studies showing LTP.

A common mechanism for plasticity is n-methyl-d-aspartate receptor (NMDAR) dependent plasticity**.** NMDAR-dependent plasticity is particularly attractive because it can account for plasticity resulting from coincident activation of inputs and provide relatively long time periods during which inputs can be integrated because of receptor kinetics. The surprising finding that the inhibitory MNTB neurons release the excitatory neurotransmitter glutamate, and that the glutamate release activates NMDARs on LSO neurons during the period of circuit

refinement, raises the possibility that NMDARs could be involved in plasticity at the MNTB-LSO pathway (Gillespie et al, 2005). Intriguingly, a number of the requirements for NMDAR-dependent plasticity (outlined below) are present in the developing MNTB-LSO pathway.

NMDA receptors are implicated in a number of forms of plasticity including potentiation and depression, at both excitatory and inhibitory synapses (for reviews see: Hunt and Castillo, 2012, Moreau and Kullmann, 2013). Although the mechanism of NMDAR-dependent plasticity can be synapse-specific, a few general characteristics are consistent across most synapses. NMDAR-dependent plasticity requires membrane depolarization for the magnesium block to be relieved, glutamate release to open the NMDAR, and calcium influx to activate intracellular pathways. NMDAR subunits are differentially associated with plasticity (for review see Yashiro and Philpot, 2008). In many developing circuits, the GluN2B subunit is expressed during critical or sensitive periods before being switched out by the GluN2A subunit (Sheng et al, 1994, Quinlan et al, 1999). GluN2B subunit containing NMDARs confer longer open times than GluN2A subunit containing NMDARs, which could increase coincidence detection and calcium influx during a period of developmental plasticity.

A number of developmental events could allow for NMDAR-dependent plasticity in the MNTB-LSO pathway during the first postnatal week. During the period of functional refinement at the MNTB-LSO synapse, GABA is co-released with glycine (Kotak et al, 1998, Nabekura et al 2004). Due to high levels of

intracellular chloride, $GABA_AR$ and glycine receptors are depolarizing and excitatory during the first postnatal week (Ehrlich et al, 1999, Kakazu et al, 1999). In addition to GABA/glycine release, the excitatory neurotransmitter glutamate is also released from MNTB terminals during early postnatal life (Gillespie et al 2005). The transient release of glutamate is supported by the expression of vesicular glutamate transporter 3 (VGLUT3) (Gillespie et al, 2005, Noh et al 2010). Slice physiology and *in situ* hybridization results suggest that there is a switch in subunit composition of NMDARs around P8, from a long-decaying GluN2B to the shorter decaying GluN2A subunit (Case and Gillespie, 2011, Singh, 2011). Collectively, these findings suggest a model such that between P3 and P8, refinement at immature MNTB-LSO terminals results from spontaneous bursts of activity from MNTB cells where GABA/glycine depolarize the membrane and relieve the magnesium block on the NMDAR, and glutamate activates the NMDARs leading to prolonged calcium entry (Kalmbach et al, 2010) dictated by the relatively long decaying GluN2B channel open times. Whether or not the immature MNTB-LSO pathway undergoes NMDAR-dependent plasticity has yet to be tested. Interestingly, the idea that glutamate release plays a role in refinement is supported by the finding that the deletion of VGLUT3 impairs functional refinement at the developing MNTB-LSO pathway (Noh et al, 2010). There are, however, several important caveats to this study.

Developmental refinement ultimately produces circuit-level changes that allow information to be integrated accurately and precisely. Below I will discuss

what influences the integration of inputs in neurons and what we have learned about integration in sound localizing neurons based on anatomical data.

Section 2: Factors influencing passive dendritic processing in binaural sound localizing neurons

Section 2.1: The effects of dendritic morphology and synapse distribution on passive filtering and integration

The ability for LSO neurons to reliably compute ILDs emerges during the period of circuit refinement. This refinement produces changes in dendritic morphology and the subcellular location of inputs. We propose that the cell optimizes these changes in dendritic morphology and synapse location to allow for fast dendritic processing, but we currently do not have a detailed knowledge of the overall dendritic morphology and synapse distribution on entire LSO bipolar principal cells. Having this information will lead to first-order models of dendritic processing in LSO bipolar principal cells. Below, I will review what we know about the detailed morphology and the distribution of synapses onto MSO cells and LSO cells. But, first I will review how morphological and passive properties of the dendrites filter synaptic inputs and how the subcellular distribution of synaptic inputs can influence synaptic integration.

First, postsynaptic potentials (PSPs) are shaped by intrinsic characteristics of the cell including the presence of transmembrane channels, cytosolic

molecules, and membrane capacitance. Although these membrane characteristics are not necessarily morphological, these characteristics do influence filtering and interact with a number of the other anatomical influences on filtering. Second, PSPs are differentially filtered depending on dendrite diameter. Intuitively, PSPs will encounter more resistance in a small diameter, high-resistance dendrite than in a large diameter, low-resistance dendrite Segev & London, 1999). Third, the further the PSP travels along a dendrite, the more resistance it will encounter. Therefore, a distal input will have a smaller effect on the soma than a proximal input, all else being equal (Spruston et al, 1999). Fourth, the complexity of the dendritic tree necessarily affects the attenuation and integration of synaptic inputs
(Spruston et al, 1999). In a complex dendritic arbor with many branch points, current flow can drift at every branch point and potentially flow in a direction that does not lead to the integration center of the neuron. By contrast, PSPs will be less attenuated in a simple, compact neuron. Another morphological characteristic that affects integration of inputs is how the dendritic tree radiates from the soma. For example, integration at the soma of a multipolar cell, where inputs from multiple dendritic arbors converge at the soma will differ from integration at the soma of unipolar or bipolar cells, where inputs converge onto one or two primary dendritic arbors.

Inputs are integrated spatially, therefore the distribution of inputs plays an important role in integration. First, the summation of 2 PSPs of the same sign

depends on their distance to each other; whereas nearby inputs result in sublinear summation, inputs that are more separated (up to a certain distance) will undergo linear summation (Spruston et al, 1999). Integration of inputs of opposite sign (ie. excitatory and inhibitory inputs), is also dependent on their relative distances and densities. Because inputs are summed temporally as well as spatially, the relative timing of inputs influences integration in an analogous way to spatial integration.

Most neurons, including principal cells of the LSO, do not integrate two inputs at a time, rather they integrate inputs from the entire cell. Therefore, the distribution of synapses along the entire cell must be considered in order to accurately model the cell. The distribution of a certain population of inputs to a specific compartment on the neuron can have significant effects on synapse integration under passive conditions. For example, perisomatic inhibition can filter or cancel out distal excitatory inputs that reach the soma. Conversely, perisomatic excitation can ensure highly reliable transmission at synapses such as the calyx of Held.

It is well known that dendrites are not only passive filters. Rather, dendrites express voltage gated channels (VGC) which confer active properties (Spruston et al, 1999). These active properties allow the dendrites to counter attenuation of current, generate dendritic spikes, and support the backpropagation of action potentials among other functions. However, quantifying dendritic morphology and synapse distribution is useful for understanding integration, to a first

approximation.

Section 2.2: Integration in Sound localizing neurons

Computations performed by principal neurons in the MSO and LSO require temporal precision. Below we will discuss what we know about synapse location, dendrite morphology and how this is achieved during development to get a better understanding of how these cells integrate their inputs. First I will describe this for MSO bipolar neurons and then for LSO bipolar neurons.

Section 2.2.1: Integration in MSO bipolar neurons

Our understanding of how MSO neurons compute ITDs has advanced greatly as a result of knowing detailed morphology, the subcellular distribution of synaptic inputs, the active properties of the dendrites, and *in vivo* extracellular and whole cell recordings.

Morphology of MSO bipolar neurons

Our understanding of dendritic characteristics of MSO neurons has evolved from the detailed qualitative observations of Cajal (Ramon y Cajal, 1909), to simple quantifications of dendrites (Rogowski and Feng, 1981), to very detailed measurements from which cable properties can be accurately predicted (Rautenberg et al, 2009). Rautenberg and colleagues filled individual MSO bipolar principal cells and then digitally rendered the cells in 3D to quantify

branch points, cell volume, surface area, and dendrite diameter (as a function of distance from the cell body) in tissue from gerbils aged postnatal day 9 to 40. They found that, between P9 and P21, there was a significant decrease in the number of branchpoints, total cell length, and cell surface area whereas the dendritic radii and cell volume increased until P27. These morphological changes will facilitate the fast postsynaptic integration that MSO bipolar cells require to detect ITDs (Rall et al, 1992, Agmon-Snir et al, 1998). Interestingly, the time at which MSO bipolar cells mature anatomically (P27) (Rautenberg et al, 2009), matches the time when these cells mature physiologically (4th postnatal week) (Scott et al, 2005), a finding which demonstrates the close relationship between structure and function in dendritic processing.

Subcellular distribution of inputs to MSO bipolar neurons

MSO bipolar neurons receive excitatory inputs from both ears; lateral dendrites are excited by the ipsilateral cochlear nucleus and medial dendrites are excited by the contralateral cochlear nucleus (Stotler, 1953). This arrangement allows MSO neurons to compare the arrival times of the converging EPSPs at the cell body, resulting in the computation of an ITD. MSO neurons receive prominent inhibitory inputs at the soma (Kapfer et al, 2002), which are thought to be critical for increasing the precision of the ITD computation, though this is debated (Grothe et al, 2010).

Slice physiology has shown that MSO dendrites contain many voltage

activated channels (HCN, K+, and Na+) which contribute to integration and filtering of EPSPs (Golding, 2011). A recent study used *in vivo* whole-cell and juxtacellular recordings in the MSO to show that computations in MSO neurons result from linear summation of EPSPs (van der Heijden et al 2013). This linear summation is consistent with slice physiology recordings which suggest that dendrites of MSO cells have many active properties. Interestingly, no evidence of well-timed inhibition was found using *in vivo* recordings, which contrasts with the suggestion that well-timed, perisomatic inhibition shapes ITD tuning (Grothe et al, 2010, van der Heijden et al, 2013). A second recent study used slice physiology on a novel thick-slice preparation to show, for the first time, that inhibition precedes excitation by 300-400ms, suggesting that inhibition could be used to shunt activity before the arrival of the coincident EPSPs (Roberts et al, 2013). This series of experiments has greatly advanced our knowledge of the influences of synapse location and dendritic filtering on sound localization.

Section 2.2.2: Integration in LSO bipolar neurons

Morphology of LSO bipolar principal neurons

Ramon y Cajal first described bipolar cells of the LSO in cat (Ramon y Cajal, 1909). He noted their bipolar morphology and restricted dendritic arbor and several thick primary dendrites. The dendritic arborizations are not as complex as those in the kitten (Scheibel and Scheibel, 1974). Since, these observations, the developmental reduction in complexity has been observed and quantified in other

species (Ollo and Schwartz, 1979, Cant, 1984, Helfert and Schwartz, 1986). The majority of these studies used Golgi staining to label neurons, but recently cells have been studied following single-cell injections and this has improved the detail in which these cells can been studied (Rietzel and Friauf, 1998). This shift in techniques has resulted in more branchpoints being detected, new cell types being identified, and more complete reconstructions of the neurons. Despite this, we currently do not have measurements that would allow us to construct first-order models of dendritic processing for fully reconstructed LSO principal cells.

Current understanding of subcellular distribution of inputs to LSO bipolar principal neurons

We have some insight into the distribution of excitatory and inhibitory inputs on LSO principal cells. There is a relationship between synapse phenotype and subcellular location; in the mature LSO, principal cell bodies are surrounded by inhibitory, glycinergic inputs from the MNTB (Cant, 1984, Helfert et al, 1992, Friauf et al, 1997, Korada and Schwartz, 1999). However, few studies have looked at both excitatory and inhibitory inputs (Cant, 1984, Helfert et al, 1992). At the cell body there are more inhibitory synapses than excitatory in a ratio of 2:1, at thick (>3 μm in diameter) dendrites the ratio is approximately even, at thin (~1 μm diameter) dendrites there are more excitatory than inhibitory synapses in a ratio of 2:1, and at the thinnest (< than 0.5 μm) dendrites there are excitatory but no inhibitory synapses (Helfert et al ,1992).

There are, however, some caveats to the above findings which constrain our understanding of synapse distribution along principal cells. First, all of these findings come from single tissue sections or single optical sections of tissue and therefore only show the distribution of synapses for a fraction of the cell. Second, the dendrites analyzed may not belong to bipolar principal cells. Although principal cells make up 70-80% of the cells in the LSO, there are 5-7 cell types and the dendrites could belong to any cell type (Helfert and Schwartz 1986, 1987, Rietzel and Friauf, 1998). Third, what one uses as a marker for a synapse is also significant. Some experiments use antibodies raised against glycine or glycine receptors to detect inhibitory synapses. The MNTB-LSO synapse had been thought to be glycinergic but it also releases GABA during early development (Kotak et al, 1998, Korada and Schwartz 1999). Therefore, staining solely for glycine could result in an underestimation the total number of inhibitory synapses. Lastly, today we have access to many synapse specific antibodies which facilitate the identification of synapses.

Just as the dendritic arbor changes during development, so does the subcellular location of inhibitory synapses in the LSO. Anatomical results suggest a re-distribution of inhibitory synapses toward the soma during the first two postnatal weeks in rat (Friauf et al, 1997). Single optical sections of glycine receptor immunoreactivity show that perisomatic staining patterns develop during the first two postnatal weeks. However, the study by Friauf et al (1997) does not give us a complete understanding of the re-distribution of inhibitory inputs along

LSO bipolar principal cells. First, the authors used glycine receptors as a marker of inhibitory synapses and could therefore underestimate the total number of inhibitory synapses because they did not quantify $GABA_A$Rs (Friauf et al, 1997). Second, it is unclear which cell types have perisomatic labeling because the cell type was not identified morphologically. Third, the authors used single optical sections to gauge the subcellular distribution of inhibitory synapses and therefore we only know about glycine receptor staining around a portion of the cell (the cell body) (Friauf et al, 1997). A 3-D reconstruction of the entire neuron and its inhibitory inputs is required for an accurate assessment of the re-distribution of inhibitory synapses along the cell.

Currently, we have no information about the subcellular distribution of excitatory synapses along LSO bipolar principal cells over development. We do, however, know that the VCN-LSO pathway undergoes functional refinement during early postnatal life (Case et al, 2011), including a reduction in the number of inputs. Therefore we might expect anatomical refinement to follow.

In light of the information given above, we still lack detailed morphological measurements and the subcellular distribution of inputs on LSO bipolar principal cells. Studies that have modeled LSO neurons used a cell morphology from Golgi staining, which underestimates the complexity of the arbor, and relatively simple distributions of excitatory and inhibitory synapses (Zackenhouse et al, 1998). Moreover, there is a clear deficit in our knowledge of how the distribution pattern is achieved during development and whether certain forms of anatomical

refinement can occur before the onset of hearing. In order to understand how dendritic morphology is optimized over development, we performed 3D reconstructions of serial confocal images of LSO bipolar cells to study changes in the distribution of inhibitory inputs and cellular morphology in the week before hearing onset (Chapter 2).

Section 3: Vesicle populations at the immature MNTB terminal

As mentioned above, the immature MNTB-LSO synapse releases GABA and glycine as well as the excitatory neurotransmitter glutamate (Kotak et al, 1998, Nabekura et al, 2004, Gillespie et al, 2005). The surprising finding that one terminal releases three fast acting neurotransmitters raises several questions about how the neurotransmitters are packaged and released at the MNTB. It is known that GABA and glycine can be co-released from the same vesicle and this co-release has been demonstrated at the MNTB-LSO synapse (Nabekura et al, 2004). The co-release of GABA and glycine from the same vesicle is facilitated by the fact that both neurotransmitters use the same transporter, vesicular inhibitory amino acid transporter (VIAAT), to load the vesicle (McIntire et al, 1997).

As for glutamate release at the immature MNTB terminal, VGLUT3 is the transporter that loads glutamate into vesicles. The transient release of glutamate at the immature MNTB-LSO synapse is correlated with the expression of VGLUT3 in presynaptic terminals of individual MNTB axons and intense

VGLUT3-IR in the LSO and SPN, two nuclei in the SOC that receive prominent projections from the MNTB during the prehearing period (Gillespie et al, 2005). Furthermore, there is no glutamatergic current in the MNTB-LSO pathway of VGLUT3$^{-/-}$ mice (Noh et al, 2010).

The release of three neurotransmitters from the immature MNTB terminal raises several fundamental questions. Is glutamate released from the same vesicle population as GABA/glycine such that each vesicle expresses both VIAAT and VGLUT3? OR Are there two populations of vesicles; one VIAAT-positive population which contains GABA/glycine and a separate VGLUT3-positive population which contains glutamate?

If GABA/glycine and glutamate are in the same vesicles then we would expect the three neurotransmitters to show the same release properties. Recent electrophysiological data from the lab show that the release properties differ between GABA/glycine and glutamate, suggesting that immature MNTB-LSO terminals contain two populations of vesicles (Case and Gillespie, 2011, Fig. 4). The finding that GABA/glycine and glutamate differ in their release probability raises new questions about what causes the different release probability between the two vesicle populations.

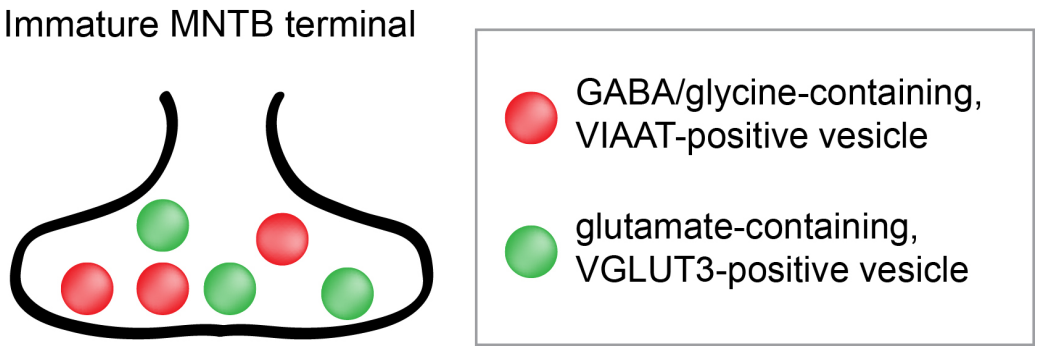

Figure 4: A schematic of our working model of vesicle populations at the immature MNTB terminal. The immature MNTB terminal contains two populations of vesicles; one population that is GABA/glycinergic and expresses VIAAT and one that is glutamatergic and expresses VGLUT3. Individual vesicles from these populations may or may not be intermingled.

Fast synchronous release of neurotransmitter at central synapses is complex and involves a lot of presynaptic machinery, but the general mechanisms of release are now well understood (Sudhof, 2013). The arrival of an action potential at the terminal opens voltage-gated Ca^{++} channels (VGCCs), resulting in the influx of Ca^{++}, which bind to calcium sensing proteins on the vesicle and initiate neurotransmitter release. Among the factors that can influence vesicular release are the VGCCs expressed at the terminal, the proximity of the vesicles to the calcium influx, the density of vesicles at the terminal, and the type of Ca^{++} sensor present on the vesicle. Here, I will specifically focus on the influence that Ca^{++} sensors have on neurotransmitter release

Variability in release can also be ascribed to the expression of different Ca^{++} sensors on the vesicle. The predominant calcium sensing proteins in the CNS belong to the synaptotagmin (Syt) family (Sudhof, 2002). Different synaptotagmin isoforms vary in calcium sensitivity and kinetics and this variance can confer different release properties to the vesicles (Hui et al, 2005, Xu et al 2007). Synaptotagmins 1, -2, and -9 are the isoforms responsible for fast, synchronous release at central synapses. When compared to other isoforms, Syt 1, -2, and -9 are very similar functionally but the three Syts do slightly differ from each other. Given that, at the immature MNTB-LSO synapse, glutamate has different release properties than GABA/glycine and that differential expression of synaptotagmin isoforms can confer different release properties, we asked the following two questions; 1) is more than one synaptotagmin isoform expressed at the MNTB terminal? and 2) is one Syt isoform specifically associated with glutamate release?

To answer this, we performed a co-localization study between calcium sensors (Syt1 and Syt2) and markers for vesicle phenotype (Chapter 3). We used VIAAT and VGLUT3 as markers for the two vesicle populations in immature MNTB terminals and VGLUT1 and VGLUT2 as markers of excitatory inputs in the SOC, such as those from the AVCN.

Section 4: Sorting of vesicular proteins at the immature MNTB-LSO terminal

Electrophysiological evidence from the lab suggests that the immature MNTB-LSO synapse contains two populations of vesicles (Case and Gillespie, 2011, unpublished observations). Furthermore, each population has different release properties which could be related to differences in presynaptic machinery, location at the terminal, or association with different VGCCs (among other factors). These two findings imply that the cell has a way to reliably sort vesicles and vesicular proteins into separate populations. For example, if single vesicles release either GABA/glycine or glutamate, then the cell must have a mechanism to ensure that VIAAT and VGLUT3 are targeted to separate vesicles. How do VIAAT-positive and VGLUT3-positive vesicles at the immature MNTB terminal achieve and maintain their identities? The mechanisms that sort vesicles and vesicular proteins at synaptic terminals that contain multiple vesicle populations are not well known. Understanding how a vesicle achieves its mature identity and how proteins are targeted to specific vesicles would be a major advance.

Synaptic vesicles are not mature when they leave the *trans* golgi network, rather synaptic vesicles mature by undergoing successive rounds of exo- and endocytosis until they acquire the proper complement of vesicular proteins (Prado and Prado, 2002, Santos et al, 2009). These rounds of exo- and endocytosis likely occur as the synaptic vesicle precursor is transported down the

axon as well as when the vesicle has reached the terminal proteins (Matteoli et al, 1992, Santos et al, 2009). However, this does not explain how specific proteins are targeted to specific vesicles or how different vesicle populations can be segregated at the terminal. Interestingly, synaptic vesicles can be directed to defined pools at the terminal depending on which modes of exo- and endocytosis they use and depending on interactions with various trafficking molecules. It is possible that such sorting happens at immature MNTB terminals but this remains to be tested.

Although vesicle recycling plays a role in vesicle maturation and different modes of exo- and endocytosis can repopulate different pools of vesicles, it is still unclear how vesicle identity can be achieved and maintained at the immature MNTB terminal. One convenient way for the cell to do this is through protein-protein interactions. If, for example, VGLUT3-positive vesicles require a specific Ca^{++} sensor and VIAAT-positive vesicles require another Ca^{++} sensor, as could be the case at the immature MNTB terminal, then perhaps there are protein-protein interactions that sort the Ca^{++} sensors to the appropriate vesicle population. Recent evidence supports the idea that protein-protein interactions can indeed influence expression and trafficking on the vesicle. Bajjalieh and colleagues found that synaptic vesicle protein 2 (SV2) targets Syt1 to synaptic vesicles (Yao et al, 2010). In cells in which SV2 was deleted, Syt1 was not targeted to the vesicle but remained on the cell surface following exocytosis. Given that vesicular proteins can target other proteins to the vesicle and that our

working model proposes that the two vesicle populations at the MNTB terminal have distinct identities, we asked if VGLUT3 was involved in targeting a particular synaptotagmin isoform to VGLUT3-positive vesicles in immature MNTB terminals (Chapter 4).

Rationale and Significance

Chapter 2: Re-distribution of Inhibitory Synapses onto Proximal Sites of LSO Principal Cells Occurs Before Hearing Onset

In neural circuits, functional refinement is commonly followed by structural changes. The structural changes can include pruning of axonal arbors, changes to the dendritic tree, and changes in the location of synapses. All of these changes presumably result in a structure that integrates information more efficiently.

Functional refinement in the MNTB-LSO synapse occurs between postnatal day 3 (P3) and P8, which is before hearing onset (P12) (Kim and Kandler, 2003). When does anatomical refinement occur? And does it require acoustical experience?

Inhibitory inputs to MSO neurons are initially diffusely distributed along the dendritic tree then redistribute toward the soma after hearing onset (Kapfer et al, 2002). This coincides with selective pruning of MNTB axonal arbors from distal dendrites (Werthat et al, 2008). Anatomical refinement of MNTB axons and LSO

neurons is also seen after hearing onset (Sanes and Siverls, 1991, Sanes et al 1992a). Together, this suggests that the MNTB-LSO circuit is first refined functionally before hearing onset and then refined anatomically in the presence of acoustical information.

In spite of the morphological changes that happen after hearing onset, there is evidence that the refinement of dendritic arbors in the LSO begins before hearing onset (Rietzel and Friauf, 1998). Little is known about the subcellular distribution of inhibitory inputs along LSO neurons or if re-distribution occurs before or after hearing onset. To better understand this, we reconstructed single LSO cells and the subcellular location of their inhibitory inputs in the pre-hearing animal.

We found that inhibitory synapses were re-distributed toward the soma and proximal dendrites of LSO principal cells in the week before hearing onset. Our results challenge the field's current working model of refinement in the SOC in two ways. First, that anatomical refinement occurs in the absence acoustically driven activity. Second, that functional refinement and anatomical refinement do not occur as two separate periods separated by some duration, rather they occur in close succession or concurrently.

Chapter 3: Synaptotagmins I and II in the Developing Rat Auditory Brainstem: Synaptotagmin I is Transiently Expressed in Glutamate-Releasing Immature Inhibitory Terminals

The developing MNTB-LSO synapse releases GABA and glycine as well as the excitatory neurotransmitter glutamate. Electrophysiological evidence suggests that GABA and glycine are released from one population of vesicles and glutamate is released from another. Interestingly, GABA/glycine and glutamate have different release properties indicating that the two pools of vesicles are located in different areas of the presynaptic terminal, are differentially associated with voltage sensitive Ca^{++} channels, and/or express different Ca^{++} sensors. Given that different Ca^{++} sensors can confer different release properties and that the GABA/glycine and glutamate have differing release properties, we asked if more than one Ca^{++} sensor is present at the immature MNTB terminal and if one Ca^{++} sensor was associated with the anomalous glutamate release. The two predominant Ca^{++} sensors at fast central synapses are synaptotagmin 1 (Syt1) and synaptotagmin 2 (Syt2). We used immunohistochemistry to study the expression patterns of Syt1 and Syt2 in the developing SOC and double immunofluorescence between Syts and markers of synapse phenotype to study which synapses contain which Ca^{++} sensors.

We found that both Syt1 and Syt2 are expressed in the developing LSO and the expression patterns suggest that one Ca^{++} sensor is associated with VGLUT3 expression and glutamate release from MNTB terminals. These findings support the idea that the differential release properties between GABA/glycine and glutamate could be related to differential expression of Ca^{++} sensors. Lastly,

these findings suggest a new working model about the organization of vesicle populations at immature MNTB terminals.

Chapter 4: Synaptotagmin I is expressed at a GABA/glycine/glutamate-releasing central synapse, independent of vesicular glutamate transporter 3 expression

In Chapter 3, we found that, in the SOC, Syt2 and VIAAT share similar temporal and spatial expression patterns and, intriguingly, that Syt1 shares the same developmentally-regulated and spatially-restricted expression pattern as VGLUT3. Based on these results, our updated working model of vesicle populations at immature MNTB terminals suggests that one population is GABA/glycinergic and expresses VIAAT and Syt2, and the other population glutamatergic and expresses VGLUT3 and Syt1. This arrangement raises several important questions about what controls the sorting of proteins onto separate vesicle pools. For example, how are proteins sorted such that Syt1 and VGLUT3 are expressed in the glutamatergic but not the GABA/glycinergic vesicle population? Also, the finding that Syt1 and VGLUT3 share the same developmentally-regulated and spatially-restricted expression pattern in the SOC, raises the question: what regulates the developmental expression of Syt1 and VGLUT3? Here, we specifically asked if VGLUT3 was required for the expression and/or targeting of Syt1 to immature MNTB terminals. To answer this, we studied Syt1 immunoreactivity in the SOC of VGLUT3$^{-/-}$ tissue and wildtype tissue.

We found that VGLUT3 influenced neither the expression nor the trafficking of Syt1 at immature MNTB terminals. This negative result does not weaken our model but suggests that the factors which influence the vesicle targeting and developmental expression of Syt1 and VGLUT3 at this synapse remain unknown.

Chapter 2: Re-distribution of Inhibitory Synapses onto Proximal Sites of LSO Principal Cells Occurs Before Hearing Onset

Abstract

The ascending projection neurons (principal cells) of the lateral superior olive (LSO) exhibit a bipolar morphology and integrate ipsilaterally-derived excitatory and contralaterally-derived inhibitory inputs. Although the subcellular location of these inputs necessarily influences signal integration, little has been known about precisely how these inputs are distributed, how their distribution affects circuit-level processing, and how their specific distribution pattern is achieved during development.

In the neighboring medial superior olive, inhibitory synapses onto principal neurons are diffusely distributed throughout the dendritic tree shortly before hearing onset, and in the next two weeks are re-distributed to occupy more proximal sites through an experience-dependent process (Kapfer et al, 2002). As the major inhibitory input to the LSO undergoes significant refinement before hearing onset in the rat (Kim & Kandler, 2003), we asked whether inhibitory synapses onto LSO principal cells are redistributed before hearing onset.

In acute slices from postnatal days 4 and 11 (P4 and P11) rats, we labeled cells in the medial and middle limbs of the LSO with a fluorescent dye using whole-cell patch clamp. Slices were fixed, resectioned at 50 µm, labeled for immunoreactivity to gephyrin, and imaged at the confocal microscope. The

resulting Z-stacks were analyzed in Imaris (Bitplane): the dendritic arbor was reconstructed in 3-D, gephyrin-positive puncta were identified, and puncta associated with the labeled neuron were selected as markers of inhibitory synapses.

In the week before hearing onset, the surface density of gephyrin puncta at the soma increased by 140% and the linear density of gephyrin along proximal dendrites increased by 90%. We also assessed dendritic complexity using the number of Sholl intersections at 5 μm intervals. The greater complexity of younger neurons was most apparent near the soma. Between P4 and P11, there was a significant reduction in the average number of intersections between 5-30 μm from the cell body but beyond 30 μm dendritic complexity was similar.

In conclusion, inhibitory synapses in the LSO undergo significant re-distribution in the absence of acoustically driven activity.

Introduction

Determining the source of a sound along the horizon is important for interpreting our environment. Azimuthal sound localization relies on the utilization of two binaural cues; interaural time differences (ITD) and interaural level differences (ILD). ILDs are first computed in binaural nuclei in the auditory brainstem, the lateral superior olive (LSO) (Boudreau and Tsuchitani, 1968). LSO bipolar principal cells are excited by sound at the ipsilateral ear and inhibited by

sound at the contralateral ear. The ipsilateral excitatory input is glutamatergic and comes from spherical bushy cells in the cochlear nucleus (Cant and Casseday 1986, Wu and Kelly 1992) whereas the inhibitory GABA/glycinergic inputs come from principal cells in the medial nucleus of the trapezoid body (MNTB, Moore and Caspary, 1983, Bledsoe et al, 1990) which are driven by excitatory inputs from globular bushy cells in the contralateral cochlear nucleus (Glendenning et al 1985, Smith et al 1991).

As objects or the listener move throughout the environment, the representation of the location of the sound source must be continually updated using cues such as ILDs. Therefore the auditory system must be capable of rapid, temporally precise computations in order to continually localize sound accurately. How does the auditory system keep up? The ascending auditory system has some of the fastest, high fidelity synapses in the brain. This temporal accuracy is seen first hand at the high fidelity end bulb of Held synapse in the AVCN and calyx of Held synapse in the MNTB where excitatory inputs envelop the soma of the postsynaptic cell, which have little processing done in the small dendrites (Englitz et al 2009, Lorteije et al 2009, Borst *et al*, 2013, Manis et al, 2013). Bipolar principal cells in the LSO, on the other hand, are large cells with long complex dendritic trees, inputs spread along the dendrites, and it is unclear how the cell integrates the converging inputs. This raises several questions; what is the optimal distribution of inputs on LSO neurons such that ILDs are accurately computed? When does this distribution appear during development? Does it

require acoustical information or can it be achieved before hearing onset?

In the medial superior olive (MSO), a neighboring nucleus that processes ITDs, inhibitory inputs from the MNTB and lateral nucleus of the trapezoid body (LNTB) are diffusely distributed along the dendrites of bipolar principal cells shortly before hearing onset and are then redistributed to the cell body and proximal dendrites over the next two weeks (Kapfer et al, 2002). Concomitant with the changes in synapse placement, the total number of MNTB axon terminals decreases and there is an increase in the proportion of axons that terminate at the cell body versus the dendrites (Werthat et al, 2008). Importantly this anatomical refinement requires normal auditory experience, as it will not occur if one of the cochleae is damaged or if the animal is raised in an environment that lacks binaural cues (Kapfer et al, 2002, Werthat et al, 2008). These findings suggest that inhibitory inputs on to MSO principal cell bodies are important for sound localization; is there a similar re-distribution of inhibitory synapses on LSO principal cells? If so, does it occur after hearing onset as in the MSO?

Given that the LSO and MSO both receive inhibitory inputs from the MNTB (Banks and Smith, 1992), one might expect the re-distribution of synapses to follow the same timeline and that structural refinement of MNTB projections to the LSO and MSO occur at the same time (after hearing onset).

Alternatively, the re-distribution of inhibitory inputs could happen before hearing onset. Structural refinement is known to follow functional refinement at

some delay (Antonini and Stryker 1993, Colman et al 1997). The developing MNTB-LSO synapses undergo functional refinement from P3 to P8 and it is unclear and controversial how long of a delay exists before structural refinement begins (Kim and Kandler 2003). There are clear examples of structural refinement of MNTB-LSO circuitry during the third and fourth postnatal weeks (Sanes and Siverls, 1991, Sanes et al, 1992a), but upon a closer look, we can see that there is some anatomical refinement in the dendritic arbors before hearing onset (Rietzel and Friauf, 1998). Here we sought to see if anatomical refinement occurs before hearing onset by asking whether there was a re-distribution of inhibitory inputs to LSO principal cells from postnatal day 4 to 11.

Methods

All experimental procedures involving animals were approved by McMaster University's Animal Research Ethics Board and conformed to guidelines outlined by the Canadian Council on Animal Care. Sprague-Dawley rats (bred on site) age postnatal days 4 and 11 (P4 and P11) were anesthetized and the brain was removed and quickly placed in artificial cerebrospinal fluid (ACSF) containing (in mM) 124 NaCl, 1 K_2SO_4, 5 KCl, 1.25 KH_2PO_4, 10 dextrose, 26 $NaHCO_3$, 2 $CaCl{\bullet}H_2O$, and1 kynurenic acid (pH 7.2, Case et al, 2011).

Coronal slices (300 μm) were cut with a vibratome and slices containing the LSO were place in a humidified, oxygenated interface chamber at room temperature. Tissue slices were allowed to recover in the chamber for at least 10

minutes before being transferred to an immersion chamber for filling. Slices were continuously perfused with ACSF superfused with 95% O2 and 5% CO_2.

Patch pipettes were pulled with borosilicate glass to a resistance of 1.5-2.5 MΩ. Pipettes were filled with 0.5% Lucifer Yellow (Sigma L-0453), freshly prepared daily in an internal solution containing (in mM) 64 d-gluconic acid , 64 cesium hydroxide•H_20, 11 EGTA, 56 CsCl, 1 $MgCl_2$•$6H_20$, 1 $CaCl_2$, 10 HEPES, 0.3 GTP-Na, ATP-Mg•3.5 H_2O (pH 7.2, Case et al, 2011).

Bipolar principal neurons in the middle and medial limbs of the lateral superior olive were visually targeted using IR-DIC optics. Cells were whole-cell patched and filled for 10 minutes. Successful cell-fills were visualized using epifluorescence and the slice was allowed to recover in the interface chamber for 20 minutes before being fixed (4% paraformaldehyde in 0.1M phosphate buffer) for 20 hours at 4°C. Only one LSO was targeted per slice. In some cases 2 cells were filled in the same LSO; one in the middle limb and the other in the medial limb.

Slices were fixed for 20 hours, transferred to 30% sucrose in 0.1 M PBS for cryoprotection, resectioned at 50 µm at a freezing microtome, and collected into 0.1 M phosphate buffer (PB; pH 7.4). Tissue sections were blocked for 24 hours in a solution containing 5% normal serum, 2.5% BSA, and 0.5% triton-X in 0.1 M PB (pH 7.4). Next, the tissue was incubated in a primary antibody raised against gephryin (mouse host; Synaptic Systems, cat. no. 147 021) diluted at 1:250 in 5% normal serum, 2.5 % BSA, and 0.5% triton-X in 0.1 M PBS, pH 7.4

for 60 hours. After washes in PBS, sections were incubated in a secondary antibody (goat anti-mouse Dylight 647, Jackson ImmunoResearch, IgG, Fc_γ subclass 1 specific) diluted at 1:500 in serum for 24 hours. Sections were washed in PBS then mounted in a mounting medium (CFM1+, Citifluor Ltd.) which has a refractive index (R.I. = 1.52) which matches the R.I. of the objective lens, immersion oil, and coverslip. A control condition in which the primary antibody was omitted was included for each staining run and showed no punctate staining.

Table 1.

Antibodies Used in This Study				
Antigen	**Immunogen**	**Host**	**Source/cat. No.**	**Dilution**
Gephyrin	Purified rat gephyrin	Mouse, monoclonal	Synaptic Systems, 147021	1:250
mouse IgG, Fc_γ subclass specific		Goat	Jackson ImmunoResearch, 115-605-205	1:500

Image Acquisition

Images were acquired at a Leica SP5 DM6000 CS confocal microscope. Filled cells were excited with the 436 nm line of an argon laser (emission window 480-600 nm) and goat anti-mouse Alexa 647 was excited with a 633 helium-neon laser and collected using a 650 nm longpass filter. Cells were initially visualized at low-magnification (20X, NA 0.17) to verify morphology and position within the LSO. High-resolution stacks of images in the Z-dimension were collected with a 63X lens (NA 1.4) at 2.5X digital zoom resulting in voxel sizes of 96 nm * 96 nm * 500 nm. Each channel was imaged sequentially and averaged twice. Most cells'

processes extended beyond a single visual field and multiple serial optical sections were taken to image the entire cell.

Analysis

Leica .lif files were converted to .ims files in Imaris 7.6.4 (Bitplane, South Windsor, CT, USA). Files containing stacks of optical sections belonging to the same cell were then stitched together in XuvStitch 1.8.099 (Emmenlauer et al, 2009). Stitched images were then imported to Imaris for image processing and analysis. Some cells displayed in Fig. 1 and 2 were stitched in another program, *Stitching* (Preibisch et al, 2009), which was used in the image processing package Fiji (Fiji is just ImageJ, Schindelin et al, 2012).

All images were median filtered with a 3x3x1 pixel filter. Dendrites were traced automatically and manually with Filament Tracer (Bitplane). Inhibitory synapses, as identified by gephyrin immunoreactive puncta, were identified and quantified in the Spots (Bitplane) application of Imaris. We developed a procedure using both automatic and manual features of Imaris to identify gephyrin puncta belonging to the labeled cell, explained in detail below. The procedure for gephyrin-Spot identification for somata and dendrites is illustrated in Fig. 3 and 4. For display purposes, some images were altered to better display the Spots (Fig. 3, 4, 5). We used 4 cells at P4 (shown in Fig 1. A, C, F, H) and 4 cells and P11 (shown in Fig 2. A-D) for 3-D reconstructions and quantification of gephyrin along the dendrites. Three-dimensional reconstructions of dendritic

arbors and quantification of puncta along the arbor are time consuming procedures, and because we had a trial version of Imaris, we could not analyze the dendrites for more than 8 cells. We used 8 cells at P4 and 9 cells at P11 for quantification of gephyrin at the soma.

Identification of gephyrin puncta at the soma

First, we created a Surface (blue) around the cell body (Fig. 3 A', B'). It was important to have the Surface hug the edge of the cell in order to accurately detect puncta belonging to the filled neuron. With an inappropriately large Surface, we would identify gephyrin clusters that were in fact outside the labeled cell. Conversely, with an inappropriately thin Surface, we would underestimate the number of gephyrin puncta. Second, a new channel that included the gephyrin puncta that were within the Surface was created (Fig. 3 A'', B''). This channel was called “Masked Gephyrin." Third, the gephyrin puncta in the “Masked Gephyrin” channel were rendered as Spots using automatic and manual processes (Fig. 3 A''', B'''). Importantly, all Spots were set to the same size, although in the future it would be valuable to have different sized puncta rendered as different sized Spots. Many quantifications could be made after the Spots were identified. For instance, Fig. 3 A'''', B'''' shows all the Spots within 1 µm of the Surface in yellow and all Spots beyond 1 µm in blue. The blue Spots (>1 µm from the Surface/cell membrane) were excluded from analyses below.

Quantification of gephyrin puncta at the soma

The surface density of gephyrin puncta at the soma was determined by dividing the number of Spots by the surface area of the soma. The surface area of the soma was obtained following the creation of the Surface around the cell body. The percent change in the number or density of gephyrin puncta at the soma between P4 and P11 was calculated using $[(P11_{ave}-P4_{ave})/P4_{ave}] * 100$.

Identification of gephyrin puncta on dendrites

The procedure to identify gephyrin puncta along the dendrites of the labeled neuron was similar to the method outlined above with some important differences. Instead of one Surface being created to mask the gephyrin, many Surfaces were created along the dendritic arbor in adjacent regions of interest. Care was taken to ensure that the dendrites within a given region of interest be of similar diameter and/or the dendritic labeling be of similar signal to noise ratio, as otherwise the Surface would either be too small or too big, leading to either an underestimation or overestimation of the number of gephyrin puncta. Fig. 4B illustrates how gephyrin puncta were identified along the dendrites.
A small area of the neuron is shown for simplicity (Fig. 4A,B). First, multiple Surfaces were created adjacent to each other (Fig. 4B). Second, gephyrin puncta under each Surface were converted to a Masked Gephyrin channel (Fig. 4B'). Third, puncta in the Masked Gephyrin channels were converted to Spots and the Spots that belonged to different Masked Gephyrin channels were merged

together (Fig. 4B''). Fourth, the distance of each Spot from the soma was measured along the dendrites traced in Filament Tracer (blue) (Fig. 4B''').

The Surface creation/Spot identification procedure was repeated over the entire cell. The end result is shown in Fig 5C. Figure 5A shows a P4 cell with multiple Surfaces and a Masked Gephyrin channel was created under each Surface. Figure 5B shows the labeled cell (red) with Spots (yellow) that were created from the multiple Masked Gephyrin channels. Figure 5C shows the same cell after the dendrites were traced in Filament Tracer (Blue) with gephyrin puncta identified as Spots (yellow). Data needed to be prepared as seen in 5C in order to for the distribution of gephyrin along entire neurons to be calculated.

Distance of synapses from the cell body can be calculated in two ways: the distance in 3D from the nearest point on the cell body, or the linear distance – following the dendrite – from the cell body. Here the linear distance was measured. Measuring the distribution of gephyrin puncta along the dendritic arbor required that the cell be rendered as a Filament in Filament Tracer. Next a beginning point of a primary dendrite was set at the soma-dendrite junction to 0 μm. The distance of each Spot along the filament was measured. If the Spot and the Filament were not in contact, the Spot mapped onto the nearest node of the filament. This 'distance along the path length' procedure was performed on every dendritic arbor that contacted the soma. The values from each branch were then amalgamated to create a database that contained the distance of every Spot from the soma.

The total length of traced dendrites, total number of traced filaments, and the total number of puncta analyzed for each dendritic tree are shown in Table 2.

Table 2.

Raw data of 8 cells analyzed for gephyrin density on dendritic arbor				
P4 Cell #	**Corresponds to cell shown in:**	**Total length of traced dendrite (µm)**	**Total number of traced filaments**	**Number of puncta analyzed**
1	Fig 1A & Fig 10A	1765	144	445
2	Fig 1C & Fig 10C	1501	82	468
3	Fig 1F & Fig 10D	613	54	138
4	Fig 1H & Fig 10B	518	26	174
P11 Cell #	**P11 Cells corresponds to cell shown in:**	**Total length of traced dendrite (µm)**	**Total number of traced filaments**	**Number of puncta analyzed**
1	Fig 2A & Fig 10F	539	33	435
2	Fig 2B & Fig 10H	884	67	393
3	Fig 2C & Fig 10G	539	19	255
4	Fig 2D & Fig 10E	932	77	490

Quantification of gephyrin puncta along the dendrite

The distance of each gephyrin punctum from the edge of the cell body was used to map out the distribution of gephyrin for each cell. The linear density of gephyrin was calculated by summing the number of Spots that were measured in a segment (e.g. 0-9.99 µm or 0-24.99 µm) then dividing it by the length of the segment (10 µm or 25 µm). The percent change in the average linear density of gephyrin in a given region was calculated as $[(P11_{ave}-P4_{ave})/P4_{ave}] * 100$.

Morphological Analyses

Dendritic complexity was measured using 3-D Sholl analysis (number of intersections between identified neuronal filaments and concentric spheres at 5 μm spacing). Only those dendritic processes considered to be fully labeled were included. The processes of the eight cells (four P4, four P11) used for Sholl analysis are shown in Fig. 10. The bipolar morphology of LSO principal cells results in ventral and dorsal dendritic arbors, which were analyzed separately, beginning at the somato-dendritic juncture.

The area of the dendritic arbor was measured from a projection of the cell in the coronal plane. The area was measured by connecting all the endpoints and the area inside the boundary was measured, as shown in Fig. 14A and B, in the image processing software package Fiji (Fiji Is Just ImageJ). The area measurements were taken from 7 P4 cells and 6 P11 cells.

The shape of the dendritic field was determined by measuring the length of a line along the long axis of the dendritic field and dividing that value by the length of a perpendicular line drawn along the widest point of the dendritic field. A high value indicates that the field is becoming more anisotropic and more restricted to its isofrequency band. Eight P4 cells and 7 P11 cells were used for analysis of cell shape.

Statistics were calculated in Matlab (Mathworks) using the Mann-Whitney U-test.

Results

We reconstructed LSO principal cells and their inhibitory inputs in 3-D at two ages before hearing onset to map the distribution of inhibitory synapses along these cells and to see how the dendritic arbors refine morphologically.

Distribution of gephyrin at the somata and along dendrites

The images acquired at P4 and P11 exhibit some salient differences, especially with regard to somatic labeling. For example, gephyrin-positive puncta at P4 appear to be fairly diffusely, and randomly, distributed throughout the field of view. Gephyrin is distributed quite differently in the LSO of tissue just one week older: in images from P11 tissue, it is possible clearly to discern the somata of un-filled neurons from the gephyrin labeling that outlines the somata of these "shadow neurons." To quantitatively analyze these differences, we used analysis tools in Bitplane Imaris software to identify (as Spots) the gephyrin puncta and (as a Surface) the cell body. For details, see Methods, Fig. 3.

At P4, gephyrin puncta (yellow) at the cell body were small and faint whereas at P11 gephyrin puncta were larger, more defined, and more abundant (see Fig. 3A" and B" for representative images). The number of gephyrin-positive puncta at the soma also increased significantly during this one-week period. The average number of gephyrin puncta at the soma increased between P4 and P11 by roughly 171% (P4 51 +/- 9; P11 139 +/- 31; Fig. 6A, p = 0.0221 Mann-Whitney). The size of the cell body also increases during this period, but not

enough to compensate for the increase in number of gephyrin-positive puncta. Thus, the density of gephyrin puncta in the somata also increased between P4 and P11, by about 125%, although this change did not quite reach statistical significance (P4 0.0675 puncta/μm^2, P11 0.1539 puncta/μm^2 Fig. 6B, $p = 0.0592$, Mann-Whitney).

The images acquired at P4 and P11 suggest a dramatic change in location of inhibitory synaptic proteins that could be caused by changes in dendritic morphology and/or a re-distribution of inhibitory synapses toward the soma. We therefore analyzed the distribution of gephyrin along the dendrites of LSO bipolar principal cells. We identified gephyrin puncta using Imaris (Bitplane) and measured their distance along the dendrite from the cell body (for details see Methods and Fig. 4). The linear density of gephyrin puncta along the dendrites was measured in 10 µm segments for P4 and P11 neurons. At P4, gephyrin was distributed rather evenly for the first 90 µm (Fig. 5A', 7). By contrast, at P11 the density of gephyrin was highest in the most proximal portions of the dendrites then steadily declined with increasing distance from the soma (Fig. 5B', 7).

The population effect is seen in the mean linear density of gephyrin along the dendrites of P4 and P11 cells. The mean linear density of gephyrin puncta within 25 µm from the cell body increased by 90% between P4 and P11 (P4 3.73 puncta/μm^2, P11 7.00 puncta/μm^2, Fig. 8). Mean linear densities of gephyrin puncta remained roughly similar for segments 25-50 µm and 50-75 µm from the cell body, but decreased between P4 and P11 from 75 µm and more distally (Fig.

8A). Cumulative frequency plots of the number of gephyrin puncta (normalized to the maximum distance of a punctum on that cell) for each cell clearly point to a salient difference between P4 and P11 cells: the majority of gephyrin puncta are found proximal to the cell body at P11 (Fig. 9).

The distribution of gephyrin along the dendritic arbor of two of the four P4 cells appeared similar to that of the P11 cells; that is gephyrin density was highest along proximal regions and gradually decreased at more distal regions Fig. 7C, 7D, 9C, and 9D). The two P4 cells that showed the P11-like distribution are shown in Fig. 1F and 1H and again in Fig. 10B and 10D. This discrepancy could be related to the sample of dendrites and gephyrin puncta in these two P4 cells. The total length of dendrite, the total number of traced segments, and number of puncta analyzed in these two P4 cells (shown in 7C, 7D) were less than those same values for the two P4 cells which showed a more diffuse distribution of gephyrin (7A, 7B, see Table 2 for measurements of each cell).

In the cell shown in Fig. 7D, only a few processes could be traced (shown in Fig. 10B) as the remaining dendrite portions were in a different tissue section, resulting in an incomplete sample of dendrites and puncta. Some of these traced dendrites were proximal, very few were distal so it is not surprising that the distribution of gephyrin puncta in this cell is different from the distribution from cells that were more fully reconstructed. The reason for the small sample for the cell in 7C was that, relative to P4 cells, the dendritic arbor was less complex and it was smaller, especially in the Z-dimension (Fig. 10D).

In conclusion, between P4 and P11 the density of gephyrin puncta increases at soma and proximal dendrites but not at distal dendrites.

Morphological refinement

Dendritic integration is influenced not only by the location of synapses but also by dendritic morphology. Thus, we examined changes in the overall complexity, size, and shape of LSO bipolar principal cell dendritic arbors between P4 and P11.

A standard measure for morphological complexity of dendritic arbors is 3-D Sholl analysis. Sholl analysis of the cells analyzed here showed a difference in the number of Sholl intersections within the first 40 μm of the cell body but little difference beyond 40 μm from the cell body (Fig. 11). Between P4 and P11, there was a significant reduction in the average number of intersections between 5-30 μm from the cell body (Fig. 12A, 10 μm; $p = 0.0325$, 15 μm; $p = 0.0195$, 20 μm; $p = 0.0065$, 25 μm; $p = 0.0173$, Mann-Whitney). Between P4 and P11, the number of intersections decreased by 60% between 5-20 μm, 30% between 25-40 μm but beyond 40 μm the number of intersections was similar (Fig. 12B). Cumulative frequency plots illustrate the reduction in the number of intersections especially between 5-40 μm in the P11 versus the P4 cells (Fig. 13).

Changes in dendritic morphology could be accompanied by changes in complexity, in shape, and in overall extent. To determine whether there were changes in overall extent of the dendritic arbors between P4 and P11, we

measured the cross-sectional area of the dendritic arbor of each cell (projected onto the coronal plane) and found that it slightly decreased between P4 and P11 (Fig. 14C). The size of the LSO also increases between P4 and P11 (see scaled schematic in Fig. 14), and the reduction in overall extent of the dendritic arbor was seen to be even more dramatic after the absolute cross-sectional area was normalized to the size of the LSO at each age. Between P4 and P11, the proportion of the LSO cross-sectional area covered by a single cell's dendritic arbor was reduced by 48% (Fig. 14D, $p = 0.0305$, Mann-Whitney).

Because the LSO is a tonotopic nucleus, and the long axes of the bipolar principal cells are generally oriented perpendicular to the tonotopic axis of the nucleus, one might expect the dendritic fields to show increasing anisotropy if morphological changes caused the cells to become physically restricted to a single isofrequency band. Therefore, we asked whether the reductions in the cells complexity and overall coverage were related to a change in shape of the dendritic field. On average, anisotropy increased between P4 and P11, with P11 neurons becoming narrower along the tonotopic axis (length of dendritic field/width of dendritic field P4 4.5, P11 7.4, Fig. 15, $p = 0.0205$, Mann-Whitney).

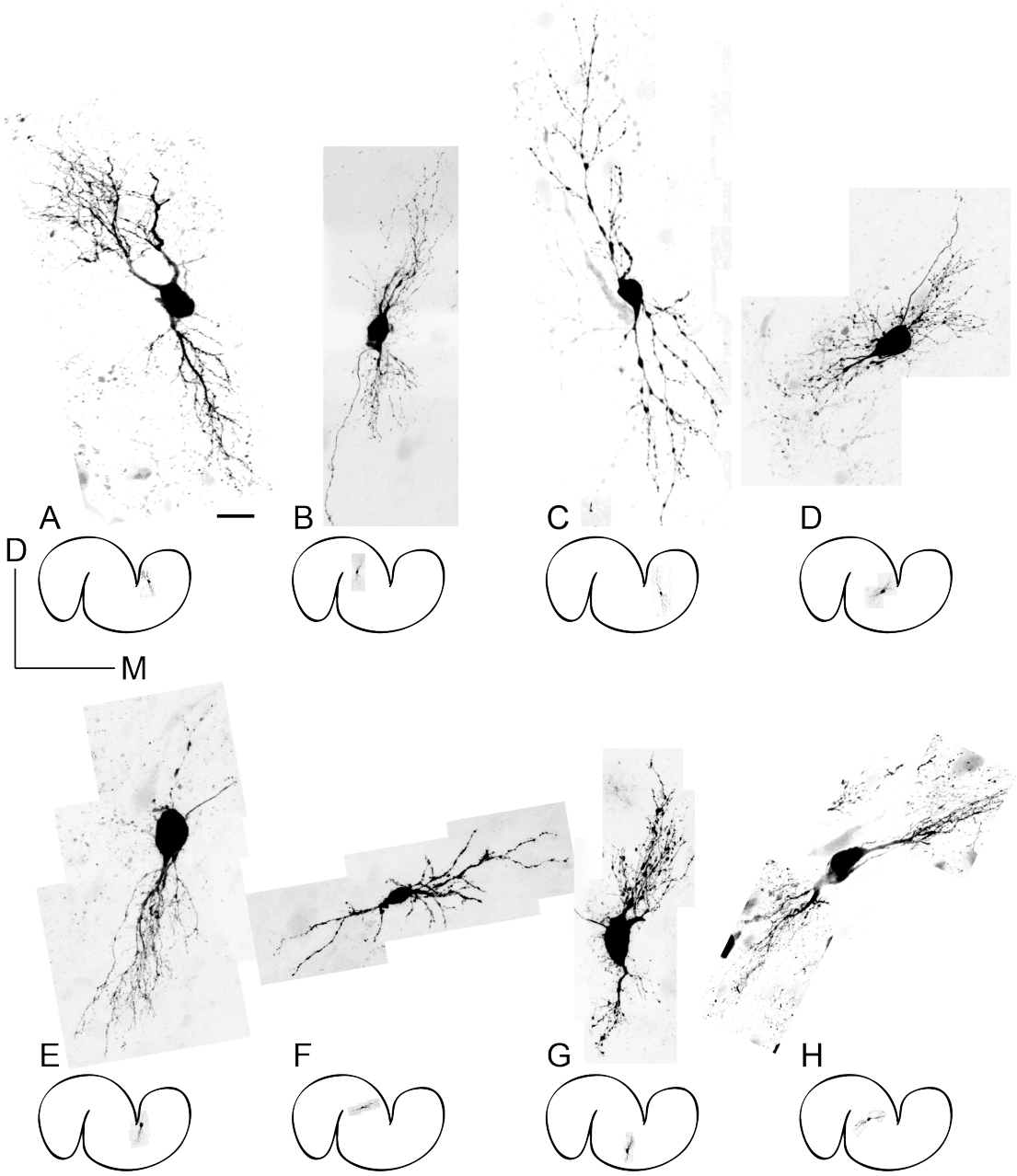
A
B
C
D
D
M
E
F
G
H

Figure 1. A-H: Examples of bipolar principal cells of the LSO filled with Lucifer Yellow from P4 animals. Each image is a Z-projection of a stack of serial optical sections acquired at a confocal microscope. Adjacent stacks of images were then stitched together to display the entire cell. Below each cell is a schematic of the location of the cell in the LSO. D, dorsal; M, medial. Scale bar = 20 μm applies to all reconstructed neurons, not the schematics of their location.

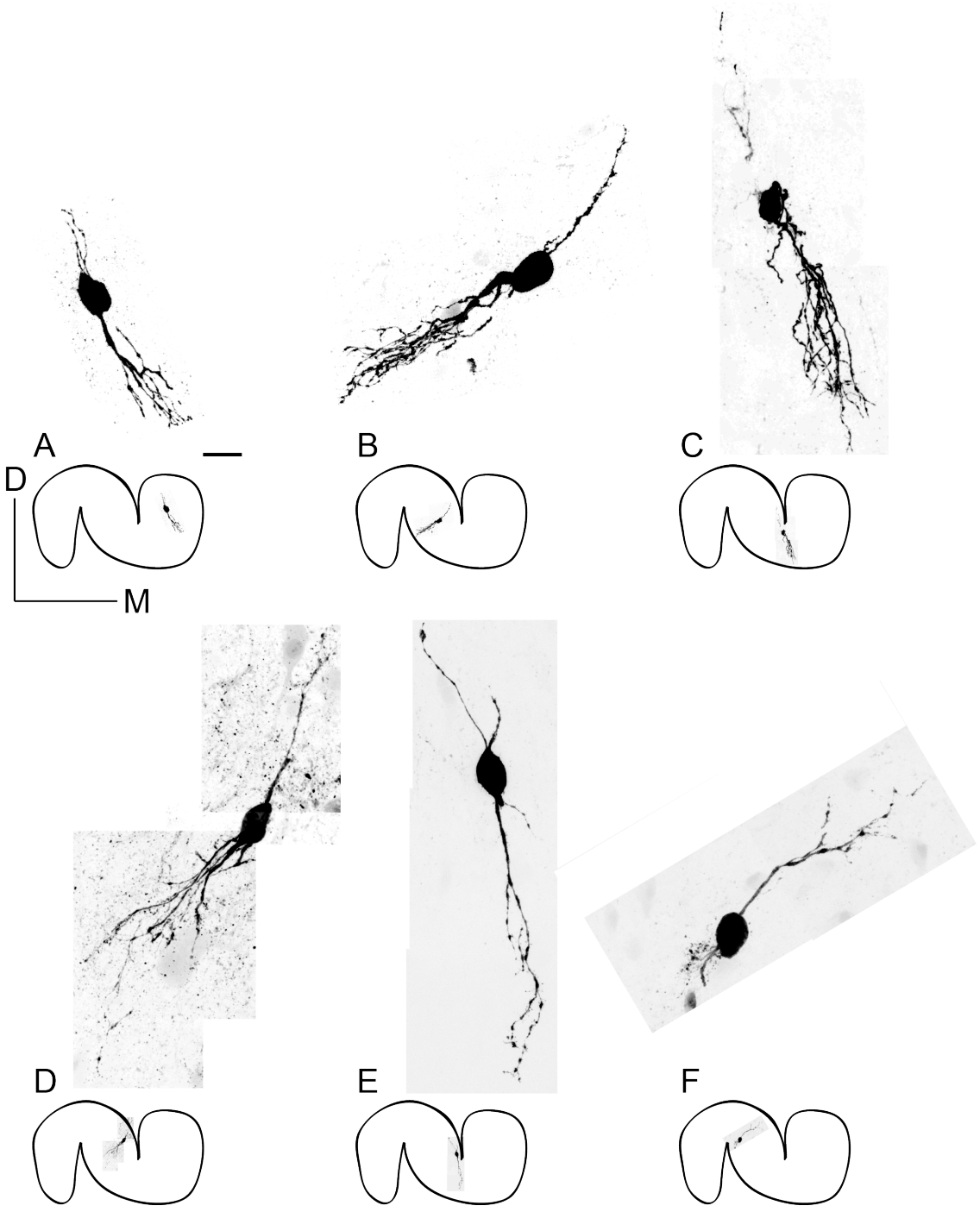
A
B
C
D
M
D
E
F

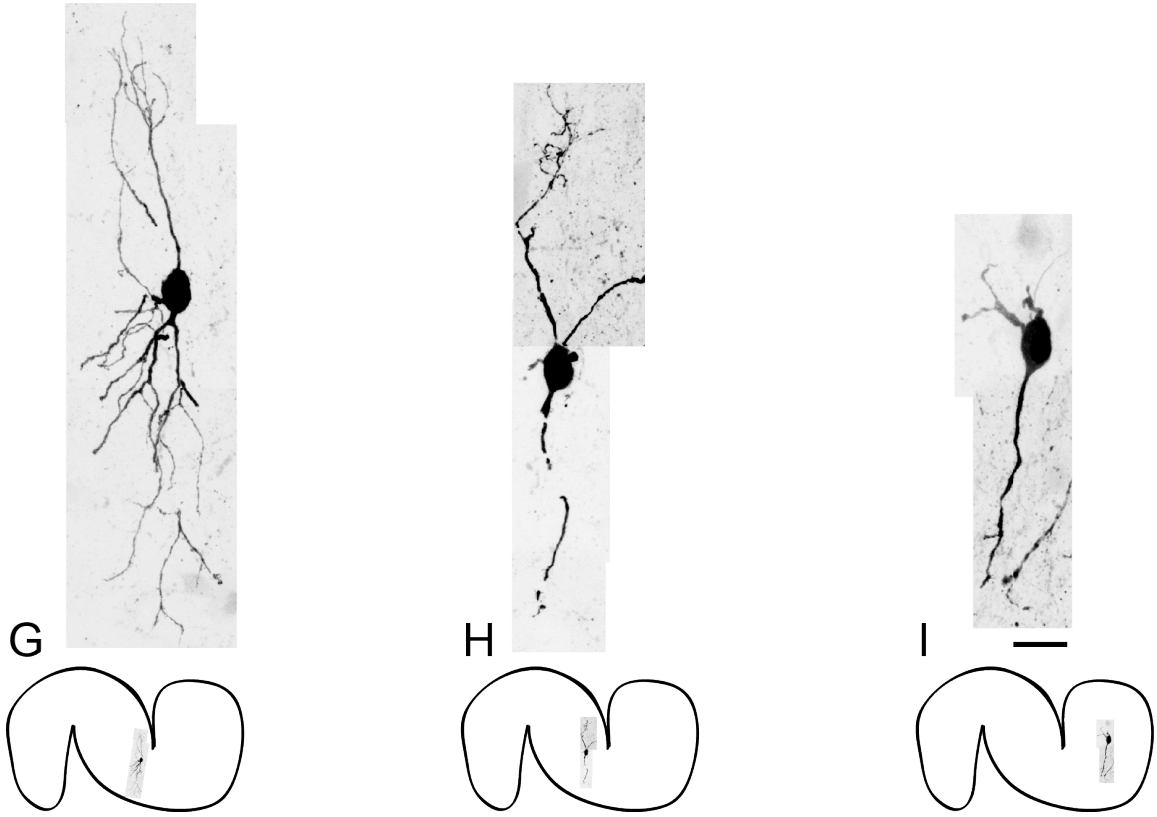

Figure 2. **A-I:** Examples of bipolar principal cells of the LSO filled with Lucifer Yellow from P11 animals. Each image is a Z-projection of a stack of serial optical sections acquired at a confocal microscope. Adjacent stacks of images were then stitched together to display the entire cell. Below each cell is a schematic of the location of the cell in the LSO. D, dorsal; M, medial. Scale bar = 20 μm applies to all reconstructed neurons, not the schematics of their location.

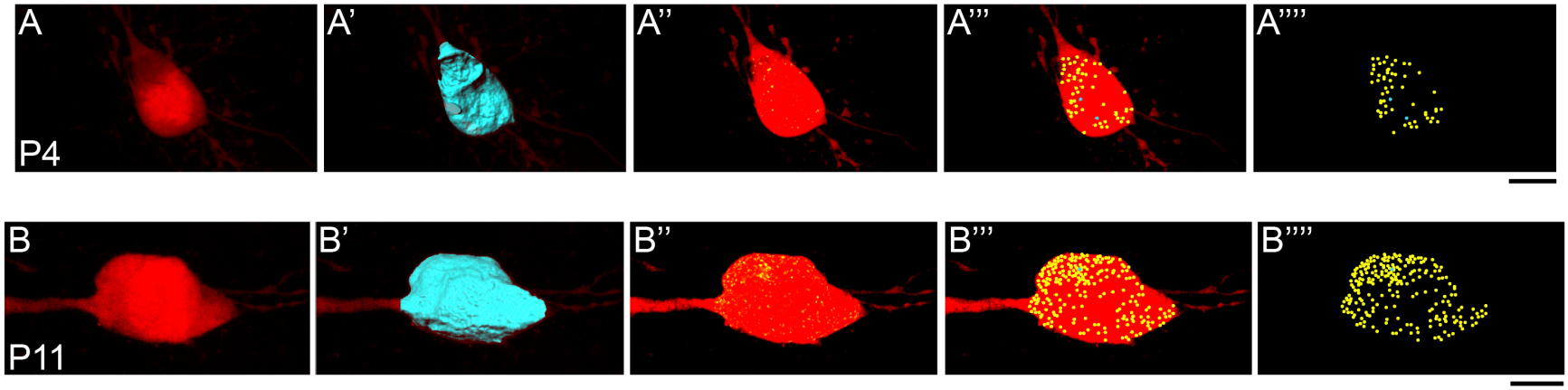

Figure 3. Identification of gephyrin puncta at the cell body. **A:** The soma of a P4 bipolar principal cell filled with Lucifer Yellow (red). **A':** A Surface (blue) is created around the cell body in Imaris (Bitplane). **A'':** Gephyrin puncta inside the Surface become a new channel – "Masked Gephyrin". Gephyrin puncta outside the Surface are excluded from further analysis. **A''':** "Masked Gephyrin" puncta are rendered as Spots using Imaris and can be quantified. **A'''':** Gephyrin Spots located within 1.00 µm of the Surface are coloured yellow and the Spots located beyond 1.00 µm of the Surface are coloured blue. The blue, intracellular Spots are excluded from analysis. **B-B'''':** The same gephyrin puncta identification procedure as outlined above for a P11 cell. Scale bars = 10 µm.

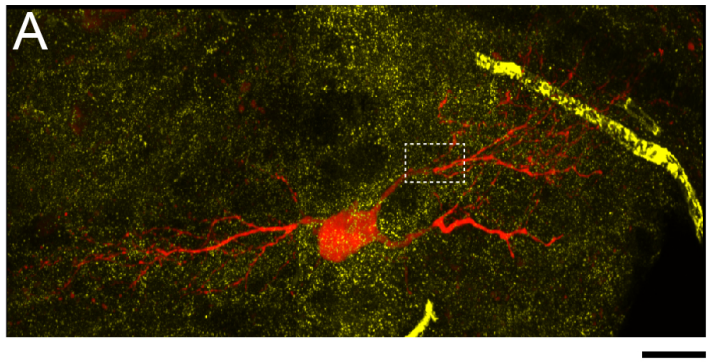
A

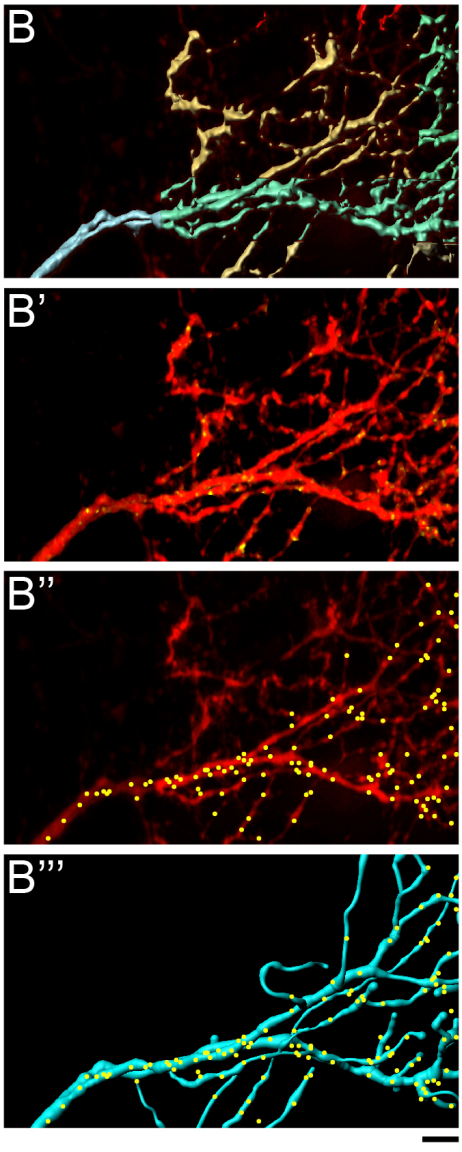
B
B'
B''
B'''

Figure 4. Identification and quantification of gephyrin puncta along the dendrites. **A:** A Z-projection of a cell labeled with Lucifer Yellow (red) and gephyrin immunolabelling (yellow) in P4 tissue. A region of interest inside the box is analyzed below. Scale bar = 20 μm. **B:** Many Surfaces (Bitplane) are created along the dendrites to isolate gephyrin puncta along the dendrite. **B':** Gephyrin puncta (yellow) inside the Surfaces are created into a new channel - "Masked Gephyrin". **B'':** Gephyrin puncta are then rendered as Spots (yellow) and their location along the dendrite can now be measured. **B''':** Spots (yellow) shown with dendrites (blue) that have been traced in Filament Tracer. The distance of a Spot to the soma was measured by measuring the distance of the Spot along the Filament from the cell body. Scale bar = 5 μm, applies to B-B'''.

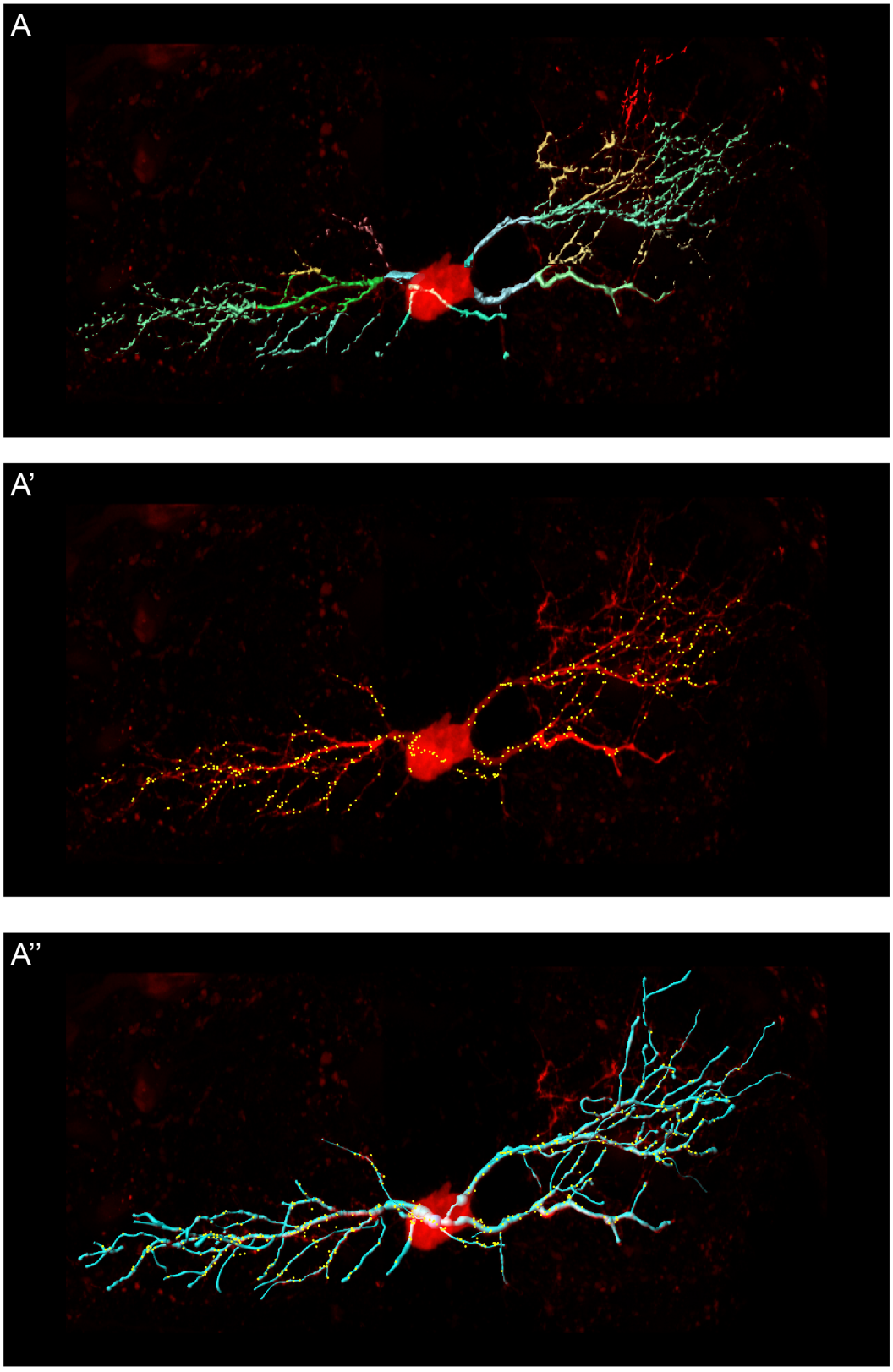
A
A'
A''

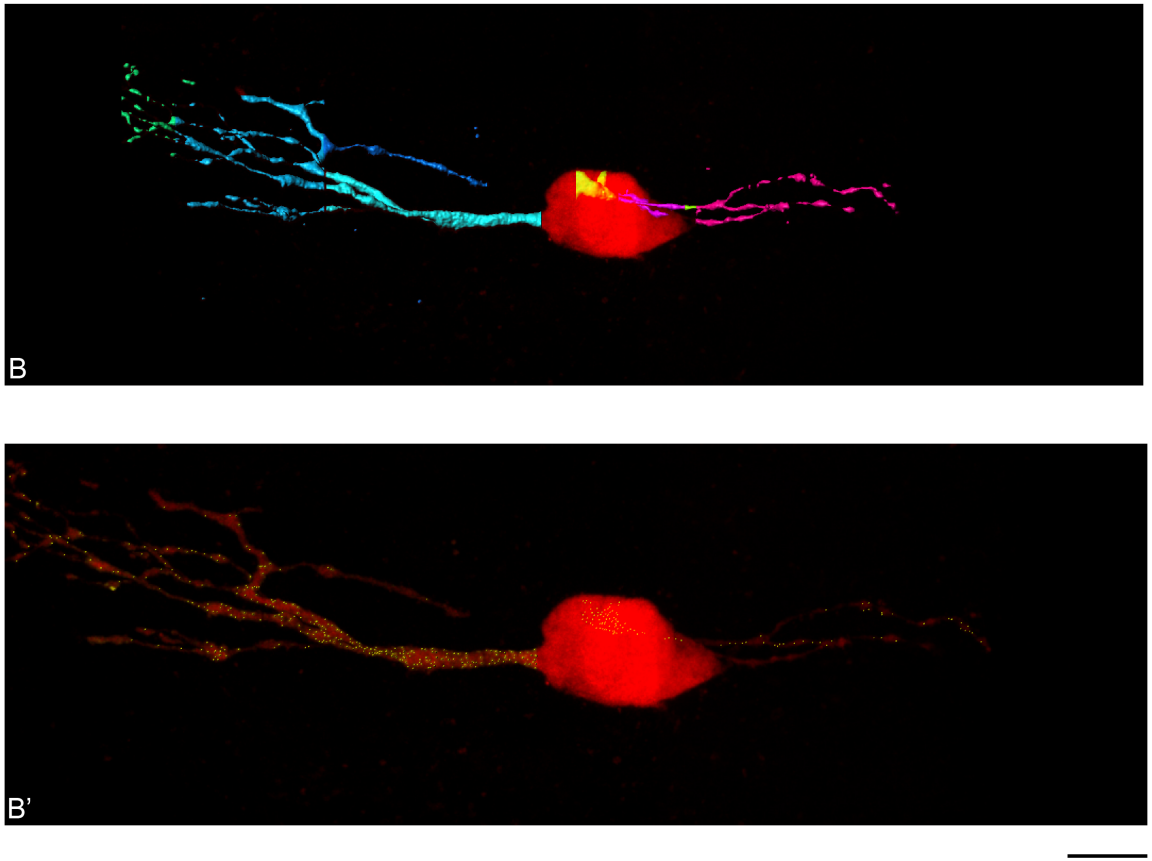

Figure 5. Examples of gephyrin puncta identified as Spots along the dendritic arbors of cells traced in Filament Tracer.

A: An image showing a P4 cell covered with Surfaces to isolate the gephyrin puncta along the dendritic tree. **A':** An image showing the cell with all isolated gephyrin puncta converted to Spots (yellow). **A'':** An image showing the cell with its gephyrin puncta identified by Spots and the dendrites traced in Filament Tracer. Scale bar = 20 μm (applies to A-A"). **B:** An image of all the Surfaces used to mask gephyrin in a sample P11 cell. **B':** An image showing the cell (red) and all of its gephyrin puncta identified as Spots (yellow). Scale bar = 15 μm applies to B, B'.

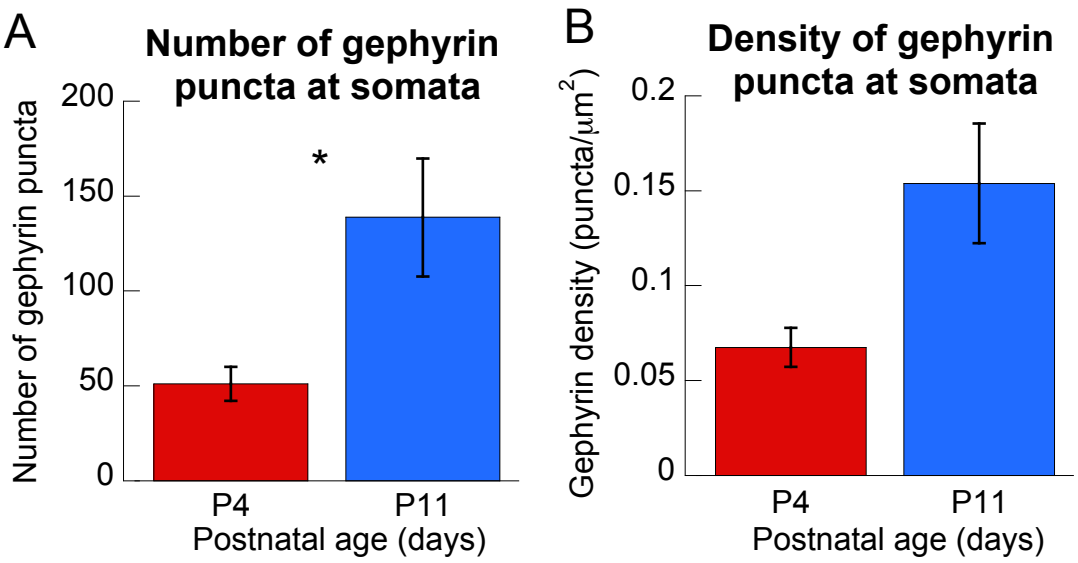

Figure 6. The number and density of gephyrin puncta at the somata at P4 and P11. **A:** The average number of gephyrin puncta within 1 μm of the Surface created on the somata of LSO bipolar principal cells increases from 50 at P4 to 140 at P11, an increase of 171% ($p = 0.0221$, Mann-Whitney). * indicates p-value of <0.05. Error bars show the standard error of the mean (s.e.m.). **B:** The average density of gephyrin puncta within 1 μm of the Surface created around the somata of LSO bipolar principal cells increases from 0.0675 puncta/μm^2 at P4 to 0.1539 puncta/μm^2 at P11, an increase of 127% ($p = 0.0592$. Mann-Whitney). Error bars represent ± 1 s.e.m.

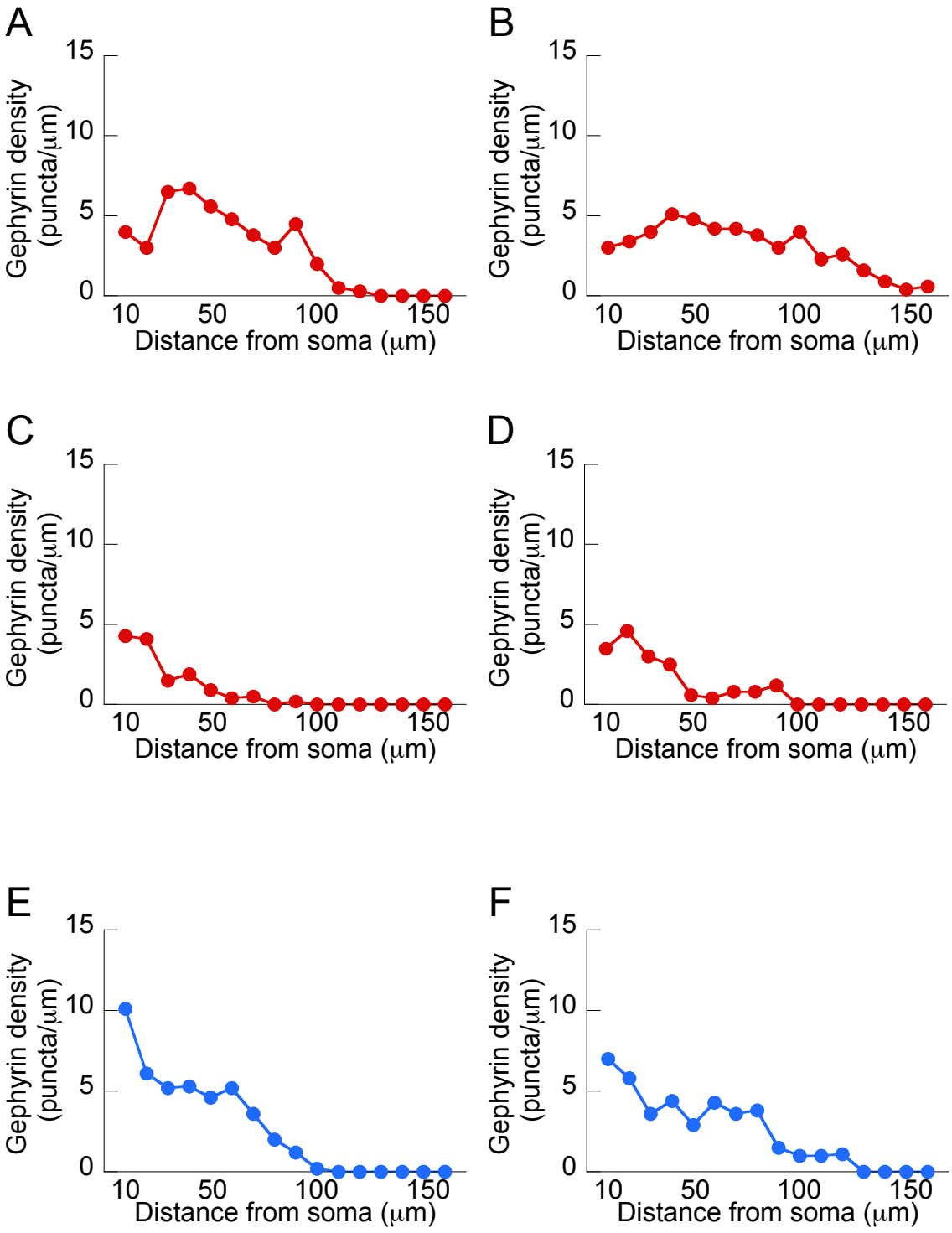
A
B
C
D
E
F
Gephyrin density (puncta/μm)
15
10
5
0
10
50
100
150
Distance from soma (μm)

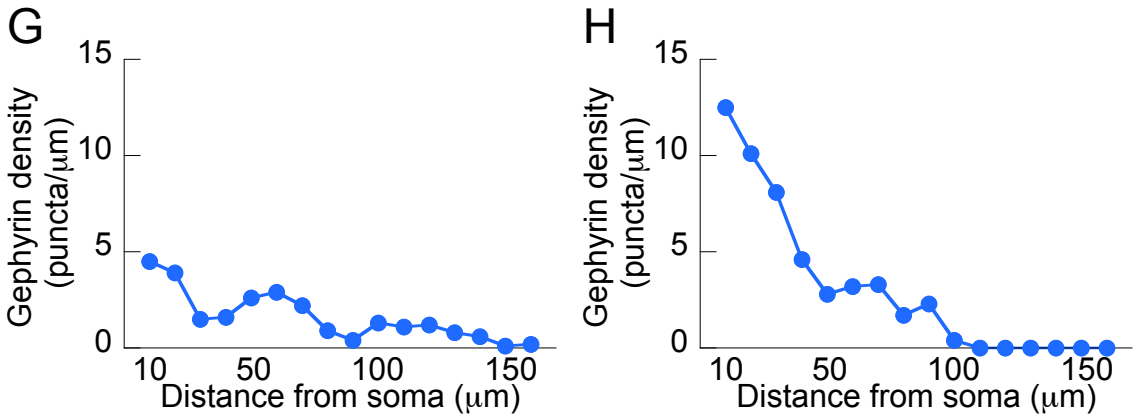

Figure 7. The linear density of gephyrin puncta along the dendrites of LSO bipolar principal cells at P4 (**A-D**, red) and P11 (**E-H**, blue). Gephyrin puncta are redistributed to more proximal dendrites between P4 and P11. The distance of each gephyrin punctum along the dendrites was measured and the value was placed in a 10 μm bin. A value of 0 μm refers to the edge of the cell body and beginning of the proximal dendrite. The linear density of gephyrin puncta along the dendrite is shown for each cell analyzed. At P4, gephyrin was distributed rather evenly along the dendrite for the first 90 μm. By contrast, at P11, the number of gephyrin puncta is highest near the somata and typically decreased steadily. The data correspond to cells shown in Figs. 1 and 2 as follows: Fig. 7A = Fig. 1A, Fig. 7B = Fig. 1C, Fig. 7C = Fig. 1F, Fig. 7D = Fig. 1H, Fig. 7E = Fig. 2A, Fig. 7F = Fig. 2B, Fig.7G = Fig. 2C, Fig. 7H = Fig. 2D.

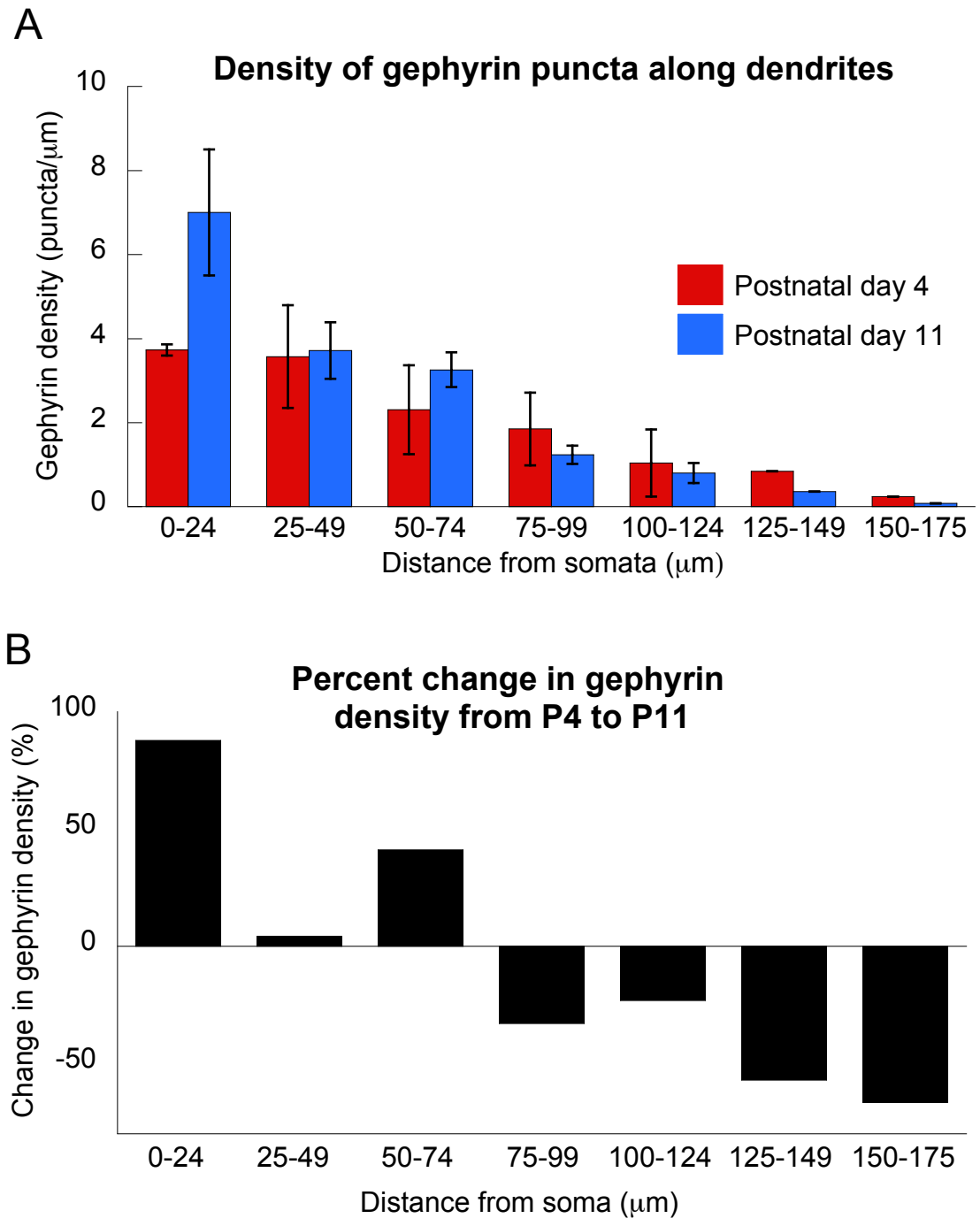

Figure 8. The average linear density of gephyrin within 25 μm of the soma is significantly higher at P11 than P4. **A:** The average density of gephyrin puncta along the dendrite in 25 μm segments at P4 and P11. The mean linear density of

gephyrin puncta within 25 µm from the cell body increased from 3.73 puncta/µm at P4 to 7.00 puncta/µm at P11. Error bars represent ± 1 s.e.m. **B:** Percent change in the average number of gephyrin puncta in 25 µm segments from P4 to P11. The average number of gephyrin puncta between 0-25 µm and 50-75 µm increased by 90% and by 40% from P4 to P11. Beyond 75 µm, the average density of gephyrin puncta consistently decreased (20-80%) from P4 to P11.

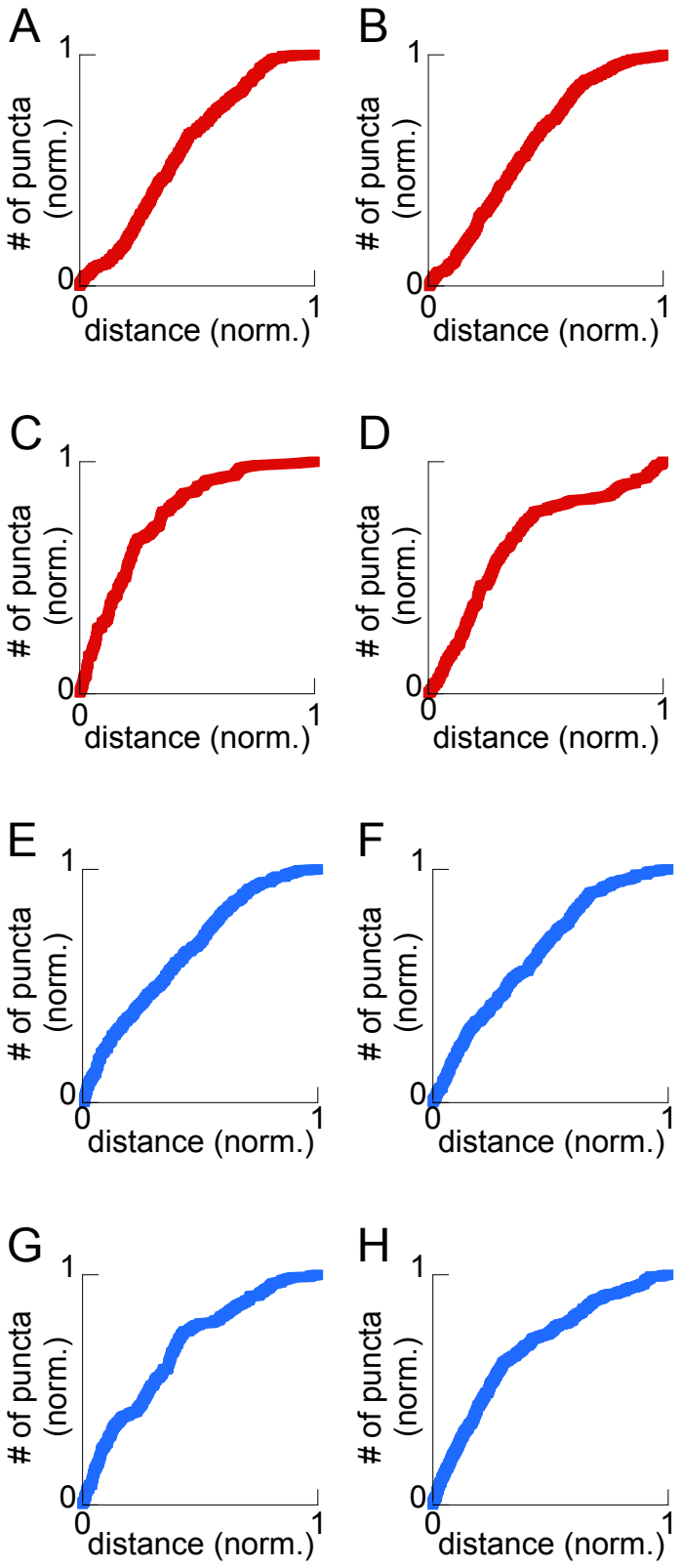
A
B
C
D
E
F
G
H
# of puncta (norm.)
distance (norm.)
0
1

Figure 9. Cumulative frequency plots showing the cumulative number of gephyrin puncta along the dendrites normalized to the maximum distance of a gephyrin punctum. **A-D:** P4 cells (red). **E-H:** P11 cells (blue). A plot is shown for each cell. The data correspond to cells shown in Figs. 1 and 2 as follows:

Fig. 9A = Fig. 1A, Fig. 9B = Fig. 1C, Fig. 9C = Fig. 1F, Fig. 9D = Fig. 1H,

Fig. 9E = Fig. 2A, Fig. 9F = Fig. 2B, Fig. 9G = Fig. 2C, Fig. 9H = Fig. 2D.

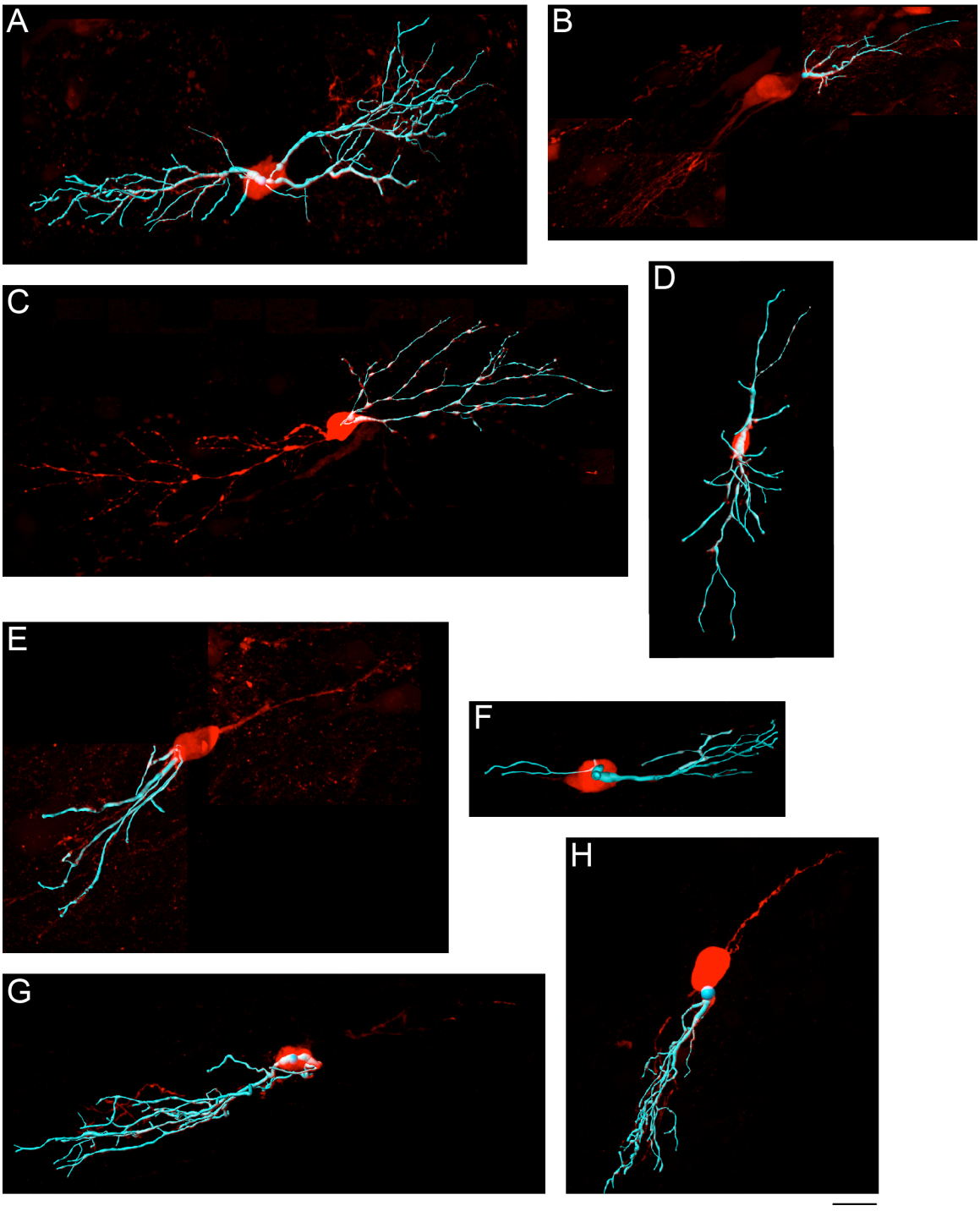

Figure 10. Filled LSO principal cells (red) traced with Filament Tracer (blue, Bitplane) for Three-dimensional Sholl analysis. **A-D:** Maximum projection images

of traced P4 cells. **E-H:** Maximum projection images of traced P11 cells. The filaments were analyzed with Sholl analysis. Sholl analysis was performed by counting the number of intersections between the traced filament and concentric spheres spaced 5 µm apart. The beginning point was the edge of the soma. Only those dendrites considered fully filled were analyzed (shown in blue). Scale bar = 20 µm.

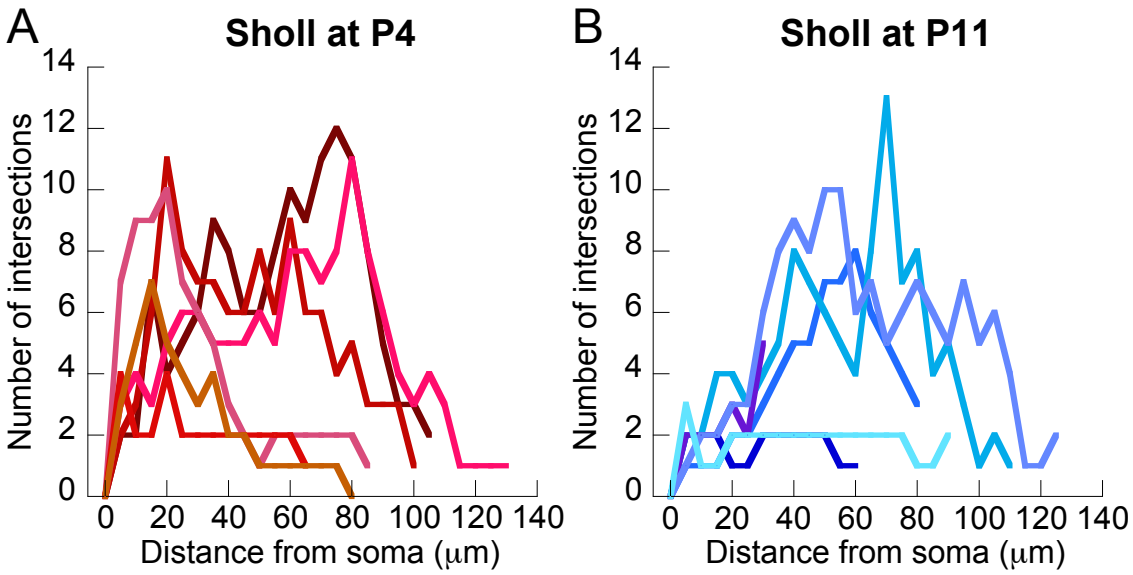

Figure 11. Results of the Sholl analysis showing the number of intersections between the traced cell and concentric spheres spaced at 5 µm intervals. Data from each analyzed dendrite are shown (**A**, P4; **B**, P11). These raw plots suggest that there are fewer intersections within the first 40 µm of the beginning point at P11 than P4.

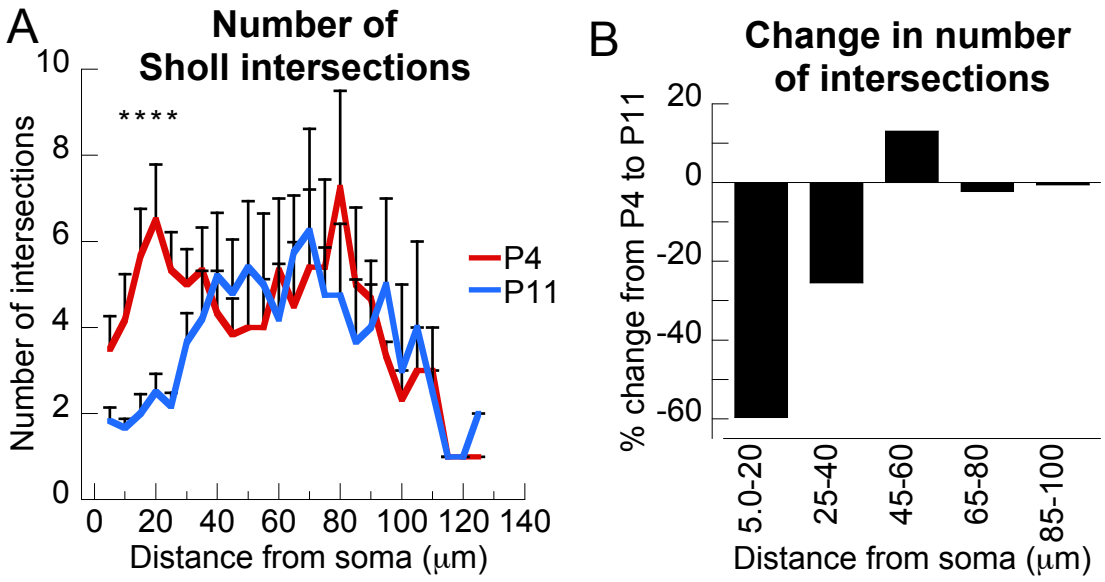

Figure 12. The average number of Sholl intersections near the somata decreases from P4 to P11. **A:** Within the first 35 μm of the beginning point, there are fewer Sholl intersections in P11 cells than P4 cells. Beyond 35 μm, there is overlap in the number of intersections at P4 and P11. (5 μm; p = 0.0801, 10 μm; p = 0.0325, 15 μm; p = 0.0195, 20 μm; p = 0.0065, 25 μm; p = 0.0173, 30 μm; p = 0.2294**,** Mann-Whitney). Error bars represent 1 s.e.m. * indicates p-value <0.05. **B:** Percent change in the average number of intersections (in 20 μm bins) between P4 and P11. There was a 60% reduction in the number of intersections between 0-20 μm from P4 to P11 and a 30% reduction in the number of intersections between 25-40 μm from P4 to P11.

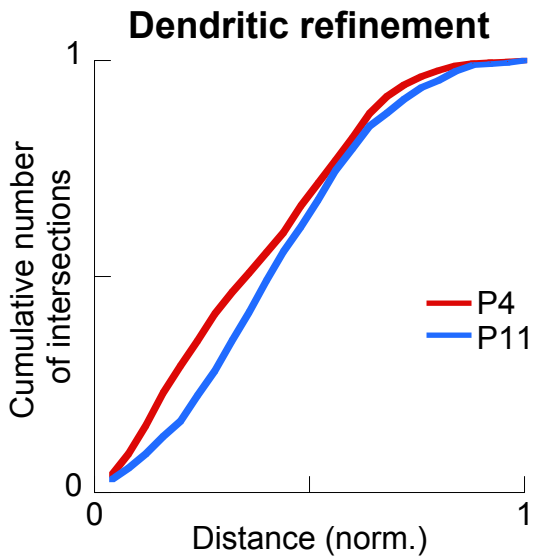

Figure 13. The ontogenic refinement in the dendritic trees is also seen in cumulative frequency plots. Cumulative frequency of the number of Sholl intersections at P4 and P11 plotted against the distance of the Sholl sphere from the cell body normalized to the maximum Sholl diameter.

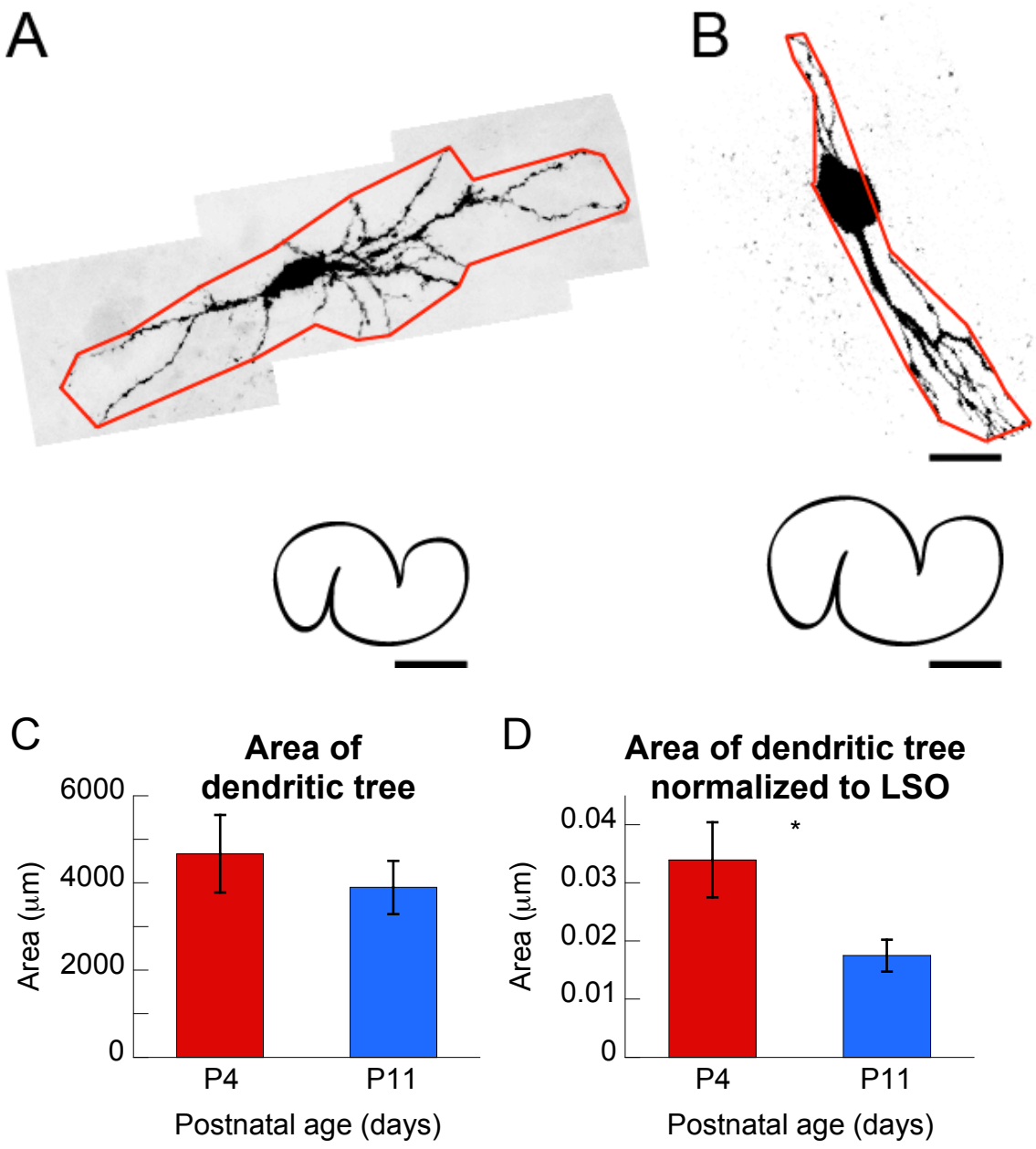

Figure 14. The areal coverage of the dendritic field of bipolar principal cells in the LSO decreases from P4 to P11. **A, B:** The size of the dendritic field was determined by connecting all the endpoints with a line and measuring the area within the boundary. Then the size of the dendritic field was normalized to the

average size of the LSO at P4 or P11. Example measurements of dendritic area are shown for a P4 (A) and P11 (B) cells. Below each cell is a schematic of the LSO scaled to each other. The area of the LSO is about 2.5x larger at P11 than at P4. Scale bar directly below cell = 20 μm (applies to A and B), scale bar below LSO schematic = 100 μm (applies to LSO schemata). **C:** The average size of the dendritic field decreases slightly from P4 to P11. Error bars represent ± 1 s.e.m. **D:** The average size of the dendritic field normalized to the cross sectional area of the LSO decreases by a factor of 2 from P4 to P11 ($p = 0.0305$, Mann-Whitney test). Error bars represent ± 1 s.e.m. * indicates p-value <0.05.

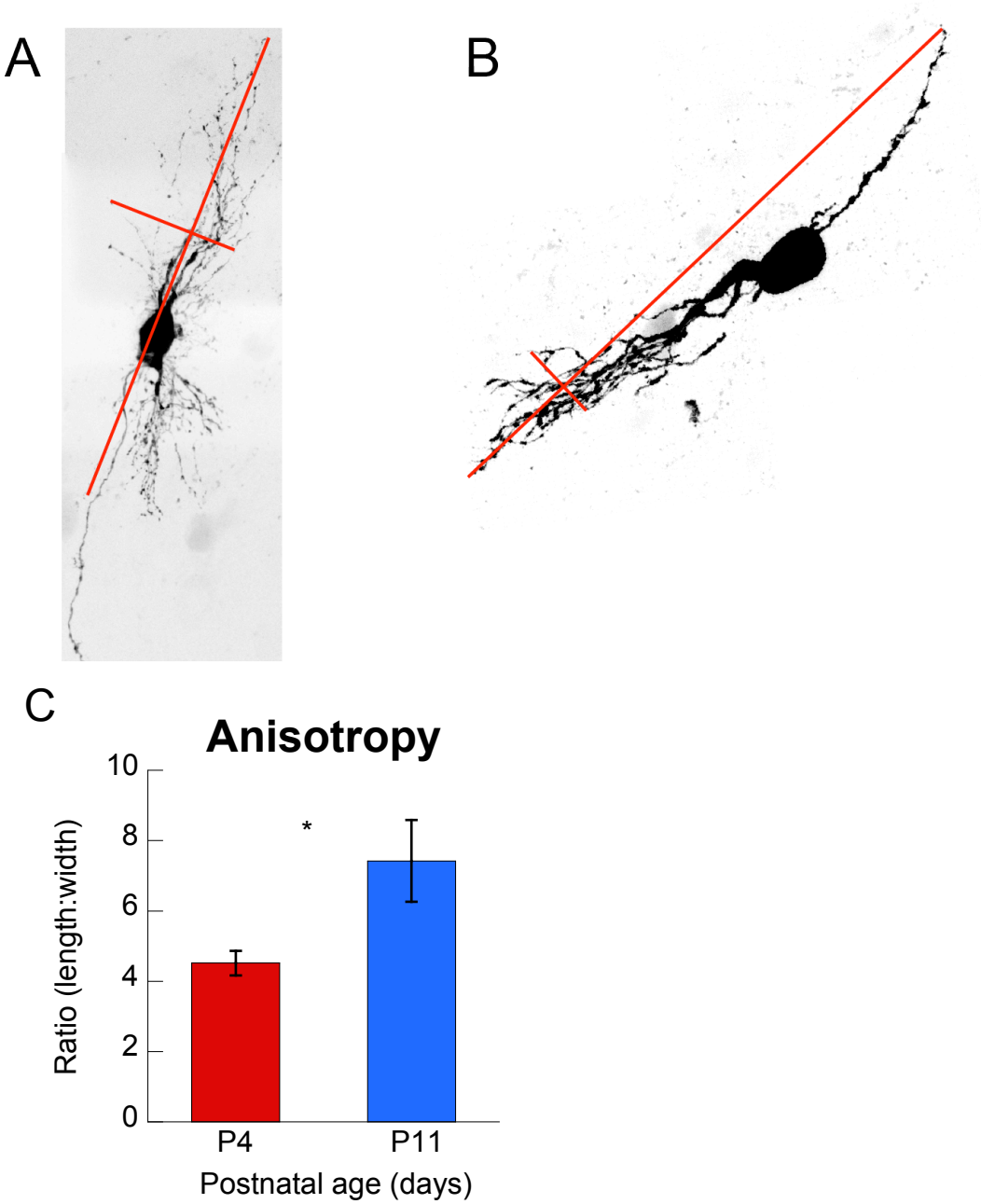

Figure 15. Anisotropy of LSO bipolar principal neurons at P4 and P11.

A, B: Images showing the 2-D projection of a cell in a coronal section and the lines used to measure anisotropy. A, P4; B, P11. Anisotropy was measured by measuring the length of a line along the long axis of the dendritic field and

dividing that value by the length of a perpendicular line drawn along the widest point of the dendritic field. **C:** The shape of the cells become more anisotropic from P4 to P11 ($p = 0.0205$, Mann-Whitney). Error bars represent ± 1 s.e.m. * indicates p-value<0.05.

Discussion

We examined the distribution of gephyrin along individual LSO bipolar principal cells at two ages before hearing onset. We found that from postnatal day 4 to P11, the number and density of gephyrin puncta at the soma increases significantly and that gephyrin puncta along the dendrites underwent significant re-distribution toward proximal dendrites. We also analyzed the morphology of the dendritic tree at P4 and P11 and found that dendritic complexity was developmentally reduced within the first 30 µm of the cell body but not more distally.

*Caveat*s

Here, we analyzed cells in 3-D by reconstructing serial optical sections obtained at a confocal microscope. It is known that resolution and brightness deteriorate when imaging deeper than 10 µm in the tissue and the principal cause is the mismatch of refractive indices between the objective lens, coverslip, mounting medium, and tissue (Pawley 1995, Staudt et al 2007). In order to counteract this problem and obtain clear images throughout the section, we used

a high refractive index (RI = 1.52) mounting medium that matches the refractive index of the lens and coverslip.

Cell fills were sometimes incomplete such that one set of branches (eg. dorsal or ventral arbor) was completely filled but the other set was not. This could have been a result of dendrites being cut off at the time the slice was taken (before the cell fill) or a result of the filled cell being sectioned on the freezing microtome. It would have been problematic to analyze completely filled and incompletely filled branches together using Sholl analysis, as the incompletely filled arbor does not accurately represent the complexity of the dendritic tree. Therefore, we divided the arbors of each cell in two (eg. dorsal and ventral arbors) and only analyzed arbors that were completely filled.

The dye, Lucifer Yellow, we used to fill cells has a very broad emission spectrum (peak emission 536 nm, emission spectrum 480-700 nm) that could excite and photobleach the Alexa 647 dye attached to the gephyrin antibodies as a result of Förster resonance energy transfer (FRET). The net result of this photobleaching would be an underestimation of the total number of gephyrin immunoreactive puncta. FRET would be most likely to occur where Lucifer Yellow was most concentrated, ie. in the cell bodies and proximal dendrites. This would result in an underestimation of gephyrin at the cell body and proximal dendrite. However, this underestimation should be equivalent in both P4 and P11 cells and therefore not contribute to any of the developmental trends we report.

Anatomical refinement occurs before hearing onset

We know that there is significant functional and structural refinement in the LSO during the first three postnatal weeks but until now we have not had a detailed view of where inhibitory synapses are located along reconstructed bipolar principal cells. We found an increase in the density of gephyrin puncta along proximal dendrites and the somata in the week preceding hearing onset (see Fig. 16). This re-distribution follows the functional refinement of the MNTB-LSO pathway and could rely on patterned spontaneous activity generated in the cochlea (Kim and Kandler, 2003, Tritsch et al, 2007, Tritsch and Bergles, 2010). Our results are in agreement with previous studies that show a high concentration of inhibitory synapses around cell bodies and proximal dendrites in the LSO (Helfert et al, 1992, Friauf et al, 1997, Korada and Schwartz, 1999). Although some of these studies suggest that a re-distribution of inhibitory synapses occurs around hearing onset (Friauf et al, 1997, Korada and Schwartz, 1999), our study is an important advance because we identified the cell type and we reconstructed cells to yield a detailed analysis of synapse location. Previous studies have used on glycine receptor immunoreactivity as a marker of inhibitory synapses in the developing LSO (Friauf et al, 1997). We now know that GABA is more prevalent than glycine in the developing MNTB-LSO pathway (Kotak et al, 1998), therefore we used the inhibitory synaptic marker gephyrin, which is found at both GABAergic and glycinergic synapses in order to simultaneously quantify all inhibitory inputs from the MNTB.

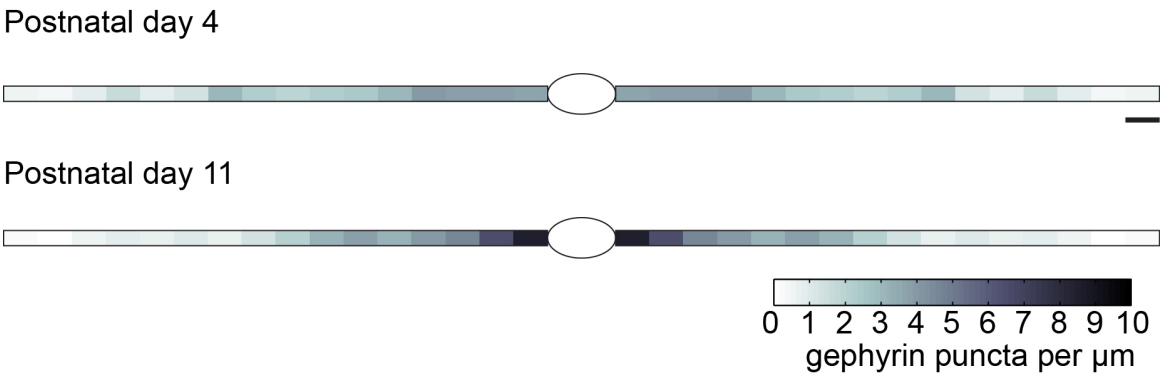

Figure 16. A schematic showing the average linear density of inhibitory synapses in the dendritic tree of LSO bipolar principal cells at P4 and P11. Gephyrin density is calculated for each 10 µm segment from 0 to 160 µm from the cell body. Gephyrin density increases on proximal dendrites between P4 and P11. Scale bar 10 µm.

Anatomical refinement of MNTB projections to MSO and LSO

Many studies have shown anatomical refinement in MNTB-MSO and MNTB-LSO projections in the weeks following hearing onset, suggesting that auditory experience drives these changes. Our results suggest that anatomical refinement begins in the absence of auditory experience. First let us consider what we know about MNTB projections.

Our results contrast with the timeline of refinement of inhibitory projections to the MSO, where both proximal re-distribution of inhibitory inputs and refinement of individual MNTB projections require acoustical information (Kapfer et al, 2003, Werthat et al, 2008). The current thinking in the field is that MNTB-

LSO projections do not undergo anatomical pruning until after hearing onset. After hearing onset, the number of terminal boutons and the spread of the boutons decrease, but these measures were not made in pre-hearing animals (Sanes and Siverls, 1991). So, perhaps MNTB projections to the LSO are pruned before hearing onset, but it has yet to be measured. The measures we have from younger animals indicate that the arbors continue to grow from P2 to P10 (increases in total length, branchpoints, and fiber area) (Sanes and Siverls, 1991). So, it remains unknown if the pruning of MNTB axons projecting to the LSO occurs concurrently with the proximal re-distribution of gephyrin (ie. before hearing onset). It is important to note that the studies of the morphology of the MNTB-LSO refinement were performed in gerbil whereas our study was performed in rat, and the timeline of anatomical refinement could differ between these species.

Anatomical refinement of LSO principal cells

Similar to our current knowledge of MNTB axonal refinement, most studies of LSO cell dendritic morphological show significant refinement following hearing onset. However, some of these studies did not look at the first two postnatal weeks. A more recent, detailed analysis of labeled cells in the LSO starting at P4 found that some anatomical changes do occur before hearing onset (Rietzel and Friauf 1998). Rietzel and Friauf (1998) found a decrease in the number of primary dendrites and a significant decrease in the number of dendritic endpoints during

the first two postnatal weeks. The decrease in the number of primary dendrites is consistent with our observation that there are fewer Sholl intersections within the first 30 μm of the cell body. Our studies are also in agreement in that we both found that LSO bipolar principal cells occupy a proportionately smaller area in the LSO from P4 to P11 and that dendritic trees change shape to become more narrow and restricted to an isofrequency band before hearing onset.

Future Questions

How can we account for the re-distribution of gephyrin toward the cell body? There are three non-mutually exclusive processes that could contribute to the proximal re-distribution of inhibitory inputs to LSO neurons.

First, the inhibitory synapses on distal dendrites could be selectively pruned. The deletion of a synapse can be a result of the retraction or pruning of an axon (Ruthazer et al, 2006). In the MSO, the proximal re-distribution of inhibitory synapses is concurrent with the selective pruning to MNTB projections to distal dendrites (Kapfer et al, 2002, Werthat et al, 2008). In the MNTB-LSO pathway, it is likely that some of the re-distribution of inhibitory synapses in the LSO is a result of distal synapses being deleted and distally projecting axons being retracted given the refinement in the spread of the axonal projections (Sanes and Siverls, 1991).

Second, the inhibitory synapses could be physically redistributed along the cell to more proximal regions. Inhibitory synapses can translocate along the cell

membrane via lateral diffusion (Meier et al 2001). Gephyrin puncta, along with their presynaptic counterparts, can move up to 5 μm per day in cultured cells (Dobie and Craig, 2011). It remains to be seen if lateral diffusion could account for the proximal re-distribution of inhibitory synapses along LSO neurons.

Third, proximal inhibitory synapses could be maintained or even added over development. We observed a 3.5-fold increase in the number of gephyrin puncta at the soma from P4 to P11, suggesting that new synapses are added or more gephyrin is added to each synapse over development.

In order to elucidate the relative contributions of synapse elimination, synapse addition, and synapse translocation, future experiments could include time-lapse imaging in slice cultures which express different fluorescent proteins in the MNTB axon, the LSO principal cells, and inhibitory synapses.

Although we see significant refinement before hearing onset, we do not think that this is the mature distribution of inhibitory inputs. Knowing the mature distribution of inputs both excitatory and inhibitory will be very important for creating models of how these neurons compute ILDs.

Chapter 3: Synaptotagmins I and II in the Developing Rat Auditory Brainstem: Synaptotagmin I is Transiently Expressed in Glutamate-Releasing Immature Inhibitory Terminals

Publication Reference:

Cooper, AP & Gillespie DC. (2011). Synaptotagmins I and II in the Developing Rat Auditory Brainstem: Synaptotagmin I is Transiently Expressed in Glutamate-Releasing Immature Inhibitory Terminals. *The Journal of Comparative Neurology*, 519(12), 2417-2433.

Abstract

The lateral superior olive (LSO), a nucleus in the auditory brainstem, computes interaural intensity differences for sound localization by comparing converging excitatory and inhibitory inputs that carry tonotopically matched information from the two ears. Tonotopic refinement in the inhibitory projection pathway from the medial nucleus of the trapezoid body (MNTB) is known to be established during the first postnatal week in rats. During this period, immature MNTB terminals in the LSO contain vesicular transporters for both inhibitory and excitatory amino acids and release glutamate. The primary Ca^{2+} sensors for vesicular release in the CNS are understood to be synaptotagmins, and in adult auditory brainstem synaptotagmin 2 is the predominant synaptotagmin. We asked here whether a different Ca^{2+} sensor might be expressed in the immature

auditory brainstem. We have found that synaptotagmin 1 is indeed expressed transiently in the immature auditory brainstem, most highly in those areas that receive glutamate-releasing immature inhibitory inputs from the MNTB, and that during the first postnatal week synaptotagmin 1 co-localizes with the vesicular glutamate transporter VGLUT3, a marker of glutamate-releasing immature inhibitory terminals from the MNTB. We suggest that immature MNTB terminals may contain two populations of synaptic vesicles, one expressing the vesicular inhibitory amino acid transporter together with synaptotagmin 2 and another expressing VGLUT3 together with synaptotagmin 1. Because Ca^{2+} sensing is an important determinant of release properties for the presynaptic terminal, differential expression of the synaptotagmins might allow the differential release of excitatory and inhibitory neurotransmitters in response to differing patterns of neural activity.

Introduction

The superior olivary complex (SOC) of the auditory brainstem includes several nuclei with major roles in sound localization. In particular, the lateral superior olive (LSO) computes interaural intensity differences (Boudreau and Tsuchitani, 1968; Caird and Klinke, 1983) by comparing converging excitatory glutamatergic inputs from the ipsilateral ventral cochlear nucleus (Cant and Casseday, 1986; Wu and Kelly, 1992) and inhibitory glycinergic inputs from the ipsilateral medial nucleus of the trapezoid body (MNTB) (Moore and Caspary,

1983; Bledsoe et al., 1990; Caspary and Finlayson, 1991), which itself receives a glutamatergic projection from the contralateral anteroventral cochlear nucleus (AVCN) at the large excitatory calyx of Held synapse (Smith et al., 1991).

A critical advance in our understanding of this nucleus would be to decipher how these converging inputs of opposite sign achieve tonotopic precision and how they are brought into register with each other in the developing brain. Although some aspects of morphological and physiological maturation are known for the AVCN-LSO pathway (Kandler and Friauf, 1993, 1995), much more is known about development in the immature inhibitory input pathway. In the MNTB-LSO pathway, tonotopic precision is understood to be established through the activity-dependent functional refinement that occurs before hearing onset at postnatal day 12 (P12) and the structural refinement that occurs after hearing onset and is complete by P21 (Kandler and Friauf, 1993; Sanes and Takacs, 1993; Kotak and Sanes, 1995; Sanes and Friauf, 2000; Kim and Kandler, 2003).

Measurable functional refinement in the MNTB-LSO pathway occurs primarily between about P3 and P8, and although the mechanisms underlying this refinement remain unclear, several concurrent events have been implicated, including release of γ-aminobutyric acid (GABA) in the immature MNTB-LSO pathway (Kotak et al., 1998; Korada and Schwartz, 1999; Nabekura et al., 2004), depolarizing action of GABA/glycine (Kandler and Friauf, 1995; Ehrlich et al., 1999), and changes in expression of calcium binding proteins and neurotransmitter transporters (Henkel and Brunso-Bechtold, 1998; Friauf et al.,

1999). Glutamate release by immature MNTB terminals within the LSO has also been demonstrated (Gillespie et al., 2005), and is thought to be required for normal refinement of the MNTB-LSO pathway (Noh et al., 2010).

The phenomenon of glutamate release at immature inhibitory terminals has led to new hypotheses for developmental inhibitory refinement, and has also created new questions about whether GABA/glycine and glutamate share vesicle populations and/or release properties. Release of GABA and glycine is associated with the sole known vesicular transporter for GABA and glycine, the vesicular inhibitory amino acid transporter (VIAAT; also known as vesicular GABA transporter [VGAT]) (McIntire et al., 1997; Dumoulin et al., 1999). Glycine release by mature MNTB terminals (and GABA release in early postnatal life) is supported by expression of VIAAT throughout life, whereas glutamate release by immature MNTB terminals is supported by the transient early expression of vesicular glutamate transporter 3 (VGLUT3) (Blaesse et al., 2005; Gillespie et al., 2005).

In recent electrophysiological studies of immature MNTB-LSO synapses, our laboratory has found that GABA/glycine and glutamate responses have different paired-pulse ratios (Case and Gillespie, unpublished results). These paired-pulse ratios are used as indicators of ‘‘release probability,’’ the probability with which an action potential invading the axon terminal elicits calcium-dependent neurotransmitter release. One way in which different paired-pulse ratios for GABA/glycine and glutamate transmission at the same MNTB-LSO

synapses could occur is for GABA/glycine and glutamate to be packaged in different synaptic vesicles, with each group of synaptic vesicles associated with a different calcium- sensor.

The calcium sensors underlying synaptic vesicular release are generally understood to belong to the synaptotagmin (Syt) protein family (Fernandez-Chacon et al., 2001;Sudhof,2002). Several synaptotagmin isoforms have been described, but only three—Syt1, Syt2, and Syt9—appear to mediate fast, synchronous (i.e., tightly action-potential coupled), vesicular release at central synapses, where the expression of a specific Syt isoform determines such presynaptic properties as calcium dependence and transmitter release kinetics (Xu et al, 2007). Of these three isoforms, Syt9 is understood to be restricted to the basal ganglia and limbic system, whereas synaptotagmins 1 and 2 show generally complementary expression throughout the adult central nervous system (CNS). Syt2, which has the fastest kinetics, has been reported to be more highly expressed than Syt1 in the adult auditory brainstem (Fox and Sanes, 2007). Here we used immunohistochemistry to study expression patterns for the two synaptotagmins Syt1 and Syt2 during the period of SOC circuit refinement, at excitatory and inhibitory synapses, and to determine which synaptotagmin is associated with the glutamate-releasing immature inhibitory terminals of the MNTB-LSO pathway.

Materials and Methods

All experimental procedures involving animals were approved by McMaster University's Animal Research Ethics Board and conformed to guidelines outlined by the Canadian Council on Animal Care. The central experiments in this study were carried out in four litters of Sprague-Dawley rats, using pups at ages postnatal day 1 (P1), P5, P9, P13, P17, and P21. Four animals were used at each age except at P21, at which time only two animals were used. Animals were euthanized with sodium pentobarbitol (120 mg/kg) and perfused transcardially with 0.1 M phosphate-buffered saline (PBS; pH 7.4), followed by ice-cold 4% paraformaldehyde in 0.1 M phosphate buffer (PB; pH 7.4). Brains were postfixed in 4% paraformaldehyde for 3 hours before being transferred to 30% sucrose in 0.1 M PBS for cryoprotection.

Tissue processing and immunohistochemistry

Coronal sections containing the superior olivary complex (SOC) were cut at 40 µm on the freezing microtome and collected into 0.1 M PB (pH 7.4). Complete sets of brains from a given litter were cut, stained, and imaged at the same time for consistency within runs. Serial sections containing SOC were stained for one of eight conditions, each section being stained for either Syt1 or Syt2 and either VGLUT1, VGLUT2, VGLUT3, or VIAAT. Primary antibodies against Syt1 (mab 48) and Syt2 (Znp-1) were used to identify Syt1-positive and Syt2-positive terminals. Primary antibodies against the vesicular transporters

VGLUT1, VGLUT2, VGLUT3, and VIAAT were used to identify synaptic vesicle phenotype. Affinity-purified secondary antibodies conjugated to either Dylight (Jackson ImmunoResearch, West Grove, PA) or Alexa fluorophores (Invitrogen, Burlingame, CA) were used at a dilution of 1:500.

All immunohistochemistry was performed on free-floating sections at 4°C. Tissue sections were blocked for 12 hours in a serum solution containing 5% normal serum, 2.5% bovine serum albumin (BSA), and 0.5% Triton X-100 in PBS (pH 7.4). Sections were then incubated in primary antibodies (diluted in 5% normal serum, 2.5% BSA in 0.1 M PBS, pH 7.4) for 48 hours. After washes in PBS, sections were incubated in secondary antibodies diluted in a normal serum solution for 12 hours. Sections were washed in PBS before being mounted and coverslipped with Gelvatol.

Antibody characterization

Antibodies used in this study are listed in Table 1. The mab 48 antibody recognizes a single protein of ~65 kDa in rat brain synaptosomal preparation (Matthew et al., 1981) and the Znp-1 a ~60 kDa protein in mouse synaptosomal preparation (Fox and Sanes 2007). Fox and Sanes (2007) used several methods to show that mab 48 and Znp-1 selectively recognize Syt1 and Syt2. First, they showed that Znp-1 recognized proteins immunoprecipitated by Znp-1 but that Znp-1 did not recognize proteins immunoprecipitated by mab 48. Second, they showed that mab 48 recognized recombinant Syt1 but not recombinant Syt2 whereas Znp-1 recognized recombinant Syt2 but not recombinant Syt1.

The staining patterns for Syt1 and Syt2 in the MNTB seen here are nearly identical to those reported using the same antibodies (Fox and Sanes, 2007) and different antibodies (Pang et al., 2006). We also examined staining patterns for Syt1 and Syt2 in the hippocampus and cerebellum and found that our staining patterns matched those previously reported (Fox and Sanes, 2007).

The VGLUT1 antibody recognizes a ~60-kDa band on immunoblots from rat cerebral cortex (Melone et al., 2005). Preabsorption of the VGLUT1 antibody with the immunogen peptide (Millipore, Bedford, MA, cat. no. AG208) eliminates immunostaining (manufacturer's worksheet). No immunostaining was observed when this antibody was used on VGLUT1 knockout mouse retina (Johnson et al., 2007).

The VGLUT2 antibody recognizes a ~55-kDa band on immunoblots from rat astrocytic cultures and this staining disappears when the antibody is preincubated with the control antigen (Montana et al., 2004).
Preabsorption of the VGLUT3 antibody with the immunogen peptide (135-2P, Synaptic Systems, Goettingen, Germany) nearly eliminated immunostaining in rat auditory brainstem tissue (data not shown).

The VIAAT antibody recognizes double bands of ~50 and ~57 kDa in PC12 cells expressing rat VIAAT (Takamori et al., 2000), one of which is thought to be the phosphorylated VIAAT (Bedet et al., 2002); on immunoblots of rat enriched synaptic vesicle preparation, the VIAAT staining pattern is blocked by the immunogen (H. Martens, personal communication).

In postnatal rat tissue, immunostaining patterns for VGLUTs 1-3 and VIAAT were nearly identical, both in localization in the brain and in subcellular distribution, to those reported previously using antibodies prepared from different sources (Gras et al., 2002; Billups, 2005; Blaesse et al., 2005; Gillespie et al., 2005). All experiments described here were done on double-immunostained tissue. Control reactions included primary deletes for each primary antibody for each staining run, and secondary deletes for each secondary antibody. Additionally, for each primary antibody, staining patterns in the double-stained tissue were compared with patterns in single-stained control tissue; patterns in single- and double- stained tissue were nearly identical.

Table 1.

Antibodies Used in This Study				
Antigen	**Immunogen**	**Host**	**Source/cat. no.**	**Dilution**
Synaptotagmin 1 (mab 48)	Rat synaptic junctional complexes	Mouse, monoclonal	Developmental Studies Hybridoma Bank	1:100
Synaptotagmin 2 (Znp-1)	1–5-day zebrafish embryo	Mouse, monoclonal	Zebrafish International Resource Center	1:500
VGLUT1	Synthetic peptide (amino acids 542–560)	Guinea pig, polyclonal	Millipore/AB5905	1:2,000
VGLUT2	Recombinant protein, GST-tagged	Guinea pig, polyclonal	Millipore/AB2251	1:1,000
VGLUT3	Recombinant C-terminal of mouse (amino acids 543–601)	Rabbit, polyclonal	Synaptic Systems/135 203	1:1,000, 1:1,500
VIAAT	Synthetic peptide, AEPPVEGDIHYQR	Rabbit, polyclonal	Synaptic Systems/131 002	1:1,000

Image acquisition and analysis

Images were acquired on the confocal microscope (Nikon D-Eclipse C1). For semiquantitative immunohistochemistry, low-magnification images of auditory brainstem were collected by using a 20x objective lens (NA 0.75), in order to compare overall intensity of synaptotagmin immunofluorescence of the different nuclei across development. For intensity measurements, PMT gain, laser intensity, and all other settings were kept constant for all images acquired within a given staining run. For co-localization measurements, high-magnification images were collected by using a 60x objective (NA 1.40), at settings optimized for co-localization analysis, and with sequential imaging of each channel. Images were converted to 8-bit tiff files for import to ImageJ.

In ImageJ, the signal channels were separated, and fluorescence intensity of Syt1- and Syt2-immunoreactivity (IR) was measured by using the low-magnification images. Mean pixel intensity was measured in each region of interest (ROI) within the SOC (these regions included the lateral LSO, middle LSO, medial LSO, MSO, SPN, and MNTB). To control for differences in background tissue fluorescence, mean pixel intensity of the reticular formation dorsal to the MNTB was subtracted from the mean pixel intensity for each ROI within the same tissue section. As these values are not absolute, descriptive statistics only are shown for these measures. To normalize for possible variability in intensity measurements between different staining runs, intensity measurements were normalized to the highest value within the run before being

averaged with intensity measurements from the remaining runs. Co-localization analysis was performed in ImageJ by using the high-magnification images. Pearson's correlation coefficients (r) and intensity correlation quotients (ICQs) (Li et al., 2004) were calculated for each co-localization image acquired.

Representative images shown in this manuscript were adjusted for brightness and contrast for the purposes of illustration. All quantitation was performed on original, unadjusted images only.

Results

We used double-immunofluorescence labeling in fixed tissue from neonatal rat pups to study overall levels and developmental expression patterns for the two synaptotagmins Syt1 and Syt2, and to determine their developmental expression in excitatory and inhibitory terminals within the SOC, with special focus on the glutamate-releasing immature inhibitory terminals found in the LSO and superior paraolivary nucleus (SPN).

Developmental expression of synaptotagmin-2 in the SOC

We first examined developmental expression of Syt2, as it is the predominant synaptotagmin found in adult brainstem. We found Syt2 to be abundantly expressed throughout the developing SOC, with Syt2 immunoreactivity (IR) visible in all the major nuclei of the SOC, including the LSO, SPN, MNTB, medial superior olive (MSO), lateral nucleus of the trapezoid

body (LNTB), and ventral nucleus of the trapezoid body (VNTB; Fig. 1A,B). Furthermore, between birth and the end of the third postnatal week, Syt2-IR increased in all the major nuclei of the SOC. Our subsequent analysis here focuses on the two SOC nuclei that contain large numbers of VGLUT3-positive terminals during early postnatal development, the LSO and the SPN, and the nucleus that provides the VGLUT3-positive glutamate-releasing inhibitory projection to these nuclei, the MNTB.

In the LSO, Syt2-IR was barely detectable at P1 (Fig. 1C). Staining intensity increased between P1 and P9 and subsequently decreased slightly from its peak value at P9 (Fig. 1C–F). As some proteins are expressed non-uniformly along the mediolateral axis of the LSO (Friauf, 1993), we examined the spatial distribution of Syt2 within the LSO by comparing intensity of Syt2-IR in the medial, middle, and lateral limbs of the LSO. Syt2 was expressed uniformly across the mediolateral axis of the LSO (Fig. 1F). In the SPN, we observed a similar developmental pattern for Syt2, in that Syt2-IR increased between P1 and P9 and then decreased slightly to a plateau value above background (Fig. 1G). In the MNTB, we found Syt2 expression at all ages, primarily localized to the prototypical fast excitatory synapse, the calyx of Held. Although measurements of intensity showed an overall decrease in Syt2-IR in the MNTB after about P9 (Fig. 1I), in fact the residual signal, localized to the presynaptic calyx of Held, remained bright into adulthood (see also Fox and Sanes, 2007).

Synaptotagmin-2 is present at both excitatory and inhibitory terminals in the SOC

Syt2 was expressed at high levels throughout the developing auditory brainstem. These areas receive classical glutamatergic inputs and glycinergic inputs, in addition to glutamate-releasing immature inhibitory inputs from the MNTB. To determine whether Syt2 was differentially expressed at excitatory and inhibitory synapses, we performed double immunofluorescence using an antibody for Syt2 together with an antibody for one of each of four presynaptic proteins associated with specific presynaptic terminal phenotypes. We used antibodies against the vesicular transporters VGLUT1 and VGLUT2 to identify classical glutamatergic excitatory synapses, VGLUT3 to identify glutamate-releasing immature inhibitory synapses, and VIAAT to identify inhibitory synapses generally. Although we examined both VGLUT1 and VGLUT2 expression, VGLUT1 and VGLUT2 have similar expression patterns in the SOC (Blaesse et al., 2005), they co-localize in the LSO (Gillespie et al., 2005), and we found that co-localization patterns for VGLUT2 were very similar to those for VGLUT1; therefore, images for VGLUT1-IR only are shown here to illustrate excitatory synapses.

Representative images showing Syt2 co-localization with vesicular transporters in the LSO, SPN, and MNTB are shown in Fig. 2 and 3. We use the terms “not co-localized” or “low co-localization” to refer to images that yielded Pearson's r values of 0.00–0.30, “moderate co-localization” to refer to images

with r values of 0.31–0.50, and “co-localized” or “highly co-localized” for images with r values > 0.50. Within the LSO, Syt2-IR was present both at excitatory terminals, as identified by VGLUT1-IR, and at inhibitory terminals, as identified by VGLUT3-IR and VIAAT-IR (Fig. 2). Syt2-IR was found both in the neuropil and at sites surrounding the somata and proximal dendrites. The co-localization of Syt2 with specific vesicular transporters appeared to be correlated with subcellular distribution. Thus, clusters of Syt2-IR that were located primarily along the neuropil were moderately co-localized with VGLUT1-IR (Fig. 2A), whereas clusters of Syt2-IR that were located primarily around somata and proximal dendrites were co-localized with VGLUT3-IR or with VIAAT-IR (Fig. 2D,G,J).

The SPN receives a prominent inhibitory projection from the ipsilateral MNTB (Helfert et al., 1989; Sommer et al., 1993), and MNTB terminals in the SPN are presumably identified by high levels of VIAAT expression at all ages, as well as by high levels of VGLUT3 expression before hearing onset (Blaesse et al., 2005). In the SPN, we found that Syt2-IR was co-localized with the salient staining for VGLUT3 and VIAAT that surrounds large cell bodies and that is found along proximal dendrites (Fig. 2E,H,K). As judged by levels of VGLUT1 or VGLUT2 relative to VGLUT3 or VIAAT staining, classical glutamatergic terminals were less prevalent than GABA/glycinergic terminals in the SPN; on average, Syt2 did not co-localize with VGLUT1 in the SPN (Fig. 2B).

In the ascending auditory pathway, the primary synapse within the MNTB is the large glutamatergic calyx of Held, which labels densely for VGLUT1. In the

calyceal terminals of the MNTB, Syt2-IR was highly co-localized with VGLUT1-IR (Fig. 2C). In addition to their large calyceal inputs, MNTB principal cell somata receive contacts from smaller VIAAT-positive inhibitory presynaptic terminals at non-calyceal sites and at presumed fenestrations of the calyx. We saw Syt2-IR in association with very few of these VIAAT-positive clusters, and Syt2 did not generally co-localize with VIAAT in the MNTB (Fig. 2I,L). The somata of the principal cells of the MNTB contain diffuse label for both VGLUT3 and VIAAT. This somatic labeling, which has been previously reported (Gillespie et al., 2005; Blaesse et al., 2005; Ito et al., 2011), does not co-localize with immunoreactivity for other presynaptic proteins, and did not co-localize here with Syt2-IR.

Developmental expression of synaptotagmin-2 at excitatory and inhibitory synapses in the LSO

As Syt2 was expressed at both excitatory and inhibitory terminals in the developing SOC, we asked whether Syt2 expression followed similar developmental trajectories in terminals of both types. To begin, we focused on Syt2 expression in the LSO, where before hearing onset Syt2 labeled both classical glutamatergic terminals (VGLUT1) and glutamate-releasing immature inhibitory terminals (VGLUT3). At P1, Syt2-IR was present in bright, well-defined clusters that did not appear to co-localize with VGLUT1-positive clusters (Fig. 3A). By P5, the number of Syt2-positive clusters had increased, and Syt2 showed moderate co-localization with VGLUT1 (Fig. 3B). From P9 onward, Syt2 was

moderately co-localized with VGLUT1, primarily in the neuropil (Fig 3C–F).

Already at P1, Syt2 was co-localized with VGLUT3 at immature inhibitory synapses (Fig. 3G). Although this co-localization occurred within small, readily identifiable clusters, neither Syt2 nor VGLUT3 clusters showed a clear pattern of subcellular distribution at this age. At P5 and P9, Syt2 co-localized with VGLUT3 near somata and proximal dendrites (Fig. 3H,I). After hearing onset, Syt2-VGLUT3 co-localization decreased with the rapid decrease in VGLUT3 expression (Fig. 3J–L). Syt2-IR remained high, however, and was highly co-localized with VIAAT near somata and proximal dendrites (Fig. 2J).

Developmental expression of synaptotagmin-1 in the SOC

In marked contrast to Syt2, which was expressed abundantly at all ages throughout the SOC, and following similar time courses in all nuclei, Syt1 was expressed at the earliest ages only, and then was differentially expressed between and even within nuclei. Syt1-IR was high in the LSO and SPN before hearing onset (Fig. 5). In the LSO, Syt1 expression followed a mediolateral gradient: after P1, Syt1 expression was higher in the lateral limb than in the middle limb and was higher in the middle limb than in the medial limb (Fig. 5C,E). In the SPN, mean levels of Syt1 expression were similar to those seen in the middle limb of the LSO. In the MNTB, Syt1-IR was barely detectable, and mean fluorescence intensity was below background. Indeed, in many cases the MNTB was most easily identified by an absence of Syt1 staining. Syt1-IR in the LNTB

(not shown) and MSO was also lower than that seen in the LSO and SPN.

The temporal expression pattern of Syt1 was distinctly different in the LSO/SPN from that in the MNTB. Whereas in the MNTB Syt1 expression was below background at all ages (Fig. 5H), in the LSO Syt1 expression followed an inverted U-shaped curve between P1 and P21. Temporal expression of Syt1 was similar in all three limbs of the LSO, peaking around P9 (Fig. 5E), and the expression profile of Syt1 in the SPN was very similar to that in the middle limb of the LSO (Fig. 5F). By P17, mean Syt1-IR within all nuclei of the SOC had fallen to levels at or below background.

Synaptotagmin-1 is present at glutamate-releasing immature inhibitory terminals in the SOC

Because Syt1 was expressed at highest levels in the LSO and SPN, the two SOC nuclei in which VGLUT3 is expressed most abundantly, we asked whether Syt1-IR was present at glutamate-releasing immature inhibitory synapses in LSO and SPN. Before hearing onset, we saw Syt1-IR at VGLUT3-positive and VIAAT-positive inhibitory terminals in the LSO and SPN (Fig. 6D,E,G,H). In contrast, we saw little or no expression of Syt1 at classical excitatory terminals, as identified by VGLUT1, in the SPN or LSO (Fig. 6A,B). These data suggest that Syt1 is specifically expressed in immature inhibitory terminals in the LSO and SPN.

In the MNTB, although overall levels of Syt1 expression were below

background, Syt1-IR was present in isolated bright clusters. In agreement with previous findings, these clusters were non-calyceal in shape and failed to co-localize with VGLUT1 (Fig. 6C) (Fox and Sanes, 2007). Although a small subset of these isolated Syt1-IR clusters co-localized with VIAAT-IR clusters, the majority did not co-localize with VIAAT (Fig. 6I,L).

Developmental expression of synaptotagmin-1 at excitatory and inhibitory synapses in the LSO

At no point in postnatal development was Syt1 co-localized with VGLUT1/2 in the LSO (Fig. 7A–F, 8A,B). This was evident in the images, in the Pearson's correlation coefficients for co-localization, and in the computed ICQs (data not shown; nearly identical patterns to Pearson's r). As Syt1 appeared to be expressed exclusively at developing inhibitory synapses within the LSO, we focused on the expression of Syt1 at inhibitory synapses during the period of synaptic refinement. At P1 and P5, Syt1-IR and VGLUT3-IR appeared in clusters of similar size that were co-localized within the LSO and SPN (Fig. 7G,H). At P9, Syt1 and VGLUT3 were still co-localized (Fig. 7I), but after P9, bright, clustered staining for both Syt1 and VGLUT3 declined, and staining became more diffuse as the expression of both proteins progressively decreased with age (Fig. 7J–L).

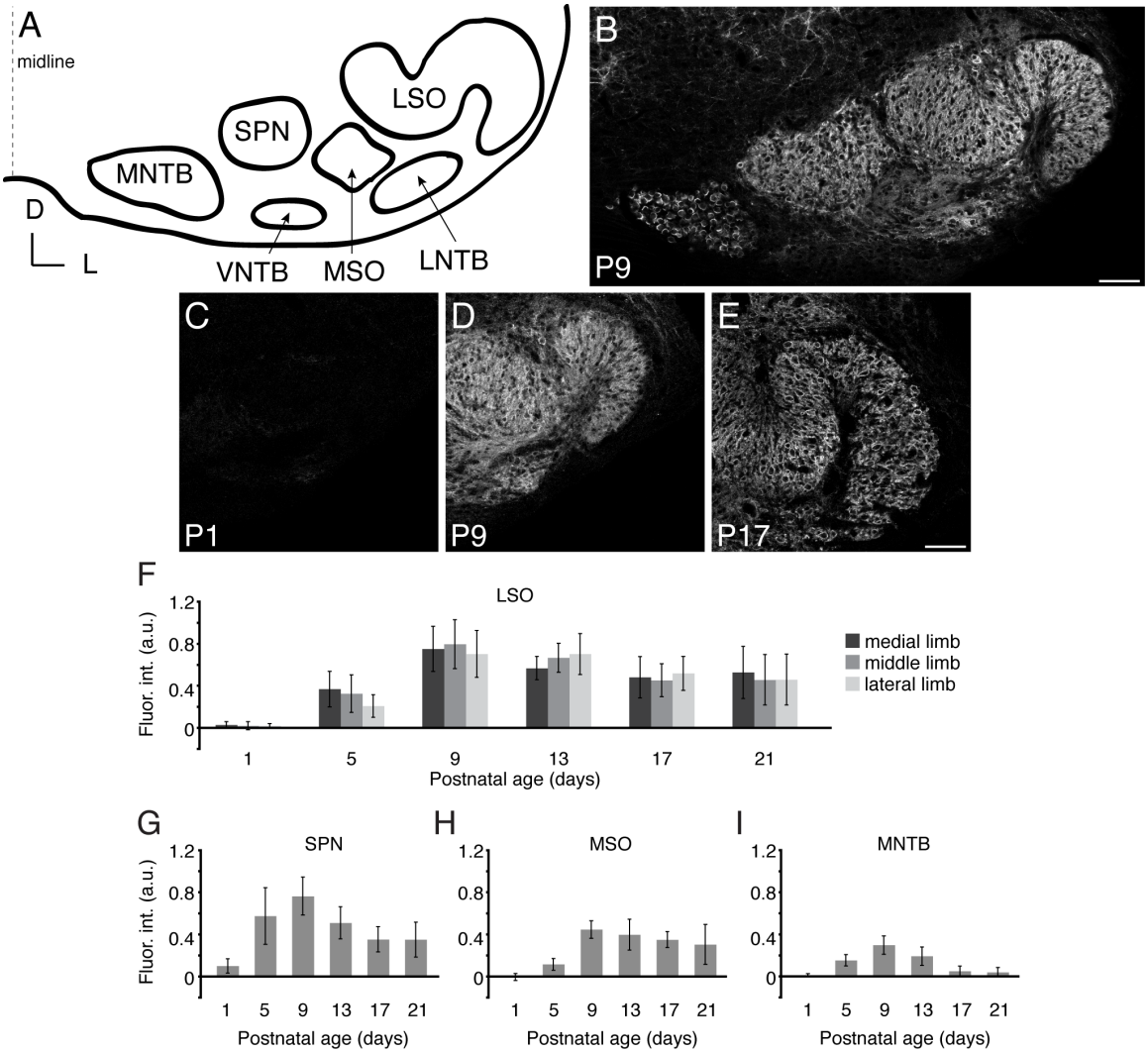

Figure 1. Syt2 levels of expression in the developing rat SOC. **A**: Schematic of the SOC, showing the LSO, SPN, MNTB, LNTB, VNTB, MSO, and MNTB. D, dorsal; L, lateral. **B**: Syt2-IR in a coronal section through auditory brainstem of a P9 rat pup. Syt2-IR can be observed in all the major nuclei of the SOC: LSO, SPN, MNTB, VNTB, MSO, and LNTB (image shown is a montage of several 20x confocal images). **C–E**: Example micrographs from a single litter, showing Syt2-IR in the LSO at three of the ages tested: P1 (C), P9 (D), and P17 (E). Syt2-IR in the LSO increases between P1 and P21, peaking around P9. **F–I**: Quantification

of fluorescence intensity across development in the three limbs of the LSO (F), SPN (G), MSO (H), and MNTB (I). Negative values indicate that staining intensity within the area of interest is below background levels (see Materials and Methods). Fluor. int., fluorescence intensity; A.u., arbitrary units. For other abbreviations, see list. Scale bar = 100 μm in B and E (applies to C–E).

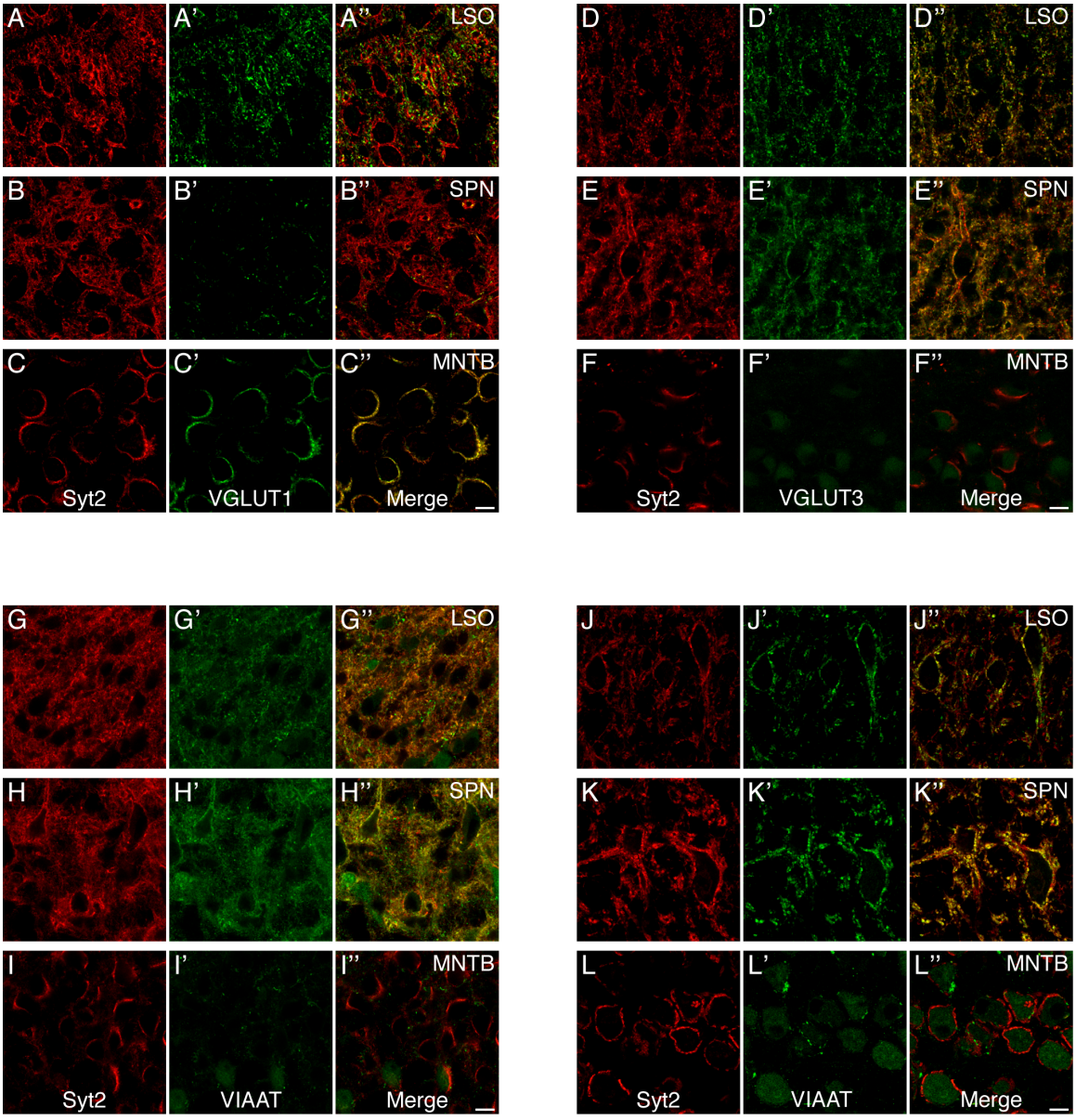

Figure 2. Syt2-IR appears at both excitatory and inhibitory terminals in the developing SOC (representative images). **A–C″**: Syt2 (red) and VGLUT1 (green) immunoreactivity in the LSO (A), SPN (B), and MNTB (C) of P9 tissue. Syt2-IR co-localizes with VGLUT1-IR in each of these nuclei. Syt2 is moderately co-localized with VGLUT1 in the LSO (for this image: Pearson's r LSO = 0.42), but not in the SPN (r = 0.23, this image). Whereas Syt2 can appear without VGLUT1 in the LSO and SPN, it nearly always co-localizes with VGLUT1 in the MNTB (for this image, Pearson's r = 0.91). **D–F″**: Syt2 (red) and VGLUT3 (green) staining in the LSO (D), SPN (E), and MNTB (F) of P5 tissue. Syt2 and VGLUT3 are highly co-localized within the LSO and SPN (r = 0.75, 0.68), but are segregated in the MNTB (r = 0.15). **G–I″**: Syt2 (red) and VIAAT (green) in the LSO (G), SPN (H), and MNTB (I) of P5 tissue. Small clusters of Syt2- and VIAAT-IR co-localize in the LSO and SPN (r = 0.57 and r = 0.69, respectively). In the MNTB, Syt2-IR is observed in the calyces, but does not co-localize with VIAAT-IR (r = 0.25), which diffusely labels principal cell bodies and brightly labels at presumed fenestrations of the calyces. **J– ″L**: Syt2 (red) and VIAAT (green) in the LSO (J), SPN (K), and MNTB (L) of P21 tissue. Clusters of co-localized Syt2 and VIAAT labeling increase in size after hearing onset and are observed surrounding the somata and along the proximal dendrites of principal cells in the LSO. After hearing onset, Syt2/VIAAT co-localization remains high in the LSO and SPN (r = 0.73 and r = 0.88, respectively), and low in the MNTB (r = 0.13). For abbreviations, see list. Scale bar = 10 μm in C″ (applies to A–C″), F″ (applies to D–F′), I″ (applies to G–

I″), and L″ (applies to J–L″).

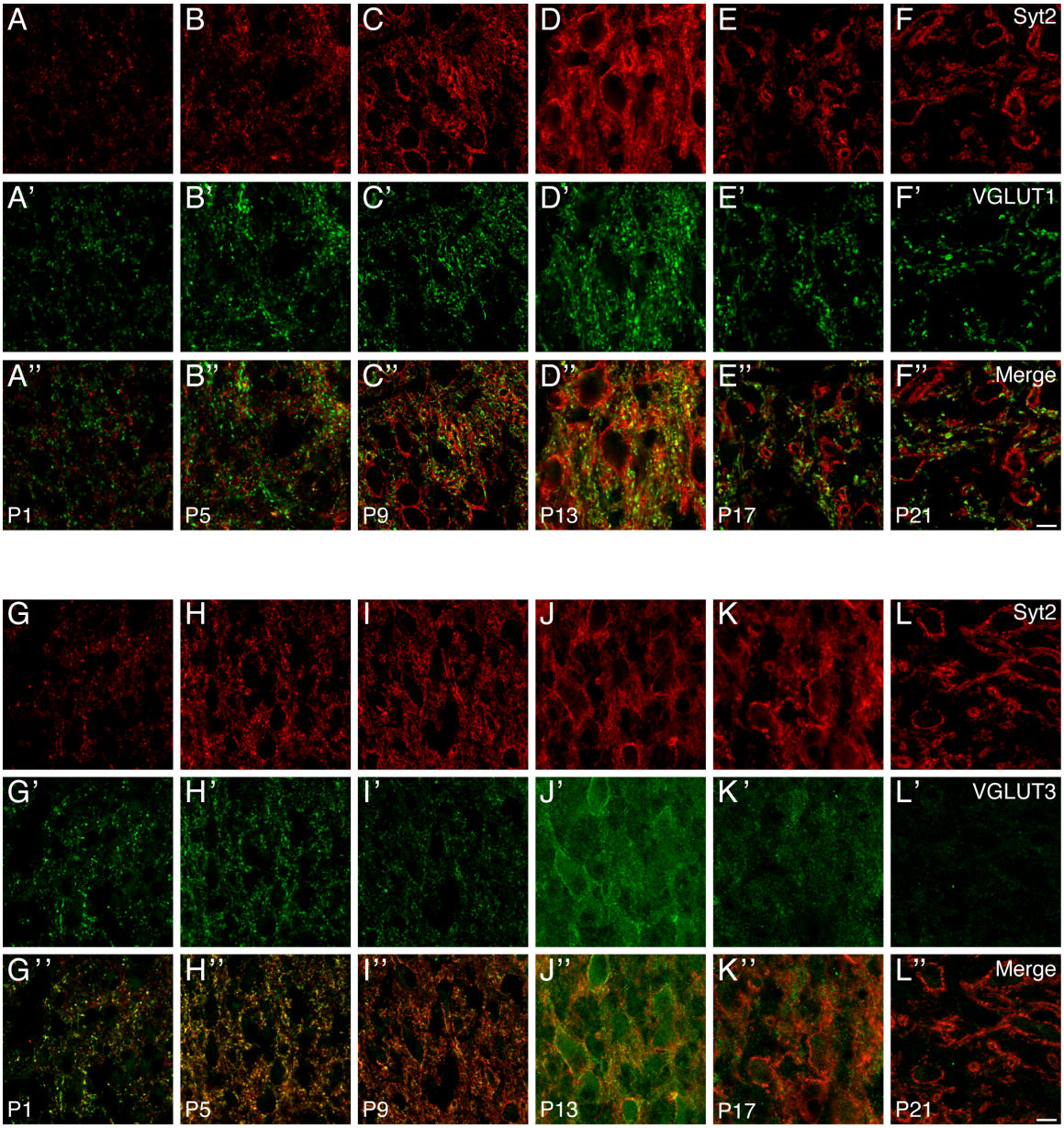

Figure 3. Developmental changes in Syt2 distribution and co-localization at glutamatergic excitatory terminals and at glutamate-releasing immature inhibitory terminals in the LSO. **A–F″**: Representative images showing that Syt2 (red) and VGLUT1 (green) immunoreactive clusters are not co-localized at P1 (r = 0.19),

but are moderately co-localized from P5 onward (P5 r = 0.34; P9 r = 0.42; P13 r = 0.43; P17 r = 0.46; P21 r = 0.40). VGLUT1 appears with Syt2 along the neuropil, but rarely around the cell body or around proximal dendrites. **G–L″**: Syt2 (red) and VGLUT3 (green) immunoreactive clusters co-localize from P1 onward. At P1 and P5, Syt2 and VGLUT3 are co-localized in well-defined clusters (P1 r = 0.65 and P5 r = 0.75, respectively). At P5, clusters are observed primarily around the somata, whereas at P9 clusters are observed surrounding the somata and along presumed proximal dendrites (arrowheads). VGLUT3-IR decreases after P9, whereas Syt2-IR clusters are still present at P13, P17, and P21. Note that acquisition parameters for these images were optimized for co-localization measurements, and that these images should not be used to make inferences about relative levels of expression. P1–17 images from the same litter. For abbreviations, see list. Scale bar = 10 μm in F″ (applies to A–F″) and L″ (applies to G–L″).

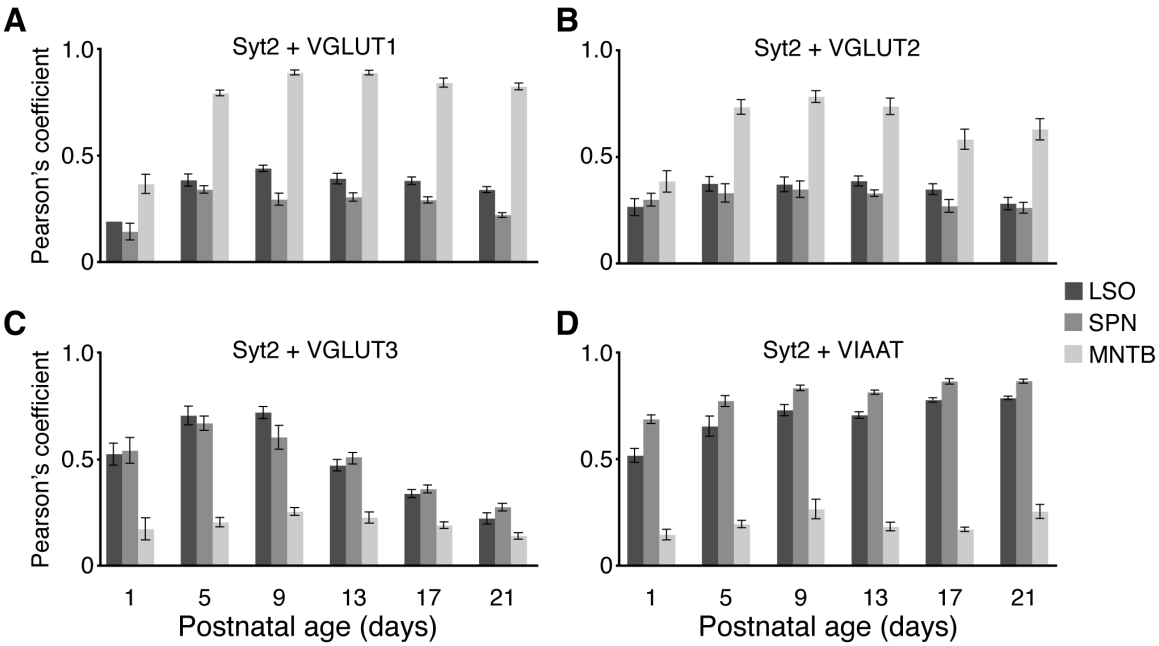

Figure 4. Group data, showing degree of co-localization of Syt2 and vesicular transporters in the developing LSO, SPN, and MNTB. **A,B**: Syt2 and VGLUT1 and -2 are moderately co-localized in the LSO and SPN and are highly co-localized in the MNTB, at all ages. **C**: During the period of VGLUT3 expression, primarily before hearing onset, VGLUT3 co-localizes with Syt2 in the LSO and SPN, but does not co-localize with Syt2 in the MNTB. **D**: Syt2 and VIAAT are co-localized in the LSO and SPN at all ages, but not in the MNTB. Shaded bars show mean Pearson's r for LSO (dark), SPN (gray), and MNTB (light gray). For abbreviations, see list. `

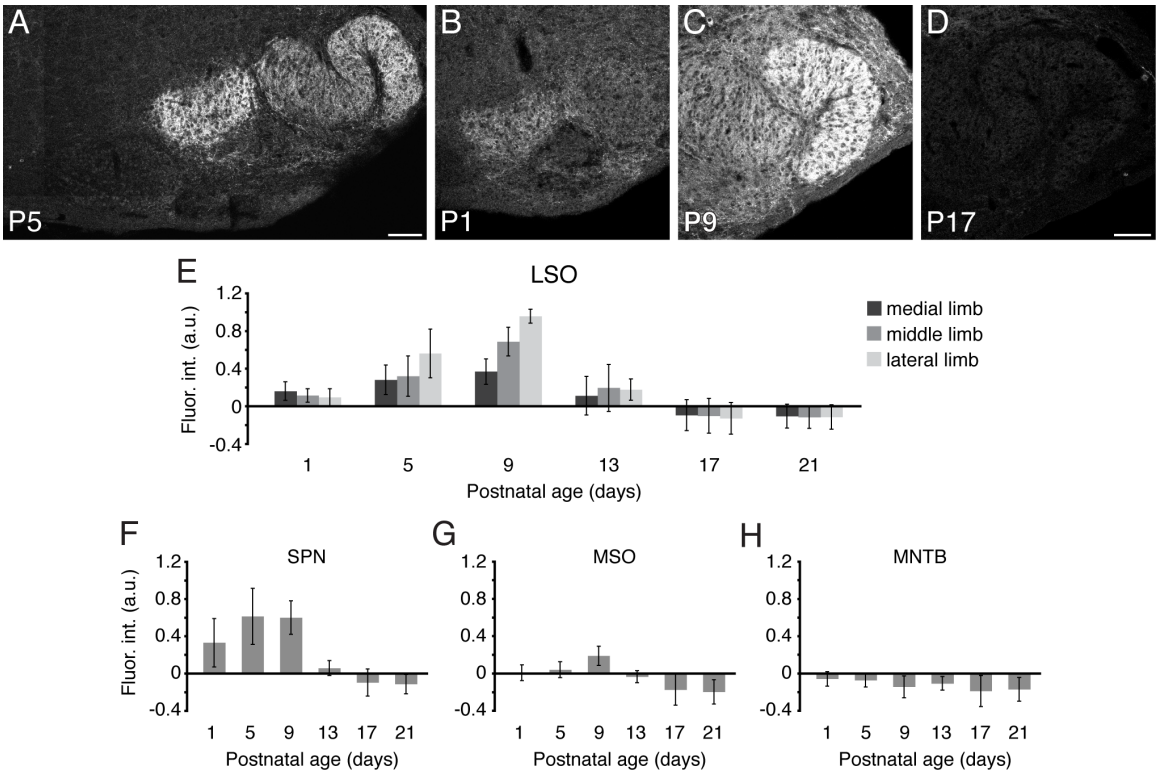

Figure 5. Syt1 levels of expression in the developing rat SOC. **A**: Syt1-IR in a coronal section of auditory brainstem from P9 tissue. Syt1-IR is highly visible in the SPN and in the LSO, especially in the lateral limb. The MNTB appears as an egg-shaped area with slightly below-background staining ventromedial to the SPN. (The image shown is a montage of several 20× confocal images; this image has been brightened slightly for display.) **B–D**: Syt1-IR in the LSO at three of the ages tested: P1 (B), P9 (C), and P17 (D). Intensity of Syt1-IR rises between P1 and P9, and decreases between P9 and P21. **E–H**: Quantification of Syt1-IR in the three limbs of the LSO (E), SPN (F), MSO (G), and MNTB (H). Negative values indicate that signal in the region of interest is lower than signal in the background (see Materials and Methods). Fluor. int., fluorescence intensity; A.u., arbitrary units. For other abbreviations, see list. Scale bar = 100 μm in A and D

(applies to B–D).

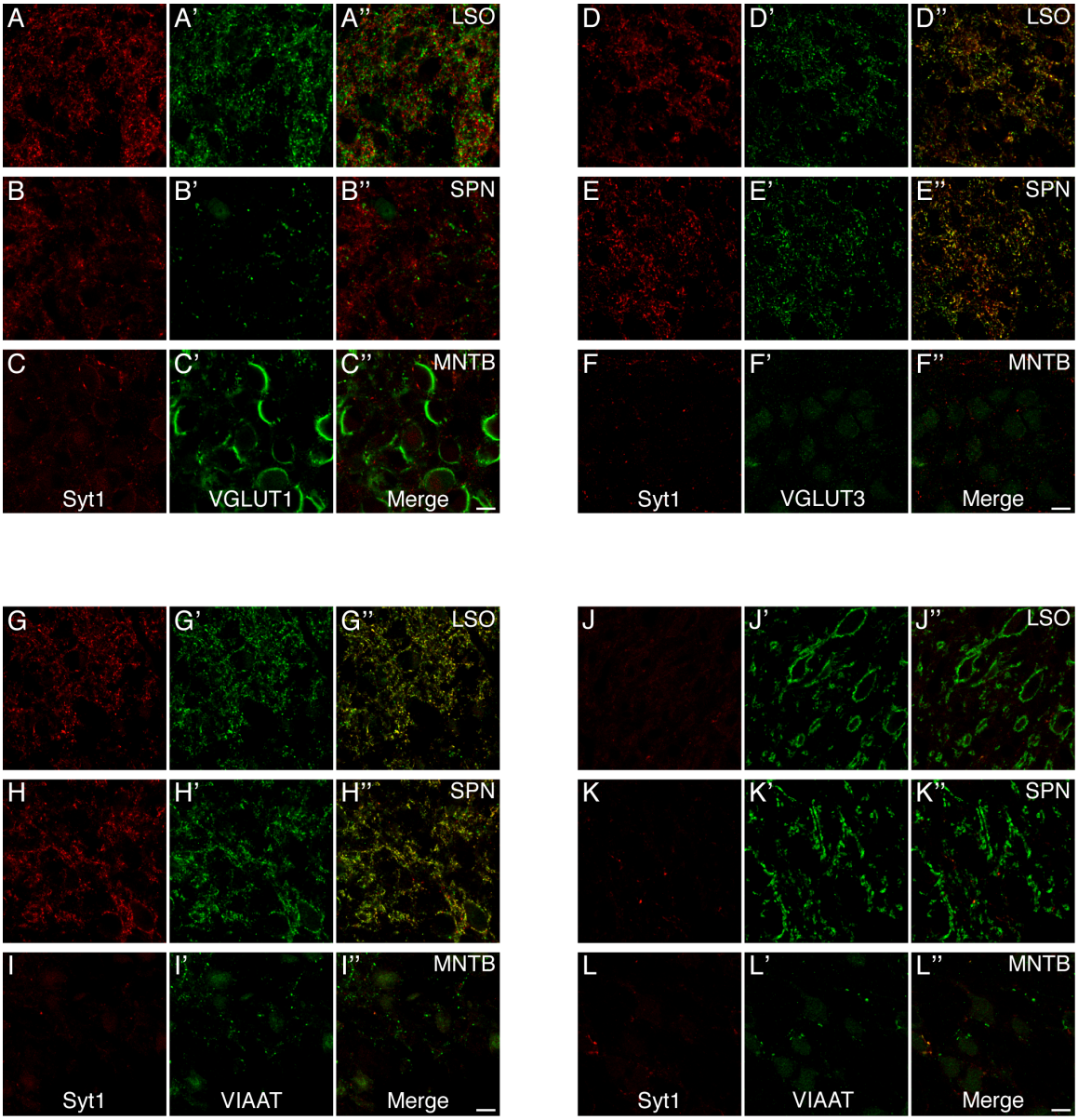

Figure 6. Syt1 is expressed at VGLUT3- and VIAAT-positive inhibitory terminals, but not at excitatory terminals, in the developing SOC (representative images). **A–C″**: Syt1 (red) and VGLUT1 (green) immunoreactivity in the LSO (A), SPN (B), and MNTB (C) of P5 tissue. Syt1 is not observed in association with VGLUT1-

positive terminals (LSO r = 0.24; SPN r = 0.09). Sparse Syt1-IR in the MNTB is not associated with the calyx of Held (r = 0.22). **D–F″**: Syt1 (red) and VGLUT3 (green) immunoreactivity in the LSO (D), SPN (E), and MNTB (F) of P5 tissue. Clusters of Syt1- and VGLUT3-IR co-localize in the LSO and SPN (r = 0.75 and r = 0.70, respectively) but not in the MNTB (r = 0.11). **G–I″**: Syt1 (red) and VIAAT (green) immunoreactivity in the LSO (G), SPN (H), and MNTB (I) of P5 tissue. Small clusters of Syt1- and VIAAT-IR co-localize in the LSO and SPN (r = 0.75 and r = 0.79, respectively). Staining for both Syt1 and VIAAT is sparse in the MNTB, and co-localization is low (mean r = 0.28; this image, r = 0.40). **J–L″**: Syt1 (red) and VIAAT (green) immunoreactivity in the LSO (J), SPN (K), and MNTB (L) of P21 tissue. Few Syt1 clusters can be observed in the LSO or SPN, and Syt1-VIAAT co-localization has largely disappeared (r = 0.25 and r = 0.23, respectively). Few Syt1 clusters remain in the MNTB, and Syt1-VIAAT co-localization is low (r = 0.29). For abbreviations, see list. Scale bar = 10 μm in C″ (applies to A–C″), F″ (applies to D–F′), I″ (applies to G–I″), and L″ (applies to J–L″).

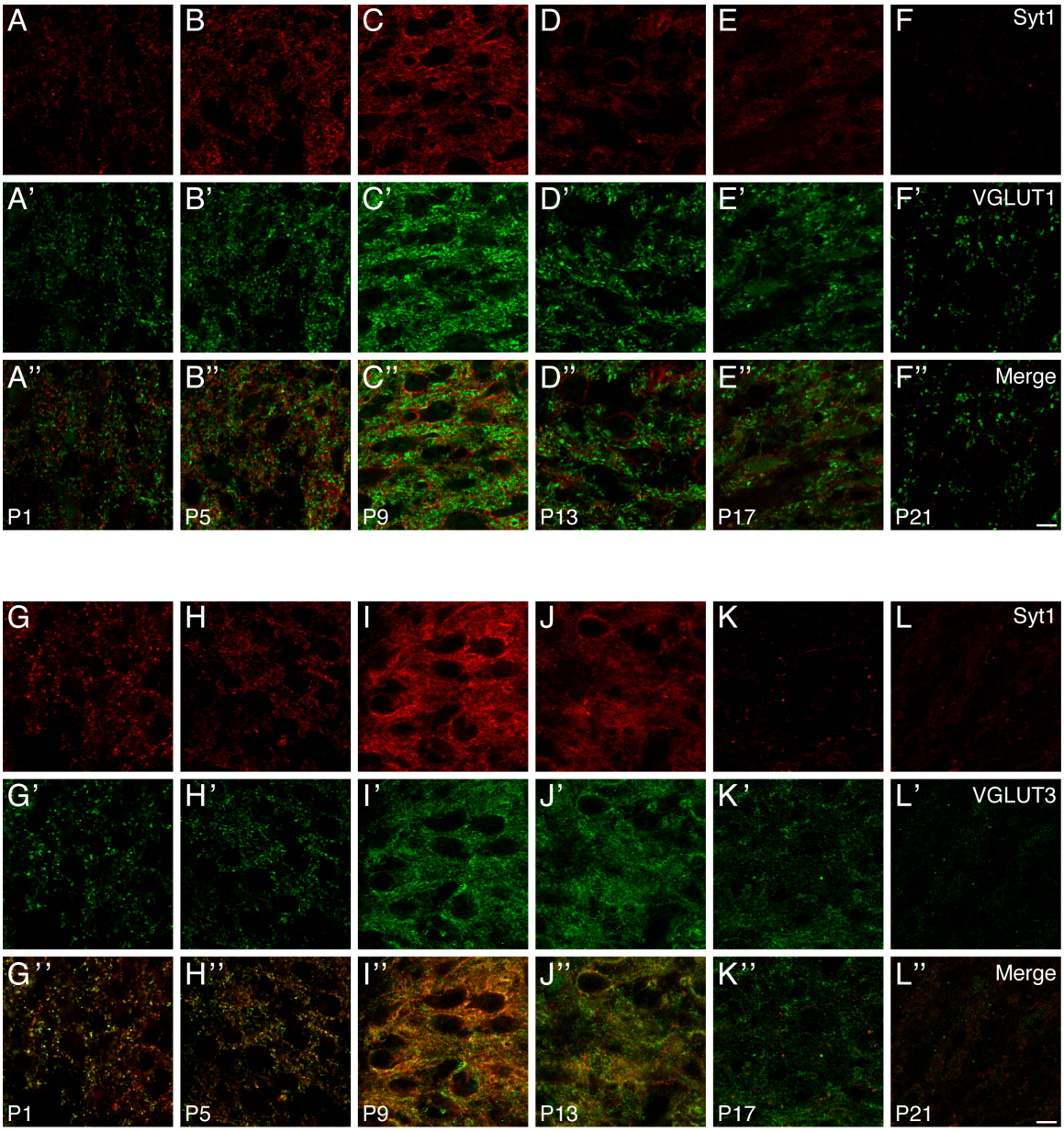

Figure 7. Developmental changes in Syt1 distribution and co-localization at glutamatergic excitatory terminals and at glutamate-releasing immature inhibitory terminals in the LSO. **A–F**: Syt1 (red) and VGLUT1 (green) are barely co-localized at any age tested (mean r = 0.20). At P13, P17, and P21, clustered Syt1 staining has largely disappeared, and residual, sparse Syt1-IR is diffusely

distributed. **G–L**: Syt1 (red) and VGLUT3 (green) immunoreactive clusters are co-localized at P1, P5, and P9 (r = 0.68, r = 0.75, and r = 0.53, respectively), when VGLUT3 expression is high. The distinct clusters of Syt1- and VGLUT3-IR exhibit no obvious pattern of subcellular distribution at P1 and P5. Staining for both Syt1 and VGLUT3 is still observed at P9, but with a more diffuse distribution. After hearing onset (P13, P17, and P21), signal-to-noise ratio and frequency of bright clusters decrease, as does Syt1/VGLUT3 co-localization (r = 0.43, r = 0.18, and r = 0.15, respectively). For abbreviations, see list. Scale bar = 10 μm in F″ (applies to A–F″) and L″ (applies to G–L″).

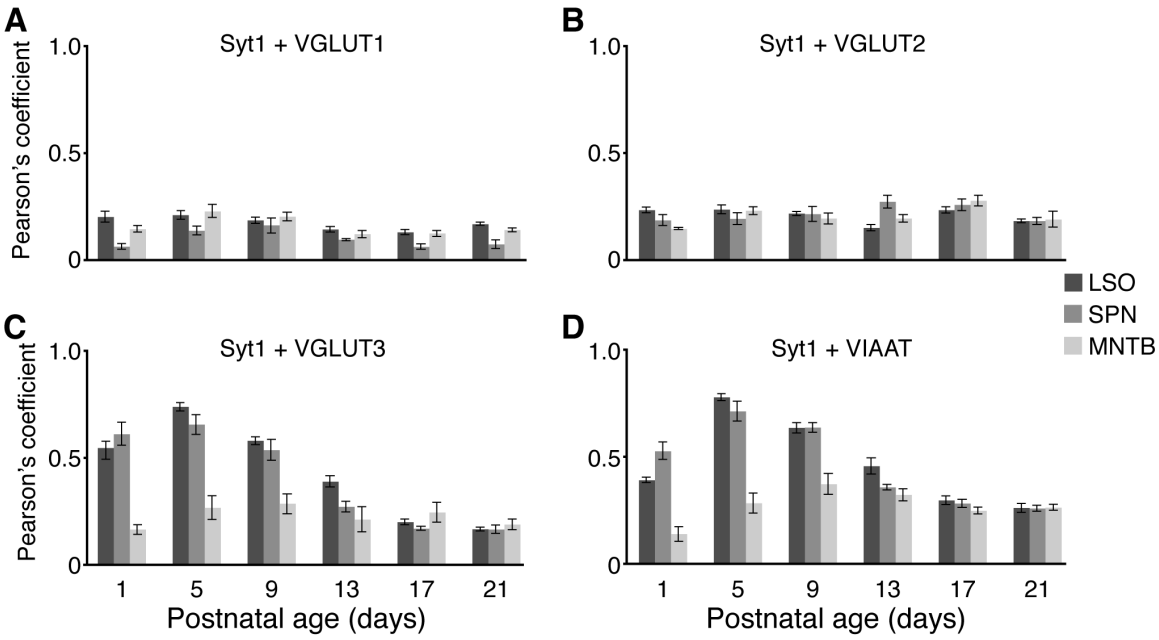

Figure 8. Group data, showing degree of co-localization of Syt1 and vesicular transporters in the developing LSO, SPN, and MNTB. **A,B**: Syt1 does not co-localize with either VGLUT1 or VGLUT2 at any age in LSO, SPN, or MNTB. **C**: Syt1 and VGLUT3 co-localize before hearing onset in the LSO and SPN; co-localization decreases with the reduction in expression of both proteins after hearing onset. **D**: Syt1 and VIAAT co-localize in the LSO and SPN before hearing onset; co-localization decreases after hearing onset. For abbreviations, see list.

Discussion

Here we have examined spatial and temporal expression of Syt1 and Syt2 in the developing auditory brainstem. We found that although both Syt1 and Syt2 are expressed during early postnatal development of the SOC, the two proteins have distinct time courses of expression, and the proteins are associated with different, but likely overlapping, populations of synaptic terminals. We further found that whereas Syt1 was expressed in the SOC, Syt1 expression was more restricted spatially and temporally than that of Syt2. In agreement with others (Xiao et al., 2010), we found that Syt1 expression was below background in the MNTB; we also saw that Syt1 was expressed at levels above background in the first 2 postnatal weeks only and then primarily within the LSO and SPN, two areas that receive VGLUT3-positive glutamate-releasing inhibitory axon terminals from the MNTB before hearing onset (~P12 in rat). Interestingly, the time course of Syt1 expression in the LSO and SPN paralleled that of VGLUT3 in the LSO and SPN, and in these nuclei Syt1-IR co-localized with VGLUT3-IR during this period. These results are consistent with the idea that Syt1 is associated with VGLUT3-expressing synaptic vesicles in immature inhibitory terminals of the auditory brainstem. These results are consistent with expression of Syt1 and Syt2 in the same immature inhibitory terminals and with the idea that the distinct release probabilities seen for GABA/glycine and glutamate at these synapses result from the association of Syt2 with VIAAT-containing vesicles and of Syt1 with VGLUT3-containing vesicles.

General patterns of synaptotagmin 1 and -2 expression

Our data corroborate previous results showing that the Syt2 isoform of the synaptotagmin family predominates in the adult brainstem (Fox and Sanes, 2007). We also found an increase in overall levels of both Syt1 and Syt2 expression over the first week, with a decrease in expression after about the age of hearing onset. In the MNTB in particular, although overall levels of Syt2-IR decreased in the second week, the remaining Syt2-IR was bright and clustered. Both the overall decrease and the localized increase in Syt2-IR within the MNTB likely result from the refinement of the presynaptic terminal, and the restriction of presynaptic proteins to the more physically confined space of the mature calyx of Held (Kandler and Friauf 1993; Ford et al., 2009). The major excitatory projection to the LSO, from the AVCN, is presumed to use VGLUT1, and yet excitatory terminals labeled by VGLUT1-IR in the LSO contained little Syt2 or Syt1 at P1.

As excitatory inputs to the LSO are functional before birth (Kandler and Friauf, 1995), one question is whether the low apparent levels of Syt1/2 seen here at birth are sufficient to support synchronous release at immature terminals, or whether another Ca^{2+} sensor might participate in exocytosis at excitatory synapses in the LSO at birth. This hypothetical alternative Ca^{2+} sensor could be an as yet unidentified double C2 domain protein (Groffen et al., 2010) or possibly another synaptotagmin. Although Syt9, the only other synaptotagmin demonstrated to promote synchronous release, has been thought to be restricted

to the striatum and limbic system (Xu et al., 2007), low levels of Syt9 transcript have been reported at early ages in another auditory brainstem nucleus (Xiao et al., 2010). Syt1 and Syt2 showed noticeably distinct spatial expression in the LSO; Syt2 was uniformly expressed within the nucleus, whereas Syt1 expression followed a mediolateral gradient before hearing onset. Expression gradients across the LSO have been seen for other proteins (Friauf, 1993; Henkel and Brunso-Bechtold, 1998). Such protein expression gradients along the tonotopic axis of the LSO may reflect variation in neuronal response properties, which can differ substantially between the low-frequency lateral limb and the higher frequency middle and medial limbs (Finlayson and Caspary, 1991).

As excitatory inputs to the LSO are functional before birth (Kandler and Friauf, 1995), one question is whether the low apparent levels of Syt1/2 seen here at birth are sufficient to support synchronous release at immature terminals, or whether another Ca^{2+} sensor might participate in exocytosis at excitatory synapses in the LSO at birth. This hypothetical alternative Ca^{2+} sensor could be an as yet unidentified double C2 domain protein (Groffen et al., 2010) or possibly another synaptotagmin. Although Syt9, the only other synaptotagmin demonstrated to promote synchronous release, has been thought to be restricted

to the striatum and limbic system (Xu et al., 2007), low levels of Syt9 transcript have been reported at early ages in another auditory brainstem nucleus (Xiao et al., 2010). Syt1 and Syt2 showed noticeably distinct spatial expression in the LSO; Syt2 was uniformly expressed within the nucleus, whereas Syt1 expression

followed a mediolateral gradient before hearing onset. Expression gradients across the LSO have been seen for other proteins (Friauf, 1993; Henkel and Brunso-Bechtold, 1998). Such protein expression gradients along the tonotopic axis of the LSO may reflect variation in neuronal response properties, which can differ substantially between the low-frequency lateral limb and the higher frequency middle and medial limbs (Finlayson and Caspary, 1991).

As expected from the low levels of glutamatergic signaling in the SPN (Caicedo and Eybalin, 1999; Blaesse et al., 2005), synaptotagmin immunoreactivity within this nucleus co-localized primarily with inhibitory synaptic proteins. Consistent with previous results (Fox and Sanes, 2007), Syt2 was highly expressed at all ages in the nervous system's prototypical fast synapse, the calyx of Held, and Syt1—expressed at low levels in the MNTB—appeared to be specifically excluded from the calyx.

Synaptotagmins at inhibitory synapses

An initial impetus for this study was provided by results showing that at synapses that utilize neurotransmitters with distinctly different phenotypes (GABA/glycine and glutamate), release properties for the two types of neurotransmitters are also distinctly different. Differing release properties between vesicle pools within the same presynaptic terminal could result from differing physical locations, vesicle-filling efficiency, or calcium sensitivity (Wu and Borst, 1999; Xu et al., 2007; Onoa et al., 2010).

The present study cannot rule out any of these possibilities, but our results are consistent with a situation in which the differential expression of two isoforms of the Ca^{2+}-sensor synaptotagmins confers different release probabilities on the two vesicle populations. As both Syt1 and Syt2 co-localize with both VGLUT3 and VIAAT in the LSO and the SPN, and as VGLUT3 and VIAAT co-localize within both LSO and SPN (Gillespie et al., 2005), we suggest that Syt1 and Syt2 are co-expressed in glutamate-releasing immature inhibitory terminals, but on separate vesicle pools. In the MNTB-LSO pathway, we propose that Syt1 is expressed on VGLUT3-positive vesicles of immature axon terminals, whereas Syt2 is expressed on VIAAT-positive vesicles in both immature and mature axon terminals. If so, release properties for glutamate at the immature MNTB-LSO synapse will be determined, at least in part, by the calcium sensitivity and kinetics of Syt1, with release properties for GABA/glycine determined by the calcium sensitivity and kinetics of Syt2.

Further questions

During approximately the first postnatal week in rat, the MNTB-LSO pathway undergoes several developmentally regulated events, including a shift from a mixed GABA/glycinergic to a primarily glycinergic phenotype (Kotak et al., 1998; Korada and Schwartz, 1999; Nabekura et al., 2004), changes in expression of calcium binding proteins, neurotransmitter transporters, ion transporters, and vesicular transporters (Henkel and Brunso-Bechtold, 1998; Friauf et al., 1999;

Kakazu et al., 1999; Gillespie et al., 2005), and maturation of receptor subunits (Friauf et al., 1997; Kungel and Friauf, 1997). The results of the current study add changes in Syt1 expression to this partial list. The striking developmental time course of Syt1 expression suggests that Syt1 could play an important role in the large-scale functional refinement that occurs in the SOC before hearing onset, but the factors that regulate Syt1 expression are unknown. For example, developmental downregulation of Syt1 could be controlled by a single event or molecule, or even by expression of, for example, VGLUT3.

We have suggested that before hearing onset, individual immature MNTB terminals in the LSO and in the SPN contain two populations of synaptic vesicles, one population that specifically expresses VIAAT and Syt2 and one population that specifically expresses VGLUT3 and Syt1. This is of course not the only possibility; expression of VGLUT3 on VIAAT-positive vesicles might act synergistically to enhance VIAAT-mediated vesicle filling (Gras et al., 2008), and in any case VIAAT and VGLUT3, and/or Syt1 and Syt2, could be randomly or nonrandomly mixed in vesicle populations of the MNTB terminal. Conclusive testing of our model for distinct Syt1/VGLUT3 and Syt2/VIAAT vesicle populations is unfortunately beyond the resolution of light microscopy, and—unless the hypothesized vesicle pools are themselves physically segregated—is also likely beyond the resolution of immunogold electron microscopy (Bergersen et al., 2003). Although it is possible that sorting of VGLUT3 and VIAAT into different vesicle recycling pathways (Onoa et al., 2010) could result in different

apparent release probabilities for glutamate and GABA/glycine, our findings here are also consistent with the possibility that differential expression of Syt1 and Syt2 on phenotypically distinct vesicles results in different release efficacies for the different neurotransmitters at individual terminals.

Why might the same synaptic terminal express two different synaptotagmins during development? One intriguing possibility is that the differential sorting of synaptotagmins to vesicles with different neurotransmitters might create a plasticity “switch” at the MNTB-LSO synapse. Developmental refinement in the MNTB-LSO pathway is dependent on neural activity (Sanes and Chokshi, 1992; Sanes and Takacs, 1993), with refinement before hearing onset likely driven by patterned spontaneous activity arising in the cochlea (Kros et al., 1998; Beutner and Moser, 1999; Kim and Kandler, 2003; Kandler, 2004; Tritsch et al., 2007; Tritsch and Bergles, 2010). The differing kinetics and Ca^{2+} affinities of the different synaptotagmin isoforms (Xu et al., 2007) could set distinct properties of synaptic release in response to differing frequencies of spiking input. At the MNTB-LSO terminal, if GABA/glycine is released specifically upon fusion of Syt2-positive vesicles, and glutamate upon fusion of Syt1-positive vesicles, spike trains of differing temporal patterns could elicit differential release of GABA/glycine or of GABA/glycine and glutamate.

The finding that animals lacking glutamate release at MNTB terminals undergo abnormal circuit refinement (Noh et al., 2010) has lent credence to the hypothesis that glutamate release supports developmental synaptic plasticity in

this pathway. If synaptic plasticity indeed requires glutamate release, and if glutamate release depends on properties of the spike train, then varying patterns of spiking activity in the neonatal MNTB could flip a “switch” (glutamate release) turning developmental plasticity on or off. It will be of interest to discover what patterns are present in the spike trains of auditory circuits before hearing onset, and to learn how the differential expression of specific synaptic proteins may interact with these spike patterns to sculpt neural circuits in the developing auditory brainstem.

Acknowledgements

The authors thank S.Y. Lee, K. Meka, and M.S. Wong for technical assistance and D. Goldreich and members of the lab for comments on the manuscript. The mab 48 antibody developed by Dr. Louis Reichardt at the University of California, San Francisco, was obtained from the Developmental Studies Hybridoma Bank maintained by the University of Iowa, Department of Biological Sciences, Iowa City, IA 52242. The Znp-1 antibody was obtained from the Zebrafish International Resource Center, which is supported by grant P40 RR012546 from the National Institutes of Health, National Center for Research Resources.

References

Bedet C, Isambert MF, Henry JP, Gasnier B. 2002. Constitutive phosphorylation of the vesicular inhibitory amino acid transporter in rat central nervous system. *J Neurochem* 75: 1654–1663.

Bergersen L, Ruiz A, Bjaalie JG, Kullmann DM, Gundersen V. 2003. GABA and GABAA receptors at hippocampal mossy fibre synapses. *Eur J Neurosci* 18: 931–941.

Beutner D, Moser T. 2001. The presynaptic function of mouse cochlear inner hair cells during development of hearing. *J Neurosci* 21: 4593–4599.

Billups B. 2005. Colocalization of vesicular glutamate transporters in the rat superior olivary complex. *Neurosci Lett* 382: 66–70.

Blaesse P, Ehrhardt S, Friauf E, Nothwang HG. 2005. Developmental pattern of three vesicular glutamate transporters in the rat superior olivary complex. *Cell Tissue Res* 320: 33–50.

Bledsoe SC Jr, Snead CR, Helfert RH, Prasad V, Wenthold RJ, Altschuler RA. 1990. Immunocytochemical and lesion studies support the hypothesis that

the projection from the medial nucleus of the trapezoid body to the lateral superior olive is glycinergic. *Brain Res* 517: 189–194.

Boudreau JC, Tsuchitani C. 1968. Binaural interaction in the cat superior olive S segment. *J Neurophysiol* 31: 442–454.

Caicedo A, Eybalin M. 1999. Glutamate receptor phenotypes in the auditory brainstem and mid-brain of the developing rat. *Eur J Neurosci* 11: 51–74.

Caird D, Klinke R. 1983. Processing of binaural stimuli by cat superior olivary complex neurons. *Exp Brain Res* 52: 385–399.

Cant NB, Casseday JH. 1986. Projections from the anteroventral cochlear nucleus to the lateral and medial superior olivary nuclei. *J Comp Neurol* 247: 457–476.

Caspary DM, Finlayson PG. 1991. Superior olivary complex: functional neuropharmacology of the principal cell types. In: Altschuler RA, et al. *Neurobiology of hearing: the central auditory system*. p 141–161.

Dumoulin A, Rostaing P, Bedet C, Lévi S, Isambert MF, Henry JP, Triller A,

Gasnier B. 1999. Presence of the vesicular inhibitory amino acid transporter in GABAergic and glycinergic synaptic terminal boutons. *J Cell Sci* 112: 811–823.

Ehrlich I, Lohrke S, Friauf E. 1999. Shift from depolarizing to hyperpolarizing glycine action in rat auditory neurones is due to age-dependent Cl^- regulation. *J Physiol* 521: 121–137.

Fernandez-Chacon R, Konigstorfer A, Gerber SH, Garcia J, Matos MF, Stevens CF, Brose N, Rizo J, Rosenmund C, Sudhof TC. 2001. Synaptotagmin I functions as a calcium regulator of release probability. *Nature* 410: 41–49.

Finlayson PG, Caspary DM. 1991. Low-frequency neurons in the lateral superior olive exhibit phase-sensitive binaural inhibition. *J Neurophysiol* 65: 598–605.

Ford MC, Grothe B, Klug A. 2009. Fenestration of the calyx of Held occurs sequentially along the tonotopic axis, is influenced by afferent activity, and facilitates glutamate clearance. *J Comp Neurol* 514: 92–106.

Fox MA, Sanes JR. 2007. Synaptotagmin I and II are present in distinct subsets of central synapses. *J Comp Neurol* 503: 280–296.

Fremeau RT Jr, Burman J, Qureshi T, Tran CH, Proctor J, Johnson J, Zhang H, Sulzer D, Copenhagen DR, Storm-Mathisen J, Reimer RJ, Chaudhry FA, Edwards RH. 2002. The identification of vesicular glutamate transporter 3 suggests novel modes of signaling by glutamate. *Proc Natl Acad Sci U S A* 99: 14488–14493.

Friauf E. 1993. Transient appearance of calbindin-D28k-positive neurons in the superior olivary complex of developing rats. *J Comp Neurol* 334: 59–74.

Friauf E, Hammerschmidt B, Kirsch J. 1997. Development of adult type inhibitory glycine receptors in the central auditory system of rats. *J Comp Neurol* 385: 117–134.

Friauf E, Aragon C, Lohrke S, Westernfelder B, Zafra F. 1999. Developmental expression of the glycine transporter GLYT2 in the auditory system of rats suggests involvement in synapse maturation. *J Comp Neurol* 412: 17–37.

Gillespie DC, Kim G, Kandler K. 2005. Inhibitory synapses in the developing auditory system are glutamatergic. *Nat Neurosci* 8: 332–338.

Gras C, Herzog E, Bellenchi GC, Bernard V, Ravassard P, Pohl M, Gasnier B, Giros B, El Mestikawy S. 2002. A third vesicular glutamate transporter expressed by cholinergic and serotoninergic neurons. *J Neurosci* 22: 5442–5451.

Gras C, Amilhon B, Lepicard EM, Poirel O, Vinatier J, Herbin M, Dumas S, Tzavara ET, Wade MR, Nomikos GG, Hanoun N, Saurini F, Kemel ML, Gasnier B, Giros B, El Mestikawy S. 2008. The vesicular glutamate transporter VGLUT3 synergizes striatal acetylcholine tone. *Nat Neurosci* 11: 292–300.

Groffen AJ, Martens S, Díez Arazola R, Cornelisse LN, Lozovaya N, de Jong AP, Goriounova NA, Habets RL, Takai Y, Borst JG, Brose N, McMahon HT, Verhage M. 2010. Doc2b is a high-affinity Ca^{2+} sensor for spontaneous neurotransmitter release. *Science* 327: 1614–1618.

Grønborg M, Pavlos NJ, Brunk I, Chua JJ, Münster-Wandowski A, Riedel D, Ahnert-Hilger G, Urlaub H, Jahn R. 2010. Quantitative comparison of glutamatergic and GABAergic synaptic vesicles unveils selectivity for few proteins including MAL2, a novel synaptic vesicle protein. *J Neurosci* 30: 2–12.

Helfert RH, Bonneau JM, Wenthold RJ, Altschuler RA. 1989. GABA and glycine immunoreactivity in the guinea pig superior olivary complex. *Brain Res* 501: 269–286.

Henkel CK, Brunso-Bechtold JK. 1998. Calcium-binding proteins and GABA reveal spatial segregation of cell types within the developing lateral superior olivary nucleus of the ferret. *Micr Res Tech* 41: 234–245.

Ito T, Bishop DC, Oliver DL. 2011. Expression of glutamate and inhibitory amino acid vesicular transporters in the rodent auditory brainstem. *J Comp Neurol* 519: 316–340.

Johnson J, Fremeau RT Jr, Duncan JL, Rentería, RC, Yang H, Hua Z, Liu X, LaVail MM, Edwards RH, Copenhagen DR. 2007. Vesicular glutamate transporter 1 is required for photoreceptor synaptic signaling but not for intrinsic visual functions. *J Neurosci* 27: 7245–7255.

Kakazu Y, Akaike N, Komiyama S, & Nabekura J. 1999. Regulation of intracellular chloride by cotransporters in developing lateral superior olive neurons. *J Neurosci* 19: 2843-2851.

Kandler K. 2004. Activity-dependent organization of inhibitory circuits: lessons

from the auditory system. *Curr Opin Neurobiol* 14: 96–104.

Kandler K, Friauf E. 1993. Pre- and postnatal development of efferent connections of the cochlear nucleus in the rat. *J Comp Neurol* 328: 161–184.

Kandler K, Friauf E. 1995. Development of glycinergic and glutamatergic synaptic transmission in the auditory brainstem of perinatal rats. *J Neurosci* 15: 6890–6904.

Kim G, Kandler K. 2003. Elimination and strengthening of glycinergic/GABAergic connections during tonotopic map formation. *Nat Neurosci* 6: 282–290.

Korada S, Schwartz IR. 1999. Development of GABA, glycine, and their receptors in the auditory brainstem of gerbil: a light and electron microscopic study. *J Comp Neurol* 409: 664–681.

Kotak VC, Sanes DH. 1995. Synaptically evoked prolonged depolarizations in the developing auditory system. *J Neurophysiol* 74: 1611–1620.

Kotak VC, Korada S, Schwartz IR, Sanes DH. 1998. A developmental shift from GABAergic to glycinergic transmission in the central auditory system. *J*

Neurosci 18: 4646–4655.

Kros CJ, Ruppersberg JP, Rüsch A. 1998. Expression of a potassium current in inner hair cells during development of hearing in mice. *Nature* 394: 281–284.

Kungel M, Friauf E. 1997. Physiology and pharmacology of native glycine receptors in developing rat auditory brainstem neurons. *Dev Brain Res* 102: 157–165.

Li Q, Lau A, Morris TJ, Guo L, Fordyce CB, Stanley EF. 2004. A syntaxin 1, Galpha(o), and N-type calcium channel complex at a presynaptic nerve terminal: analysis by quantitative immunocolocalization. *J Neurosci* 24: 4070–4081.

Matthew WD, Tsavaler L, Reichardt LF. 1981. Identification of a synaptic vesicle-specific membrane protein with a wide distribution in neuronal and neurosecretory tissue. *J Cell Biol* 91: 257–269.

McIntire SL, Reimer RJ, Schuske K, Edwards RH, Jorgensen EM. 1997. Identification and characterization of the vesicular GABA transporter. *Nature* 389: 870–876.

Melone M, Burette A, Weinberg RJ. 2005. Light microscopic identification and immunocytochemical characterization of glutamatergic synapses in brain sections. *J Comp Neurol* 492: 495–509.

Montana V, Ni Y, Sunjara V, Hua X, Parpura V. 2004. Vesicular glutamate transporter-dependent glutamate release from astrocytes. *J Neurosci* 24: 2633–2642.

Moore MJ, Caspary DM. 1983. Strychnine blocks binaural inhibition in lateral superior olivary neurons. *J Neurosci* 3: 237–242.

Nabekura J, Katsurabayashi S, Kakazu Y, Shibata S, Matsubara A, Jinno S, Mizoguchi Y, Sasaki A, Ishibashi H. 2004. Developmental switch from GABA to glycine release in single central synaptic terminals. *Nat Neurosci* 7: 17–23.

Noh J, Seal RP, Garver JA, Edwards RH, Kandler K. 2010. Glutamate co-release at GABA/glycinergic synapses is crucial for the refinement of an inhibitory map. *Nat Neurosci* 13: 232–238.

Onoa B, Li H, Gagnon-Bartsch JA, Elias LA, Edwards RH. 2010. Vesicular

monoamine and glutamate transporters select distinct synaptic vesicle recycling pathways. *J Neurosci* 30: 7917–7927.

Pang ZP, Sun J, Rizo J, Maximov A, Sudhof TC. 2006. Genetic analysis of synaptotagmin 2 in spontaneous and Ca^{2+} triggered neurotransmitter release. *EMBO J* 25: 2039–2050.

Pothos EN, Larsen KE, Krantz DE, Liu Y, Haycock JW, Setlik W, Gershon MD, Edwards RH, Sulzer D. 2000. Synaptic vesicle transporter expression regulates vesicle phenotype and quantal size. *J Neurosci* 20: 7297–7306.

Sanes DH, Chokshi P. 1992. Glycinergic transmission influences the development of dendrite shape. *Neuroreport* 3: 323–326.

Sanes DH, Friauf E. 2000. Development and influence of inhibition in the lateral superior olivary nucleus. *Hear Res* 147: 46–58.

Sanes DH, Takacs C. 1993. Activity-dependent refinement of inhibitory connections. *Eur J Neurosci* 5: 570–574.

Smith PH, Joris PX, Carney LH, Yin TCT. 1991. Projections of physiologically characterized globular bushy cell axons from the cochlear nucleus of the

cat. *J Comp Neurol* 304: 387–407.

Sommer I, Lingenhöhl K, Friauf E. 1993. Principal cells of the rat medial nucleus of the trapezoid body: an intracellular in vivo study of their physiology and morphology. *Exp Brain Res* 95: 223–239.

Südhof TC. 2002. Synaptotagmins: why so many? *J Biol Chem* 277: 7629–7632.

Takamori S, Riedel D, Jahn R. 2000. Immunoisolation of GABA-specific synaptic vesicles defines a functionally distinct subset of synaptic vesicles. *J Neurosci* 20: 4904–4911.

Tritsch NX, Bergles DE. 2010. Developmental regulation of spontaneous activity in the mammalian cochlea. *J Neurosci* 30: 1539–1550.

Tritsch NX, Yi E, Gale JE, Glowatzki E, Bergles DE. 2007 The origin of spontaneous activity in the developing auditory system. *Nature* 450: 50–55.

Wu LG, Borst JG. 1999. The reduced release probability of releasable vesicles during recovery from short-term synaptic depression. *Neuron* 23: 821–832.

Wu SH, Kelly JB. 1992. Synaptic pharmacology of the superior olivary complex studied in mouse brain slice. *J Neurosci* 12: 3084–3097.

Xiao L, Han Y, Runne H, Murray H, Kochubey O, Luthi-Carter R, Schneggenburger R. 2010. Developmental expression of synaptotagmin isoforms in single calyx of Held-generating neurons. *Mol Cell Neurosci* 44: 374–385.

Xu J, Mashimo T, Sudhof TC. 2007. Synaptotagmin-1, -2, and -9: Ca(2+) sensors for fast release that specify distinct presynaptic properties in subsets of neurons. *Neuron* 54: 567–581.

Xu J, Pang ZP, Shin OH, Südhof TC. 2009. Synaptotagmin-1 functions as a Ca^{2+} sensor for spontaneous release. *Nat Neurosci* 12: 759–766.

Chapter 4: Synaptotagmin I is expressed at a GABA/glycine/glutamate-releasing central synapse, independent of vesicular glutamate transporter 3 expression

Abstract

The continuing discovery of synapses that use multiple transmitters has raised new questions about synaptic transmission, vesicular phenotype, and protein targeting. During an early period of circuit refinement, synaptic terminals in the brainstem MNTB-LSO pathway release the three classic small amino acid transmitters: GABA, glycine, and glutamate. Slice physiology strongly suggests that these terminals contain two vesicle populations, one a GABA- and glycinergic population characterized by the expression of the vesicular inhibitory amino acid transporter (VIAAT) and the other a glutamatergic population characterized by expression of vesicular glutamate transporter 3 (VGLUT3).

We recently found that the immature MNTB-LSO synapse expresses both synaptotagmin 1 (Syt1) and synaptotagmin 2 (Syt2). As Syt1 and VGLUT3 exhibit similar spatial and temporal expression patterns and co-localize in MNTB terminals, the working model for this synapse posits a population of vesicles uniquely characterized by co-expression of VGLUT3 and Syt1. Similarly, Syt2 and VIAAT are both prominently expressed in the SOC and co-localize in MNTB terminals at all ages of postnatal development, and the working model suggests that Syt2 and VIAAT are co-expressed on another population of vesicles. This

model raises the question of whether one of these synaptic proteins might influence expression and/or trafficking of the other protein.

We asked whether VGLUT3 is necessary for Syt1 expression in MNTB synaptic terminals by immunostaining for Syt1 in tissue from both wildtype and VGLUT3 knockout mice. We found that Syt1 was expressed at normal levels, and that Syt1 protein was present in the MNTB-LSO synaptic terminals, regardless of VGLUT3 expression. Thus, in the MNTB-LSO pathway, VGLUT3 expression is not necessary either for Syt1 expression or for targeting of Syt1 to synaptic terminals.

Introduction

The superior olivary complex in the auditory brainstem includes several nuclei involved in sound localization. The lateral superior olive (LSO) computes interaural level differences (ILDs) by comparing converging excitatory glutamatergic inputs from the ipsilateral ventral cochlear nucleus (VCN) with inhibitory glycinergic inputs from the ipsilateral medial nucleus of the trapezoid body (MNTB), which are driven by glutamatergic inputs from the contralateral VCN (Tollin, 2003). The ILD computation performed by LSO principal neurons requires the converging inputs to be tonotopically aligned and this alignment happens during early postnatal life through successive periods of refinement (Kandler et al, 2009). Although some aspects of refinement in the VCN-LSO

projection are known (Case et al, 2011), more is known about refinement in the MNTB-LSO projection.

In the MNTB-LSO pathway, inputs are strengthened or weakened resulting in a functional tonotopic map being achieved by postnatal day 8 (P8) (Kim and Kandler, 2003). The mechanisms underlying refinement at this inhibitory synapse are poorly understood. Before hearing onset, the MNTB projection, which was traditionally thought to be purely glycinergic, also releases GABA and the two neurotransmitters are released from the same vesicle (Kotak et al 1998, Korada and Schwartz, 1999, Nabekura et al 2004). Interestingly, before hearing onset, MNTB terminals also release the excitatory neurotransmitter glutamate and this glutamate release coincides with transient expression of vesicular glutamate transporter 3 (VGLUT3) in MNTB terminals (Gillespie et al, 2005). This raises new questions about whether glutamate is released from the same vesicles as GABA/glycine or if there are two populations of vesicles.

Electrophysiological evidence from the lab suggests that glutamate is released from a separate pool of vesicles than GABA/glycine (unpublished observations). Based on these data, we propose that there are two populations of vesicles at immature MNTB terminals, one a GABA- and glycinergic population characterized by the expression of VIAAT and the other a glutamatergic population characterized by expression of vesicular glutamate transporter 3 (VGLUT3).

Recent findings from the lab show that the GABA/glycine and glutamate have different paired pulse ratios, suggesting that the two populations differ in their synaptic machinery (Case and Gillespie, 2011, Alamilla and Gillespie, 2013). Among the factors that can influence release properties are: location in the presynaptic terminal, association with voltage-gated calcium sensors, and the calcium sensor present on the vesicles. Recently, we found that two calcium sensors, synaptotagmin 1 (Syt1) and synaptotagmin 2 (Syt2), are present at immature MNTB terminals (Cooper and Gillespie, 2011). Syt2 is expressed across development and at both excitatory and inhibitory terminals in the LSO. Syt1, on the other hand, is only expressed during the first two postnatal weeks (the period of glutamate release from MNTB terminals) and is specifically associated with inhibitory terminals in the LSO. Interestingly, the temporal and spatial expression patterns of Syt1 and VGLUT3 are closely matched and our working model suggests that Syt1 and VGLUT3 are co-expressed on the glutamatergic population of vesicles whereas Syt2 and VIAAT are co-expressed on the GABA/glycinergic population of vesicles (see schematic below).

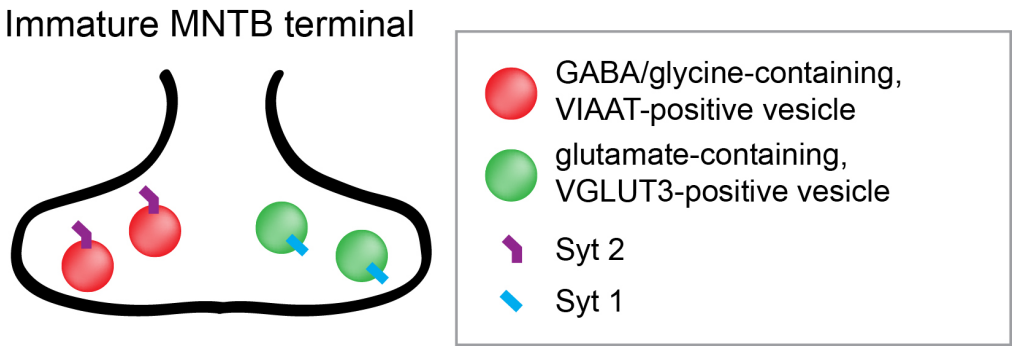

A schematic of our updated working model of vesicle populations at the immature MNTB terminal. The immature MNTB terminal contains two populations of vesicles; one population that is GABA/glycinergic and expresses VIAAT and Syt2 and one that is glutamatergic and expresses VGLUT3 and Syt1. This arrangement is based on the spatial and temporal expression patterns of Syt1, Syt2, VGLUT3, and VIAAT seen in Chapter 2 of this thesis.

If GABA/glycine and glutamate are released from separate vesicle populations, then the precise sorting of vesicular transporters to separate vesicles must be maintained, and, according to our model, Syt1 and Syt2 must also be precisely sorted to the correct population. The idea that the cell can tightly regulate the expression of certain proteins on synaptic vesicles has recently been shown. Analysis of single vesicles from whole-brain samples shows that the copy number of certain vesicular proteins exhibits little variance (Mutch et al, 2011). The number of copies of synaptic vesicle protein 2 (SV2), VGLUT1, and Syt1 showed little intervesicle variability, indicating their expression

was tightly regulated. In contrast, the copy number of synaptophysin and synaptobrevin 2 was considerably variable, indicating their expression was less regulated. This raises an interesting question: what regulates the copy number of proteins on a vesicle? The mechanisms that control the expression and number of vesicular proteins are poorly understood but there is evidence that protein-protein interactions are among the potential mechanisms. For example, the expression and trafficking of Syt1 to vesicles is controlled by SV2 (Yao et al, 2010). Regarding the immature MNTB-LSO terminal, if the Syt1:VGLUT3 and Syt2:VIAAT arrangement is accurate, then how is the arrangement maintained and could the expression of one vesicular protein influence the expression and/or trafficking of another vesicular protein?

We focused on a possible interaction between Syt1 and VGLUT3. First, we asked if VGLUT3 was required for the expression of Syt1. To answer this we performed immunostaining for Syt1 in wildtype and VGLUT3$^{-/-}$ mice and looked for Syt1-immunoreactivity in the LSO and SPN, two nuclei that receive prominent inhibitory projections from the MNTB**.** Second, we asked if VGLUT3 was required for targeting Syt1 to MNTB terminals in wildtype mice and VGLUT3$^{-/-}$ mice. Using VIAAT as a marker of MNTB terminals, we looked for Syt1 at VIAAT positive sites in the LSO and SPN of wildtype and VGLUT3$^{-/-}$ mice.

Methods

All experimental procedures involving animals were approved by McMaster University's Animal Research Ethics Board and conformed to guidelines outlined by the Canadian Council on Animal Care. Mice heterozygous for VGLUT3 (gift of Salah el Mestikawy) were bred resulting in litters of wildtype (+/+), heterozygous (+/-), and knockout (-/-) mouse pups. The central experiments in this study were carried out in two litters of mice, using pups at ages postnatal day 3 (P3) and P7. Animals were euthanized and perfused transcardially with 0.1 M phosphate-buffered saline (PBS; pH 7.4), followed by ice-cold paraformaldehyde in 0.1 M phosphate buffer (PB; pH 7.4). Brains were postfixed in 4% paraformaldehyde for 18 hours before being transferred to 30% sucrose in 0.1 M PBS for cryoprotection.

Genotyping

DNA was obtained from tail samples that were cut at the time of tissue harvesting. Mice were identified by PCR analysis using primers located in the VGLUT3 wildtype (278bp) and VGLUT3 knockout cassette (604bp) primers (Gras et al, 2008, Mobix Lab, McMaster University). Primer bands were identified using gel electrophoresis.

Tissue processing and immunohistochemistry

Coronal sections containing the superior olivary complex (SOC) were cut at 40 µm on a freezing microtome and collected into 0.1 M PB (pH 7.4). Both the P3 and the P7 litters contained a brain from a wildtype mouse, a heterozygote mouse, and a VGLUT3-/- mouse. The data from the heterozygote mice will not be shown nor discussed in this manuscript. The brains from each litter were cut, stained, and imaged at the same time for consistency within runs. The P7 litter was processed first and was stained only for Syt1. The P3 litter was processed next and was double-stained for Syt1 and VIAAT. The results shown below are from a total of four brains (P3 wildtype, P3 VGLUT3-/-, P7 wildtype, and P7 VGLUT3-/-. Each brain yielded 2-6 SOCs to study. Affinity-purified secondary antibodies conjugated to Alexa dyes were used at a dilution of 1:500.

Table 1.

Antibodies Used in This Study				
Antigen	**Immunogen**	**Host**	**Source/cat. No.**	**Dilution**
Synaptotagmin 1 (mab 48)	Rat synaptic junctional complexes	Mouse, monoclonal	Developmental Studies Hybridoma Bank	1:50
VIAAT	Synthetic peptide, AEPPVEGDIHYQR	Rabbit, polyclonal	Synaptic Systems, 131 002	1:1000
gtXms ALEXA 647 IgG2B		Goat	Jackson Immunoresearch,	1:500
gtX rb Alexa 555		Goat	Jackson Immunoresearch,	1:500

All immunohistochemistry was performed on free-floating sections at 4° C. Tissue sections were blocked for 24 hours in a serum solution containing 5%

normal goat serum, 2.5% bovine serum albumin (BSA), and 0.5% triton X-100 in PBS (pH 7.4). Sections were then incubated in primary antibodies (diluted in 5% normal goat serum, 2.5 % BSA in 0.1 M PBS, pH 7.4) for 72 hours. After washes in PBS, sections were incubated in secondary (diluted in 5% normal goat serum, 2.5 % BSA in 0.1 M PBS, pH 7.4) for 12 hours. Sections were washed in PBS before being mounted and coverslipped with mounting medium (DAKO).

Image acquisition and analysis

Images were acquired on the confocal microscope (Nikon D-Eclipse C1). Low-magnification images of auditory brainstem were collected using a 20X objective lens (NA 0.75) to study the expression of Syt1 in the developing SOC and for semi-quantitative immunohistochemistry. For intensity measurements, the laser intensity, PMT gain, and all other settings were kept constant for all images acquired within a given staining run. Images were converted to 8-bit tiff files for import to Fiji (Fiji Is Just ImageJ, Schindelin et al, 2012). In Fiji, the signal channels were separated, and fluorescence intensity of Syt1-immunoreactivity was measured by using the low-magnification images. Mean pixel intensity was measured in the lateral LSO, the medial LSO and the SPN. To control for differences in background tissue fluorescence, mean pixel intensity of the reticular formation dorsal to the MNTB was subtracted from the mean pixel intensity for each ROI within the same tissue section. As these values are not absolute, descriptive statistics only are shown for these measures.

High-magnification images were collected using a 60X objective (NA 1.40) at settings that used the full dynamic range of the pixel values. Tissue sections labeled with two fluorophores were imaged sequentially.

Representative images shown in this manuscript were adjusted for brightness and contrast for the purposes of illustration. Quantification was performed on original, unaltered images.

Results

We used single and double-immunofluorescence labeling in fixed tissue from wildtype and VGLUT3$^{-/-}$ mouse pups to study the patterns of Syt1-IR in the LSO and SPN and to study the position of Syt1-IR relative to a marker of inhibitory terminals, VIAAT.

Syt1-IR in wildtype and VGLUT3$^{-/-}$ mice

We first examined Syt1 expression in the LSO and SPN of wildtype mice at postnatal day 3 (P3) and P7. We found Syt1 to be expressed in both the LSO and the SPN during the first postnatal week (Fig. 1). At P3, Syt1-IR appeared equally bright across the mediolateral axis of the LSO (Fig. 1, 2) except for a characteristic bright strip of Syt1-IR at the medial, marginal border of the LSO (Fig. 1B). At P7, Syt1-IR also appeared uniformly bright across the mediolateral axis of the LSO. The sample image of the LSO in the P7 wildtype brain contained only a portion of the LSO, therefore we did not see the characteristic strip of Syt1-

IR at the medial edge of the nucleus. In the SPN, Syt1-immunofluorescence was consistently brighter than that in the LSO (Fig. 1, 2).

Syt1-IR was also present in the LSO and SPN of VGLUT3$^{-/-}$ mice at P3 and P7. At both P3 and P7, Syt1-IR was uniformly bright across the LSO (Fig. 1, 2) and a bright strip of Syt1 expression at the medial, marginal border. The sample image of the LSO from a VGLUT3$^{-/-}$ mouse at P3 shows an incomplete LSO; however, the characteristic strip was still present. As was the case in the wildtype, Syt1-IR was stronger in the SPN than the LSO.

In order to be confident in the Syt1-IR in the LSO and SPN, we looked for clusters of Syt1-IR at high magnification. There were clearly identifiable Syt1-IR puncta in both the LSO and SPN in the wildtype and the VGLUT3$^{-/-}$ mice (Fig. 3, 4). In the LSO, there was no obvious subcellular distribution pattern of Syt1 puncta (Fig. 3A-D) whereas in the SPN, the pattern of Syt1 puncta in the P7 wildtype tissue suggested that Syt1 was located around the somata and proximal dendrites (Fig. 4B). Based on these results, the answer to our first question is that VGLUT3 is not required for the expression of Syt1 in the LSO or SPN.

Although VGLUT3 is not required for Syt1 expression in MNTB terminals, it is possible that VGLUT3 targets Syt1 to MNTB terminals and/or glutamatergic vesicles. If VGLUT3 directs the targeting of Syt1 to the terminal, then we would not expect to see any Syt1 at VIAAT-positive inhibitory terminals in VGLUT3$^{-/-}$ mice. Next, we did a double stain for VIAAT and Syt1 to see if VGLUT3 was required to direct Syt1 to the terminal (Fig. 5). Syt1-IR clusters co-localized with

VIAAT-IR clusters in the LSO of wildtype and VGLUT3$^{-/-}$ mice (Fig. 6A-B''). Syt1-IR clusters also co-localized with VIAAT-IR clusters in the SPN of wildtype and VGLUT3$^{-/-}$ mice (Fig. 7A-B')'. In conclusion, VGLUT3 is not required for targeting Syt1 to the terminals of immature inhibitory projections from the MNTB to the LSO or to the SPN.

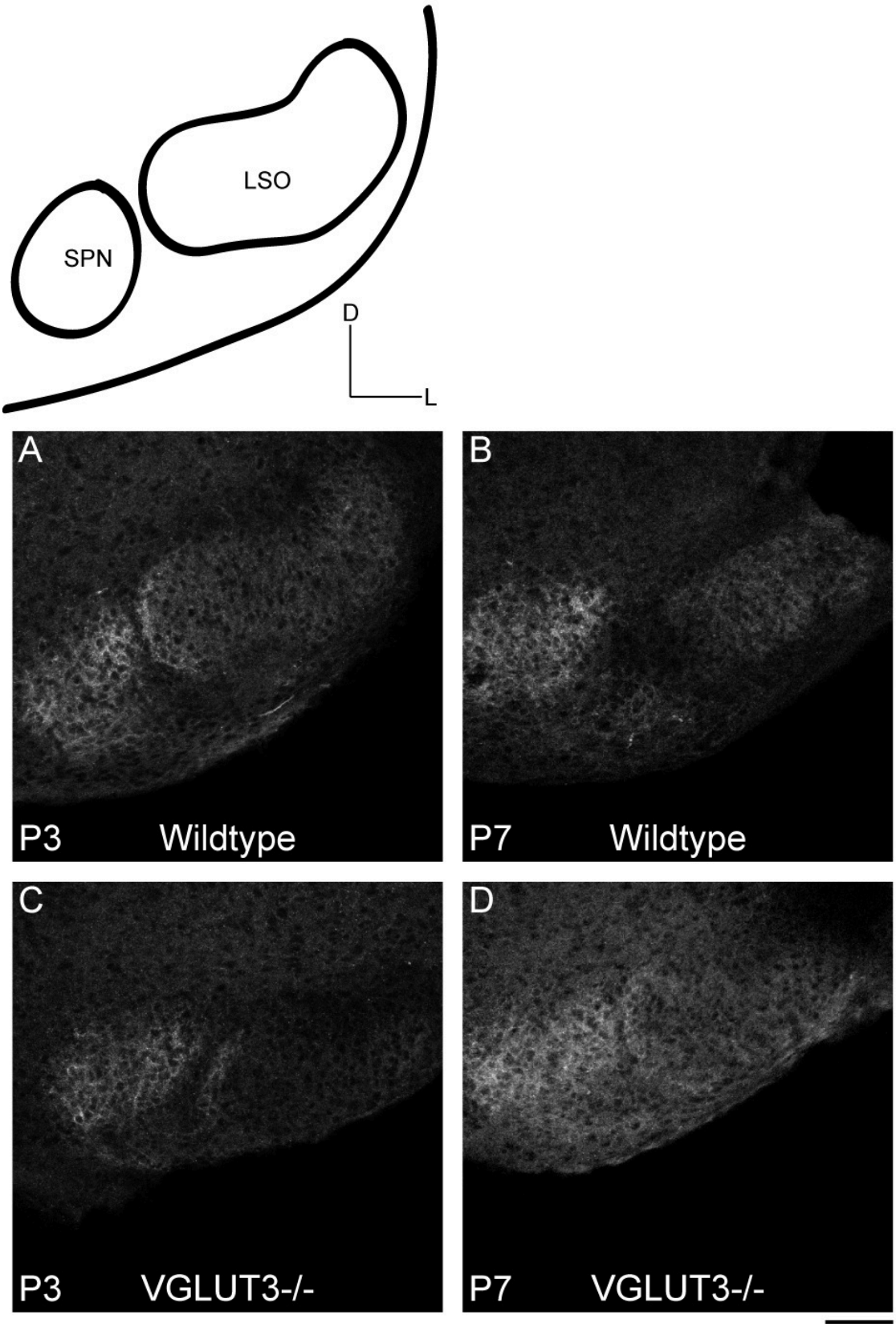
LSO
SPN
D
L
A
P3 Wildtype
B
P7 Wildtype
C
P3 VGLUT3-/-
D
P7 VGLUT3-/-

Figure 1. Syt1-IR appears in the LSO and SPN of both wildtype and VGLUT3$^{-/-}$ mice. **A:** Schematic of the LSO and SPN from a coronal section through early postnatal mouse auditory brainstem. L is lateral, D is dorsal. **B-E:** Example micrographs of Syt1-IR in the LSO and SPN of a P3 wildtype mouse (B), a P7 wildtype mouse (C), a P3 VGLUT3$^{-/-}$ mouse, and a P7 VGLUT3$^{-/-}$ mouse (D). Syt1-IR in the LSO is weaker than Syt1-IR in the SPN. Syt1-IR appears consistently bright across the medio-lateral axis of the LSO, except for a strip of strong Syt1-IR wrapping around the medial margin of the LSO.
Scale bar = 100 μm.

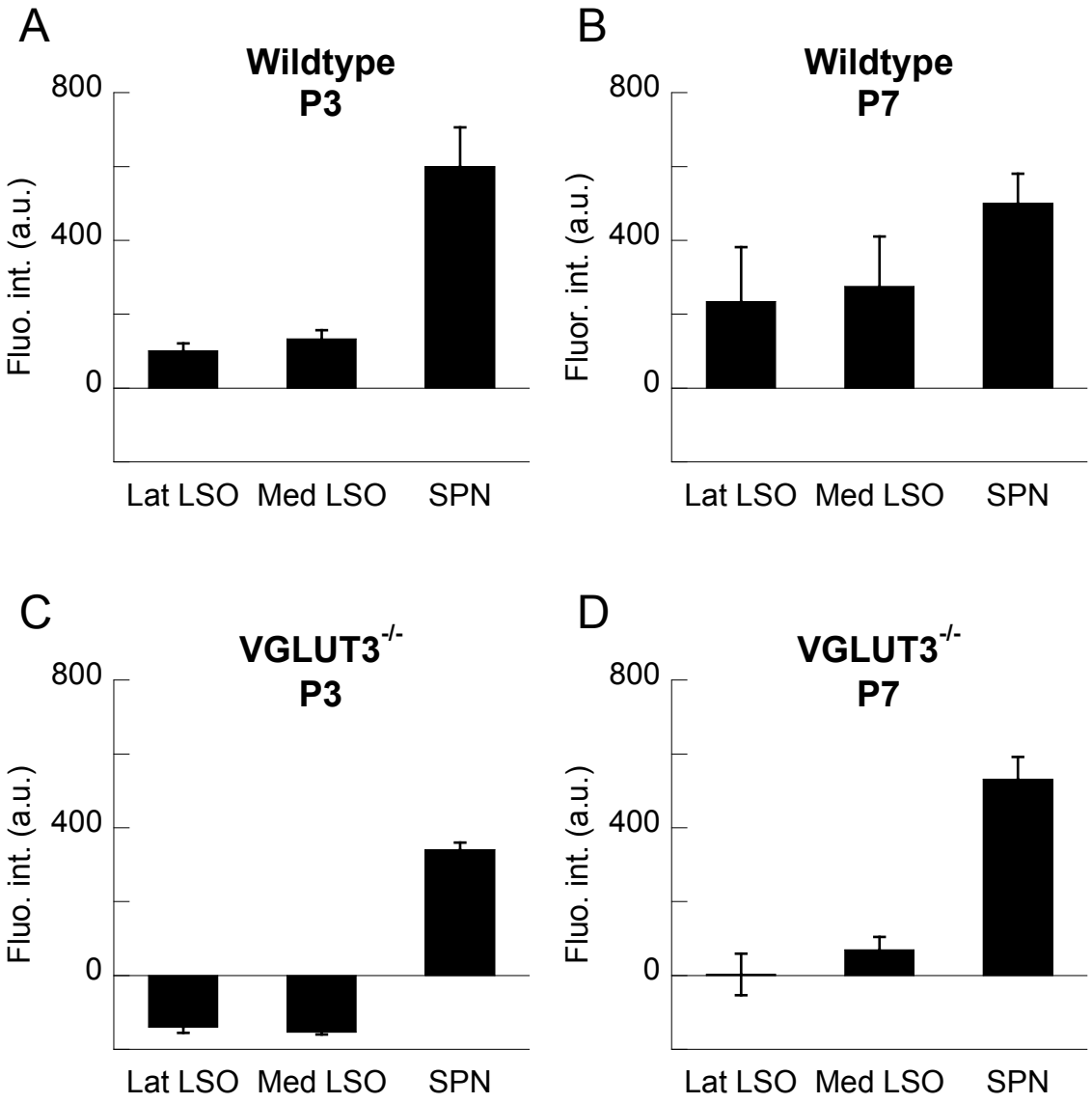

Figure 2. Syt1 expression levels in the LSO and SPN of wildtype and VGLUT3$^{-/-}$ mice. **A-D:** Quantification of fluorescence intensity of Syt1-IR in the lateral limb of the LSO (Lat LSO), medial limb of the LSO (Med LSO), and the SPN from P3 wildtype mice (A), P7 wildtype mice (B), P3 VGLUT3$^{-/-}$ mice (C), and P3 VGLUT3$^{-/-}$ mice(D). Fluorescence intensity is consistently higher in the SPN than in the LSO. Negative values indicate that staining intensity with the area of interest is

below background levels. Fluor. int., fluorescence intensity; a.u. arbitrary units. Error bars represent ± 1 s.e.m.

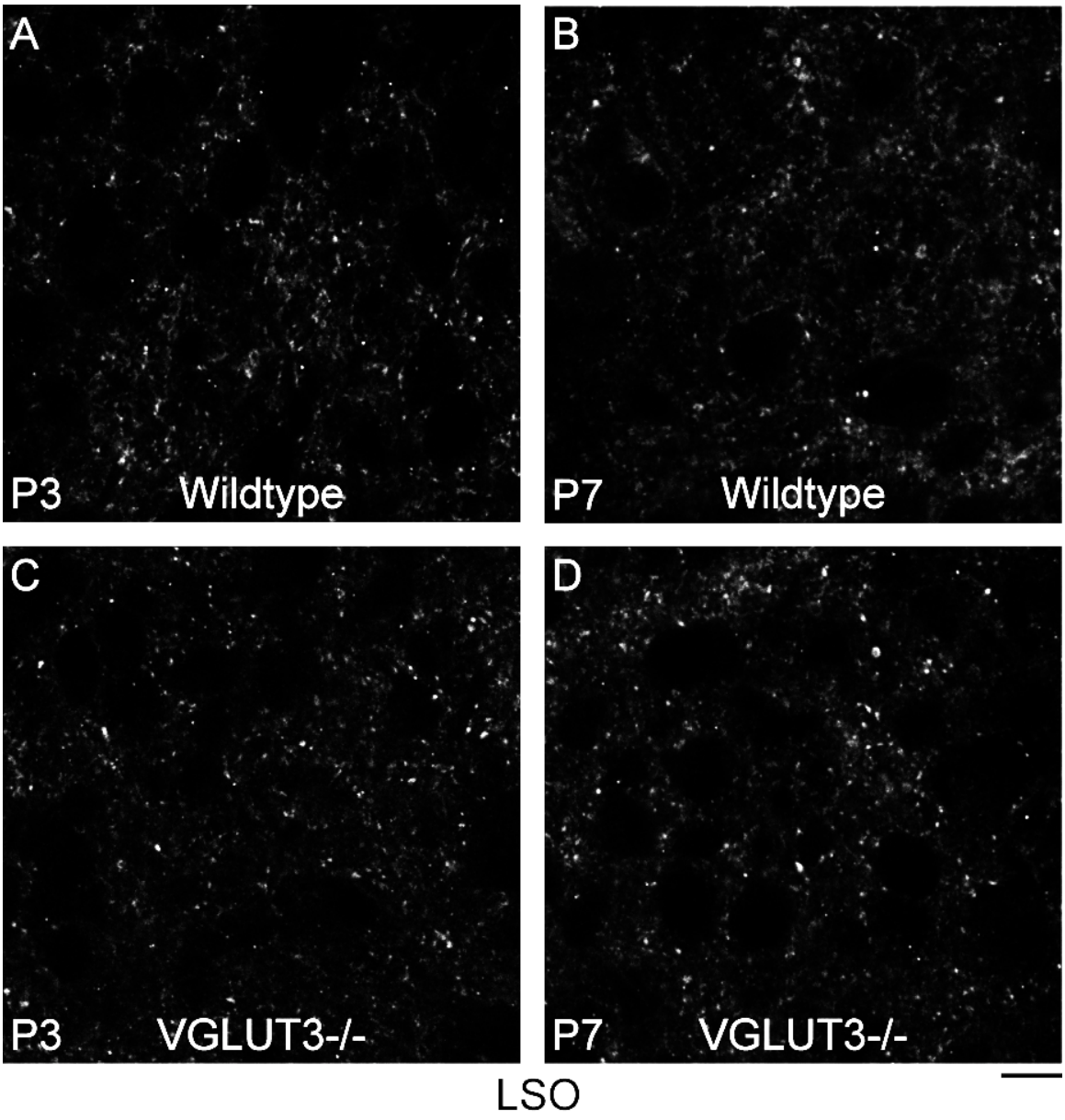

Figure 3. Syt1-IR clusters are present in the LSO of both wildtype and VGLUT3$^{-/-}$ mice. **A-D:** Example micrographs of Syt1-IR in the LSO of a P3 wildtype mouse (A), a P7 wildtype mouse (B), a P3 VGLUT3$^{-/-}$ mouse (C), and a P7 VGLUT3$^{-/-}$ mouse (D). Scale bar = 10 µm.

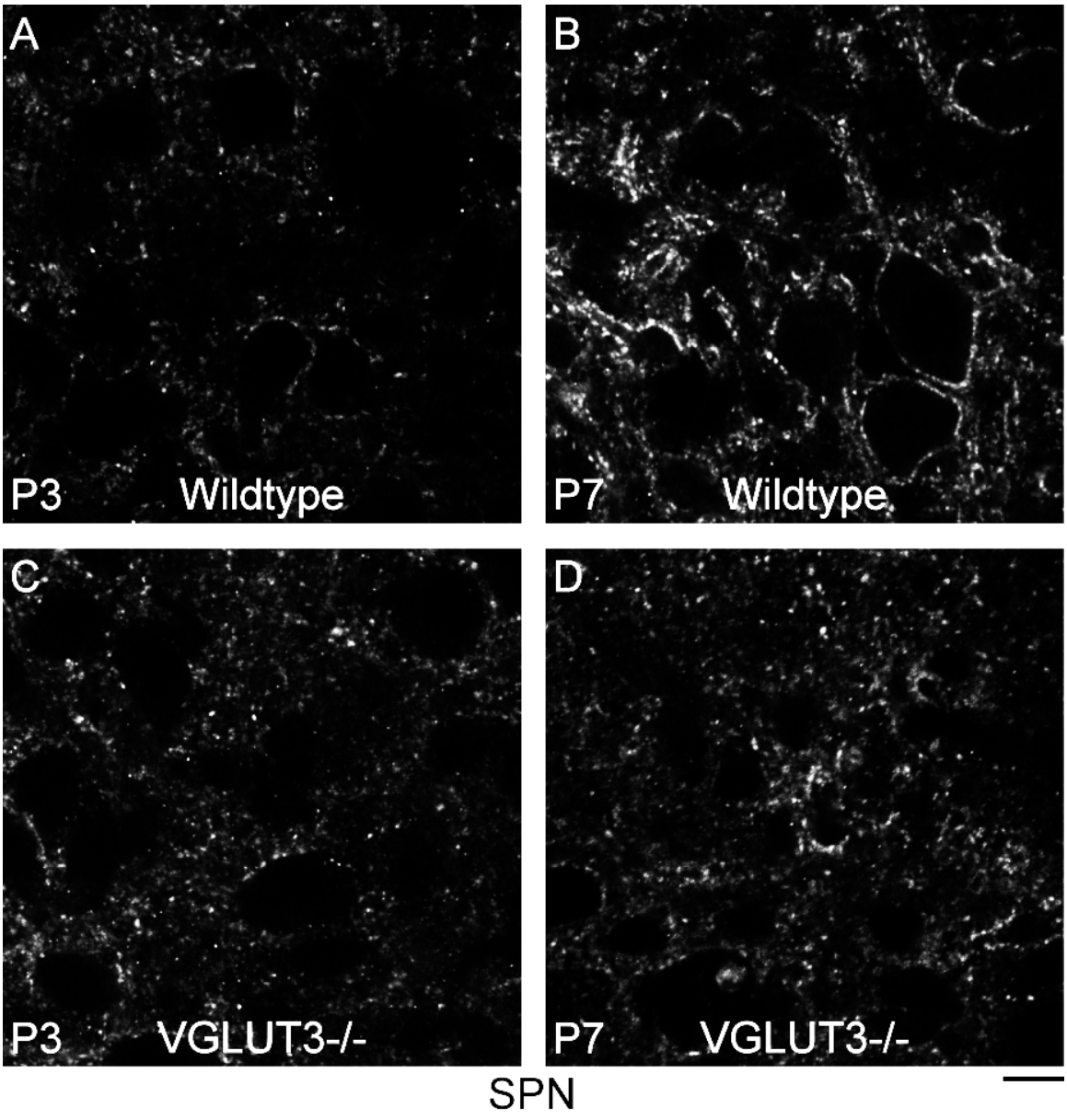

Figure 4. Syt1-IR clusters are present in the SPN of both wildtype and VGLUT3$^{-/-}$ mice. **A-D:** Example micrographs of Syt1-IR in the SPN of a P3 wildtype mouse (A), a P7 wildtype mouse (B), a P3 VGLUT3$^{-/-}$ mouse (C), and a P7 VGLUT3$^{-/-}$ mouse (D). Syt1-IR clusters appear to outline the somata and proximal dendrites

of SPN neurons in the P7 wildtype tissue (B), but not in the P3 wildtype nor in the VGLUT3$^{-/-}$ knockout tissue. Scale bar = 10 μm.

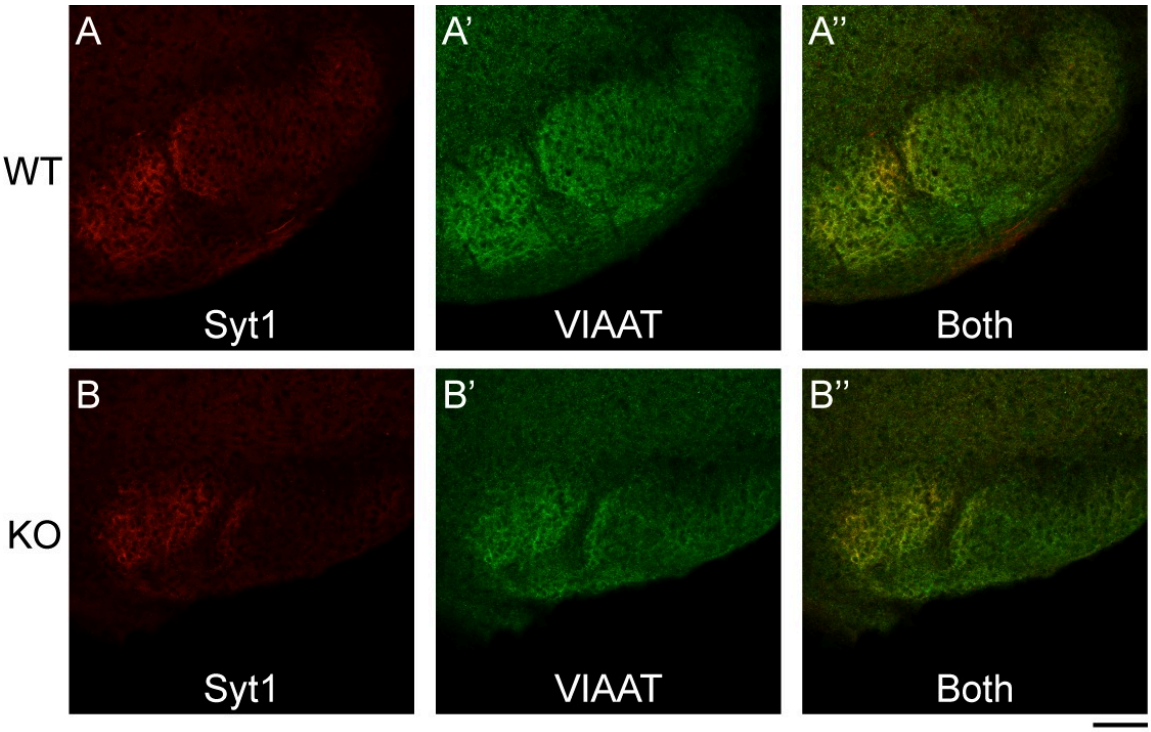

Figure 5. Syt1 (red) and VIAAT (green) in the LSO and SPN of wildtype and VGLUT3$^{-/-}$ mice. **A-B":** Representative images show expression of Syt1-IR (red) VIAAT-IR (green), and both from a wildtype mouse pup (P3, A-A") and a VGLUT3$^{-/-}$ pup (P3, B-B"). Each image is a single confocal image taken with a 20X lens. Scale bar = 100 μm.

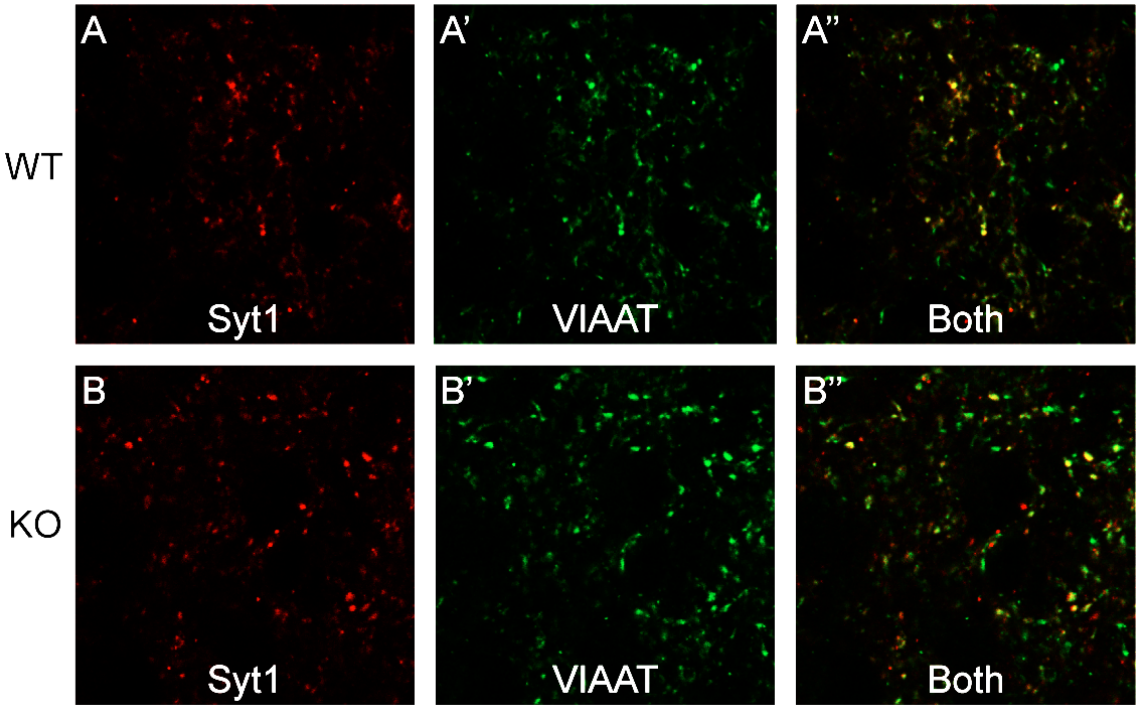

Figure 6. Syt1-IR is at VIAAT-positive inhibitory terminals in the LSO of both wildtype and VGLUT3$^{-/-}$ mice. **A-B''**: Representative images showing that Syt1-IR (red) co-localizes with VIAAT (green) immunoreactivity in the LSO of a P3 wildtype mouse (A-A'') and a VGLUT3 $^{-/-}$ mouse (B-B''). Scale bar = 5 μm.

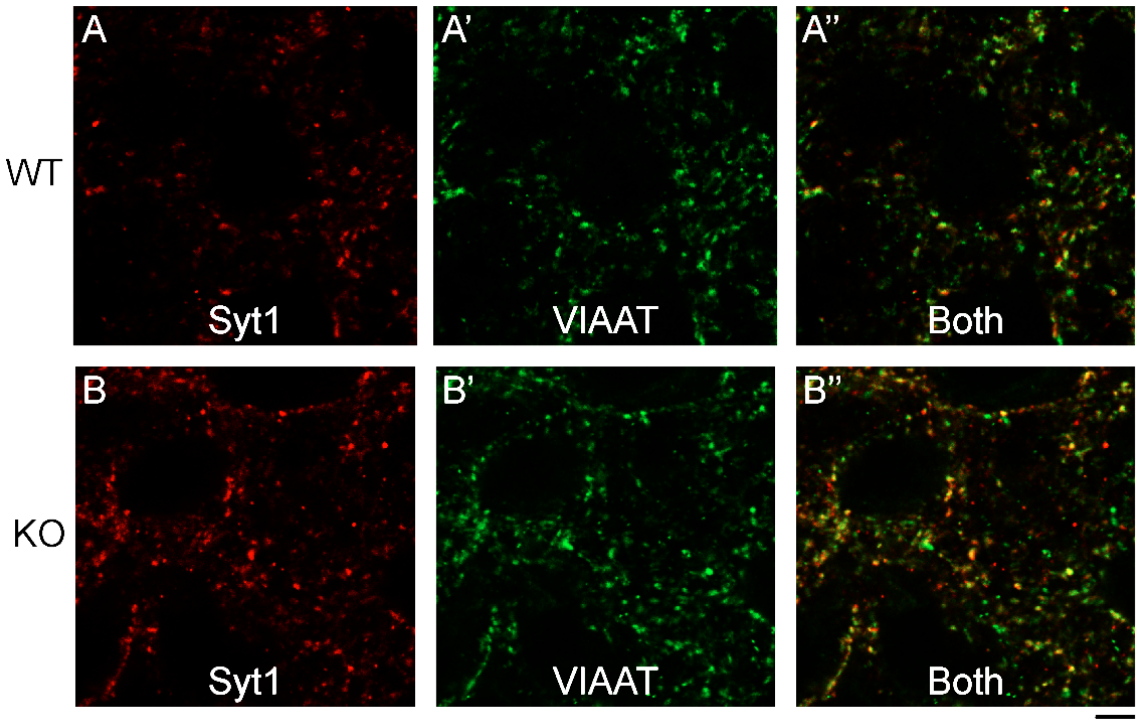

Figure 7. Syt1-IR is at VIAAT-positive inhibitory terminals in the SPN of both wildtype and VGLUT3$^{-/-}$ mice. **A-B'':** Representative images showing that Syt1-IR (red) co-localizes with VIAAT-IR (green) in the SPN of a P3 wildtype mouse (A-A'') and a P3 VGLUT3 $^{-/-}$ mouse (B-B''). Scale bar = 5 µm.

Discussion

Immature MNTB terminals release GABA/glycine, supported by the expression of VIAAT, and glutamate supported by the expression of VGLUT3. The immature terminal also expresses two calcium sensors, Syt1 and Syt2, and together these findings suggest a working model with Syt1 expressed on VGLUT3-positive vesicles and Syt2 expressed on VIAAT-positive vesicles. Here,

we asked if the expression or targeting of Syt1 was influenced by VGLUT3. We found that neither the expression nor the targeting of Syt1 was significantly affected by the deletion of VGLUT3. The fact that Syt1 is expressed in spite of the deletion of VGLUT3 does not necessarily weaken our working model, as a different synaptic vesicle protein could be mediating the targeting of the transporters and calcium sensors to the proper vesicles. It remains to be seen if Syt1 controls the expression or targeting of VGLUT3. This experiment was not conducted here because $Syt1^{-/-}$ tissue was unavailable.

Caveats

Although there were clear Syt1-IR puncta in both the wildtype and knockout mice, the noise levels were too high to measure correlational coefficients between Syt1- and VIAAT-IR puncta. It is expected to get some noisy labeling when using a primary antibody raised in the same species from which tissue is taken for staining. We did try to reduce this noise with our choice of secondary antibody. Since the isotype of our primary antibody is known (IgG2b), we used an IgG2b specific secondary antibody in order to reduced cross-reactivity between the secondary antibody and other protein isotypes.

It's possible that the deletion of VGLUT3 does impair the targeting of Syt1 to the vesicle, though not the terminal, and this would go undetected at the light microscopy level due to resolution limits. The scenario that Syt1 is transported to the terminal and remains at the terminal at normal levels without being used in

transmission seems unlikely because it would not serve the cell to have an extra spectator protein present at the active synapse. Regardless, whether Syt1 is present at the terminal or on the vesicle in VGLUT3$^{-/-}$ mice could potentially be resolved with higher resolution microscopy such as immunoelectron microscopy, stimulated-emission depletion microscopy (STED) microscopy, or total internal reflection fluorescence (TIRF) microscopy.

What could be controlling the expression and targeting of Syt1 to VGLUT3-positive vesicles?

The recent finding that certain synaptic proteins are expressed with little intervesicular variance suggests that there must be mechanisms that control the stoichiometry of vesicular proteins (Mutch et al, 2011). What regulates protein expression on the vesicle? Recently it was shown that SV2 can regulate a vesicle's sensitivity to calcium by altering the number of synaptotagmins on a vesicle (Yao et al, 2010). Given the proposed VGLUT3:Syt1 relationship at the immature MNTB terminal, it will be interesting to know what controls their expression.

Another major unanswered question is what signals the two populations into separate vesicle pools? We are beginning to understand how other groups of synaptic vesicles are sorted and trafficked at the terminal. At many central and peripheral synapses, synaptic vesicles are divided into three pools (or populations); a readily releasable pool (RRP), a recycling pool, and reserve pool.

These pools are released by different stimuli and are usually located in separate areas of the terminal bouton (Rizzoli and Betz, 2005). Interestingly, vesicles from a given pool often return to that same pool suggesting there are signals to return the vesicle/vesicular proteins back to its origin (Rizzoli and Betz, 2005). An important question has been how a given vesicle gets trafficked to one of the three pools following exocytosis. Evidence suggests that the adaptor proteins (AP) AP2, and AP3 play a role in recycling vesicles to distinct vesicle pools. AP2 is involved in restoring vesicles to the recycling pool, and AP3 is involved in repopulating the reserve pool (Voglmaier and Edwards, 2007). Exciting new research has shown that a number of vesicular proteins differentially interact (directly or indirectly) with AP2 and AP3, resulting in different vesicular proteins being trafficked to different vesicle pools. Interestingly, the vesicular proteins that have been shown to interact with adaptor proteins, and may therefore play a role in vesicle sorting, trafficking, and targeting, include VGLUT1, VIAAT, and Syt1 (Foss et al, 2013, Santos et al, 2013).

Could separate VIAAT-positive and VGLUT3-positive vesicle populations be maintained through the use sorting motifs on vesicular transporters or Ca^{++} sensors that differentially interact with population-specific adaptor proteins? Is the Syt1:VGLUT3/Syt2:VIAAT pairing achieved during endocytosis or at a subsequent stage in the synaptic vesicle cycle? Answering these questions will require pushing technical boundaries in order to reliably get single-vesicle resolution at a synapse with multiple vesicle populations. Nevertheless, answers

to these questions will give us a new understanding of vesicle sorting, protein targeting, and organization of co-releasing synapses.

Chapter 5: General Discussion

Summary

Most circuitry in the ascending auditory system must be refined and tonotopically aligned in order to perform computations reliably and fast. This refined circuitry is not initially present but develops during the first few postnatal weeks as a result of several activity-dependent processes. Interestingly, some of this refinement occurs before the onset of hearing and could rely on spontaneously generated patterns of neural activity to drive the refinement. At present it is not clear which refinement processes occur in the absence of hearing and we do not understand the mechanisms by which plastic changes occur.

Here, we focused on the development of the inhibitory projections from the MNTB to the LSO, a major sound localization nucleus. During early postnatal life, MNTB-LSO synapses are selectively strengthened and weakened and this functional refinement happens before hearing onset. The current working model in the field is that these functional changes are followed by anatomical changes and that the latter depend on acoustically-driven activity. However, until now, the supposition that anatomical refinement in the MNTB-LSO pathway requires auditory experience has not been directly tested.

Our understanding of the mechanisms that lead to plastic changes at the immature MNTB-LSO synapse is incomplete. The finding that immature MNTB

terminals release the excitatory neurotransmitter glutamate and that glutamate release activates NMDARs has led to the intriguing suggestion that glutamate release is involved in refinement. Consistent with this idea, deleting the protein which loads glutamate into vesicles at immature MNTB terminals, VGLUT3, impairs functional refinement at the MNTB-LSO synapse. If glutamate is involved in plasticity at the MNTB-LSO synapse, then perhaps there are specific patterns of activity which trigger the release of glutamate and result in plasticity. Interestingly, evidence from slice physiology shows that glutamate is released under different stimulation conditions than GABA/glycine. This raises the question, what could regulate the different release properties for GABA/glycine and glutamate? Given that vesicular Ca^{++} sensors confer release properties, we asked if immature MNTB terminals express more than one Ca^{++} sensor and if one was specifically associated with glutamate release.

Electrophysiological data suggest that the MNTB terminal contains two phenotypically distinct vesicle populations and that the populations differ in their release properties. Since the phenotype and release properties of a vesicle can depend on which proteins it expresses, the two populations of synaptic vesicles at the immature MNTB likely differ in their constituent vesicular proteins. A major question in cell biology is how the cell sorts proteins onto the two different vesicle populations. Although there are a number of molecules that could influence protein expression on the vesicle, for our final question we specifically asked if if VGLUT3 controls the targeting of Syt1 to immature MNTB terminals.

Summaries of Chapters 2-4

Chapter 2 Summary: Re-distribution of Inhibitory Synapses onto Proximal Sites of LSO Principal Cells Occurs Before Hearing Onset

The developing MNTB-LSO pathway undergoes both functional and anatomical refinement. The current working model in the field suggests that anatomical refinement follows functional refinement (complete by ~P8) at some delay, and that anatomical refinement requires acoustical experience and therefore begins at hearing onset (P12). This model is consistent with evidence from inhibitory circuitry in a neighboring nucleus involved in sound localization, the MSO, where anatomical refinement of MNTB-MSO projections and re-distribution of inhibitory inputs require auditory experience (Kapfer et al, 2002).

Here, we asked if inhibitory synapses along LSO neurons are redistributed before the onset of hearing. We filled individual principal neurons of the LSO and labeled inhibitory synapses with a gephyrin antibody in order to quantify the distribution of inhibitory inputs along the entire cell in rats aged P4 and P11. We found a significant re-distribution of inhibitory inputs toward the proximal dendrites and the soma between P4 and P11. This re-distribution was a result of an increase in the density and the total number of gephyrin puncta along the proximal dendrites and at the soma. During this same period, we found a significant decrease in dendritic complexity with the first 30 μm of the cell body, whereas there was no change in dendritic complexity in distal regions. Lastly, the

dendritic fields of LSO bipolar principal cells change shape between P4 and P11, such that by P11 they cover a more restricted area.

This study shows that, unlike the anatomical refinement in MSO, re-distribution of inhibitory inputs on LSO neurons occurs in the absence of acoustical information. Moreover, in contrast to the idea that there is a 4+ day delay between functional and anatomical refinement in the MNTB-LSO pathway, anatomical refinement quickly succeeds or occurs concurrently with functional refinement.

Chapter 3 Summary: Synaptotagmins I and II in the Developing Rat Auditory Brainstem: Synaptotagmin I is Transiently Expressed in Glutamate-Releasing Immature Inhibitory Terminals

The developing MNTB-LSO pathway releases the inhibitory neurotransmitters GABA and glycine as well as the excitatory neurotransmitter glutamate (Gillespie et al, 2005). Slice physiology studies of the MNTB-LSO pathway suggest that GABA and glycine are released from one population of vesicles that express VIAAT and that glutamate is released from a distinct population of vesicles that express VGLUT3 (Nabekura et al, 2004, Gillespie et al, 2005). Interestingly, GABA/glycine and glutamate differ in their release properties at this synapse. Differential release properties could be related to differential expression of Ca^{++} sensors on the synaptic vesicles but, until now, it was not clear which Ca^{++} sensors were present at immature MNTB terminals.

Here, we used immunohistochemistry to study the expression of the Ca^{++} sensors Syt1 and Syt2 in the developing rat SOC, with a focus on the LSO and SPN, two nuclei which receive prominent projections from the MNTB.

We found that both Syt1 and Syt2 were expressed in the developing SOC. Syt2 was expressed in all the major nuclei of the SOC at all stages of development, which is consistent with the idea that Syt2 is the predominant calcium sensor in the SOC (Fox and Sanes, 2007). Interestingly, Syt1 was only highly expressed in the LSO and SPN. Moreover, Syt1 was only expressed during the pre-hearing period, which is the same time when the MNTB axons release glutamate and express VGLUT3. These results suggest that the developing MNTB terminals express two Syt isoforms and lead to a model such that Syt1 is expressed on VGLUT3-positive, glutamatergic vesicles, and Syt2 is expressed on VIAAT-positive, GABA/glycinergic vesicles.

Chapter 4 Summary: Synaptotagmin I is expressed at a GABA/glycine/glutamate-releasing central synapse, independent of vesicular glutamate transporter 3 expression

Based on anatomical evidence presented in Chapter 3, our updated working model for the immature MNTB-LSO synapse suggests that Syt1 and VGLUT3 are co-expressed on one vesicle population and that Syt2 and VIAAT are co-expressed on the other population. From this model we infer that the cell has a mechanism to ensure the proper sorting and trafficking of vesicular proteins

to the appropriate vesicle, but it remains unknown what could be regulating this organization. Here, we asked if VGLUT3 controls the expression and/or trafficking of Syt1 at immature MNTB terminals. First, we compared Syt1 immunoreactivity in tissue from wildtype and VGLUT3$^{-/-}$ mice. We found no obvious difference in Syt1 staining patterns in the LSO and SPN, two nuclei which receive prominent projections from the MNTB. Second, we asked if VGLUT3 was required for trafficking Syt1 to immature MNTB terminals. Using VIAAT as a marker of inhibitory terminals, we found that the deletion of *vglut3* did not affect trafficking of Syt1 to MNTB terminals. Although VGLUT3 and Syt1 share similar spatial and temporal expression patterns in developing MNTB terminals, VGLUT3 influences neither the expression nor the trafficking of Syt1 to the terminal.

Implications & Future Questions

A Role for VGLUT3 in Anatomical Refinement?

Maturation of sound localization circuitry is understood to depend on patterned neural activity that results in functional and anatomical refinement (Kandler et al, 2009). The mechanisms for this refinement are not well understood. The surprising finding that glutamate is released and activates NMDARs at the immature inhibitory MNTB-LSO synapse has led to the intriguing suggestion that glutamate release could be involved in refinement at MNTB

terminals (Gillespie et al, 2005). Recently, it was shown that the deletion of *vglut3*, a gene that is required for glutamate release from the MNTB, impairs functional refinement in the MNTB-LSO projection (Noh et al, 2010). This provides evidence that VGLUT3, and possibly glutamate release from the MNTB, is involved in functional refinement of MNTB-LSO circuitry. If functional refinement leads to anatomical refinement, then, based on our knowledge that functional refinement is impaired in VGLUT3$^{-/-}$ mice, we would expect anatomical refinement to be impaired in VGLUT3$^{-/-}$. This raises the question: does the deletion of *vglut3* alter anatomical refinement in LSO circuitry? To answer this question, a future study could look at changes in cell morphology and synapse distribution across development in the VGLUT3 mouse.

Some inferences about the role of VGLUT3 in anatomical refinement can be made from the Syt1 staining in the SPN of P7 wildtype and VGLUT3$^{-/-}$ mice (Chapter 4, Fig. 4B). The SPN receives prominent inhibitory projections from the MNTB and labels intensely for Syt1 and VIAAT during early postnatal development (Cooper and Gillespie, 2011). In fact, both Syt1-IR and VIAAT-IR are stronger in the SPN than in the LSO and Syt1-IR and VIAAT-IR puncta can be seen surrounding the large cell bodies of the SPN (Blaesse *et al*, 2005, unpublished observations). In the wildtype mouse, Syt1-IR puncta clearly outline the cell bodies in the SPN (Chapter 4, Fig. 4B). The distribution of Syt1-IR puncta appears qualitatively different in the VGLUT3$^{-/-}$ mice, as perisomatic staining is not as apparent (Chapter 4, Fig. 4D). This preliminary observation suggests that

anatomical refinement may be impaired in the VGLUT3$^{-/-}$ mice. In light of the effects of *vglut3* deletion on functional refinement, the presumed causal relationship between functional and anatomical refinement, and the preliminary observations of perisomatic labeling in the SPN of VGLUT3$^{-/-}$, it will be exciting to see if and how anatomical refinement is affected by the deletion *vglut3*.

Anatomical refinement of the AVCN-LSO pathway and subcellular distribution of AVCN-LSO and MNTB-LSO inputs

In contrast to what we know about anatomical refinement in the MNTB-LSO pathway, we know very little about anatomical refinement and the subcellular distribution of inputs in the AVCN-LSO pathway both during development and in the adult. Excitatory inputs to from the AVCN to MSO bipolar cells show little re-distribution during postnatal development which raises the following questions: does the subcellular distribution of excitatory AVCN-LSO inputs along LSO cells change during the period of refinement? If so, is the mature distribution of AVCN-LSO inputs achieved at the same time as the mature distribution of MNTB-LSO inputs? Given that functional refinement in the AVCN-LSO and MNTB-LSO pathways occurs concurrently (Kim and Kandler, 2003, Case et al, 2011), one might expect that anatomical refinement in both pathways is concurrent.

In addition to learning the subcellular distribution of excitatory inputs to LSO neurons, it will be interesting to know how close the AVCN and MNTB inputs

are to each other along LSO neurons during development. Physiological studies show that, between P3 and P8, glutamate release from the MNTB pathway activates NMDARs in the AVCN pathway, and vice versa (Alamilla and Gillespie, 2011). The substantial glutamatergic crosstalk suggests that AVCN and MNTB inputs are located close enough for glutamate to diffuse throughout the extracellular space and activate NMDARs at neighboring synapses (Rusakov et al, 1999). Knowing the distributions of AVCN and MNTB inputs along immature LSO principal neurons will clarify the role that relative distances between of the two inputs plays in glutamatergic crosstalk.

Our knowledge of how mature principal cells of the LSO integrate binaural inputs to compute ILDs will also be advanced by knowing the subcellular location of both excitatory and inhibitory inputs. The existing models of integration in LSO neurons are based on relatively simple interpretations of cell morphology and synapse distribution (Zacksenhouse et al, 1998). With current technology and techniques, it is possible to generate more realistic models which incorporate detailed cell morphology and the subcellular distribution of inputs throughout the entire, reconstructed dendritic tree. It is clear that our knowledge of computation in LSO cells will advance by having such anatomical data, which could itself be built upon with electrophysiological studies showing the strength and interactions of different inputs along neurons of the LSO.

Are MNTB projections refined at different times in the LSO and MSO?

In bipolar principal cells of the MSO, it seems that the proximal re-distribution of inhibitory inputs is related to the maintenance of MNTB projections to the proximal regions of the cell (Kapfer et al, 2002, Werthat et al, 2008). Both of these events require auditory experience and occur between P12 and P25. We found that proximal re-distribution of inhibitory inputs to LSO principal cells occurs before hearing onset. Since the re-distribution of synapses is closely related to anatomical refinement of axonal projections, it is possible that MNTB axonal projections to the LSO are refined before hearing onset. Given that the MNTB projects to both the LSO and MSO, and in some cases the same MNTB neuron projects to both nuclei (Banks and Smith, 1992), it is surprising that they could undergo refinement at different times. Is the refinement of MNTB axons target-specific?

The possibility that anatomical refinement of MNTB projections is target-specific is exciting, but we must first consider the following two points. Firstly, the studies looking at the MNTB-MSO projections were done in gerbil whereas our study was performed in rat. Therefore the differences in refinement could be species-specific. In order to test this, one would need to track pruning to the MSO and LSO in the same species. Secondly, MNTB projections to the LSO, which relay information on relatively high-frequency information, might undergo refinement sooner than MNTB projections to the MSO, which relay information on relatively low-frequency information, because auditory regions that process high-

frequency information have been shown to mature faster than auditory regions that process low-frequency information (Sanes et al, 1992a, Kandler and Friauf, 1993, Friauf et al, 1997). The reason high-frequency regions of the auditory system mature faster or differently is unknown.

Although it is intriguing to consider that MNTB projections are refined in a target-specific fashion, other possibilities such as the two stated above must also be tested.

Identities of vesicle pools at the immature MNTB terminal

The vesicular identities of the glutamatergic and GABA/glycinergic populations remain a major unanswered question. Future experiments can attempt to test our working model that Syt1 is on VGLUT3-positive vesicles and Syt2 is on VIAAT-positive vesicles. This could be deciphered using high-resolution imaging techniques or physiological techniques.

High-resolution imaging, such as electron microscopy or superesolution light microscopy could provide valuable information about the co-expression of vesicular transporters and synaptotagmin isoforms on vesicles at the immature MNTB terminals. Double-immunolabel, post-embedding electron microscopy can provide valuable information on the localization of vesicular proteins at a co-releasing synapse because the technique offers high-resolution. A major caveat of this approach is reliably identifying which proteins are expressed on a given vesicle. Synaptic vesicles are 30-40 nm in diameter and the distance from the

antigen to the electron dense gold particle on the secondary antibody is about 30 nm. Therefore, if, for example, VGLUT3 and Syt1, were on the same vesicle, then the gold particles there are indirectly labeled with could still be 90 nm apart. Meanwhile, two particles corresponding to Syt1 and VGLUT3 could be side-by-side (suggesting vesicular co-expression) and still be on different vesicle populations. Because the different vesicle populations could be intermixed at the terminal, reliably identifying the proteins expressed by a *single vesicle* could be difficult. An alternative approach is to measure the distance between two proteins in question (eg. VGLUT3 and Syt1) for a population of vesicles and compare it to the distance between a protein and a random point. If the proteins in question are co-expressed on the same vesicle, then the majority should be within 90 nm of each other and they should be closer to each other than the protein and the random point are to each other, on average (Stensrud et al, 2013).

Another advantage to using electron microscopy is that different vesicle phenotypes have different ultrastructural and density characteristics. For example, in the mature LSO, glutamatergic terminals contain round vesicles and glycinergic terminals contain flat vesicles (Ollo and Schwartz, 1979, Helfert et al, 1992). Whether or not synaptic vesicles at the immature MNTB terminal can be differentiated ultrastructurally is unknown. If there are two different types of synaptic vesicles, such as round and flat, it could provide corroborative evidence that there are two populations of vesicles. Furthermore, one could see if a particular synaptotagmin is preferentially with ultrastructurally different vesicles.

Electron microscopy is technically demanding and can only be used to visualize *ex vivo* tissue. An alternative to electron microscopy is super-resolution light microscopy, such as stimulated excitation depletion (STED) microscopy. STED microscopy has achieved a resolution of ~45 nm in the neuroscience literature, can be used in living samples, and tissue preparation for STED microscopy is simpler than that for electron microscopy (Willig et al, 2006, Westphal et al, 2008). Two-colour STED microscopy could be used to distinguish the relative co-expression of transporters and synaptotagmins on vesicles at the immature MNTB terminal. In addition, STED microscopy could also be used to monitor different recycling pathways the two populations could take, which would also provide useful information about how the terminal is organized (Hoopman et al, 2010).

Interpretation of the results from the above immunolabeling techniques are likely to be complicated by the degree to which the glutamatergic and GABA/glycinergic vesicle populations are intermixed at the terminal and the resolution of the imaging technique. Given these caveats with anatomical techniques, one wonders if there is a way to study it functionally. Determining the identity of the vesicle pools in the MNTB terminal pharmacologically is difficult because there are no known pharmacological inhibitors of Syt1 or Syt2. There are, however, genetic and optical tools that could be useful. Using genetic and optical tools, Syt1 can be temporarily and focally inactivated at the NMJ in Drosophila (Marek and Davis, 2002). The inactivation of Syt1 results in a

decrease in the amplitude of the EPSP. It is possible that one could use these tools in experiments in the rodent nervous system to clarify whether Syt1 is specifically targeted to a vesicle populations at immature MNTB terminals. If these tools could be applied to *syt1* in mice, then one could photoinactivate Syt1 and see which component(s), GABA/glycine and/or glutamate, is/are affected. To date, this particular photoinactivation technique has not been demonstrated in any species other than Drosophila but it is theoretically possible (Habets and Verstreken, 2011) and it could help decipher the details of vesicle populations at the developing MNTB-LSO synapse.

Concluding Remarks

The proper development of sound localization circuitry in the auditory brainstem is important for allowing organisms to interpret the auditory world. The circuitry is both functionally and anatomically refined and this refinement is thought to be activity-dependent. The patterns of activity that are involved in refinement are not yet known and it will be important to study the patterns of activity sent from the cochlear nuclei to the SOC using *in vivo* recordings. The finding that different activity patterns result in the release of GABA/glycine and glutamate, which could be related to the differential expression of Ca^{++} sensors on VIAAT-positive and VGLUT3-positive vesicles, is consistent with the idea that MNTB neurons release glutamate in response to activity patterns that are involved in plasticity.

References

Agmon-Snir H, Carr CE, & Rinzel J. (1998). The role of dendrites in auditory coincidence detection. *Nature*, 393, 268-272.

Alamilla, J & Gillespie, DC. (2011). Glutamatergic inputs and glutamate-releasing immature inhibitory inputs activate a shared postsynaptic receptor population in lateral superior olive. *Neuroscience*, 196, 285-296.

Alamilla J & Gillespie DC. (2013). Maturation of calcium-dependent GABA, glycine, and glutamate release in the glycinergic MNTB-LSO pathway. PLoS One, 8, e75688.

Antonini A & Stryker MP. (1993). Rapid remodeling of axonal arbors in the visual cortex. *Science*, 260, 1819-1821.

Banks MI & Smith PH. (1992). Intracellular recordings from neurobiotin-labeled cells in brain slices of the rat medial nucleus of the trapezoid body. *J Neurosci*, 12, 2819-2837.

Borst JGG & Rusu SI. (2011). "The Calyx of Held Synapse." *Synaptic mechanisms in the auditory system*. Eds Trussell LO, Popper AN, & Fay RR. New York, Springer, 95-134.

Brand A, Behrend O, Marquadt T, McAlpine D, & Grothe B. (2002). Precise inhibition is essential for microsecond interaural time difference coding. *Nature*, 417, 543-547.

Cant NB. (1984). The fine structure of the lateral superior olivary nucleus of the cat. *J Comp Neurol*, 227, 63-77.

Case DT & Gillespie DC. (2011). Pre- and postsynaptic properties of glutamatergic transmission in the immature inhibitory MNTB-LSO pathway. *J Neurophysiol*, 106, 2570-2579.

Case DT, Zhao X, & Gillespie DC. (2011). Functional refinement in the projection from ventral cochlear nucleus to lateral superior olive precedes hearing onset in rat. PLoS One, 6, e20756.

Chang EH, Kotak, VC, and Sanes DH. (2003). Long-term depression of synaptic inhibition is expressed postsynaptically in the developing auditory system. *J Neurophysiol*, 90, 1479-1488.

Citri A & Malenka RC. (2008). Synaptic plasticity: multiple forms, functions, and mechanisms. *Neuropsychopharmacology*, 33, 18-41.

Colman H, Nabekura J, & Lichtman JW. (1997). Alterations in synaptic strength preceding axon withdrawal. *Science*, 275, 356-361.

Cooper AP & Gillespie DC. (2011). Synaptotagmins I and II in the developing rat auditory brainstem: Synaptotagmin I is transiently expressed in glutamate-releasing immature inhibitory terminals. *J Comp Neurol*, 519, 2417-2433.

Cramer KS. (2005). Eph proteins and the assembly of auditory circuits. *Hear Res*, 206, 42-51.

Dobie FA & Craig AM. (2011). Inhibitory synapse dynamics: coordinated presynaptic and postsynaptic mobility and the major contribution of recycled vesicles to new synapse formation. *J Neurosci*, 31, 10481-10493.

Emmenlauer M, Ronneberg O, Ponti A, Schwab P, Griffa A, Filippi A, Nitschke R, Driever W, & Burkhardt H. (2009). XuvTools: free, fast and reliable stitching of large 3D datasets. *J Microsc*, 233, 42-60.

Englitz B, Tolnai S, Typlt M, Jost J & Rubsamen R. (2009). Reliability of synaptic transmission at the synapses of Held in vivo under acoustic stimulation. *PLoS One, 4*,10, e7014. doi: 10.1371/journal.pone.0007014..

Foss SM, Li H, Santos MS, Edwards RH, & Voglmaier SM. (2013). Multiple dileucine-like motifs direct VGLUT1 trafficking. *J Neurosci*, *33*, 10647–10660.

Galli L & Maffei L. (1988). Spontaneous impulse activity of rat retinal ganglion cells in prenatal life. *Science*, 242, 90-91.

Golding NL. (2011). "Neuronal response properties and voltage-dated ion channels in the auditory system." Synaptic mechanisms in the auditory system. Eds. Trussell LO, Popper AN & Fay RR. New York, Springer, 7-41.

Grothe B, Pecka M, & McAlpine D. (2010). Mechanisms for sound localization in mammals. *Physiol Rev*, 90, 983-1012.

Habets RL & Verstreken P. (2011) FlAsH-FALI inactivation of a protein at the third-instar neuromuscular junction. *Cold Spring Harb Protoc*, April 1; 2011, doi:10.1101/pdb.prot5597.

Helfert RH & Schwartz IR. (1986). Morphological evidence for the existence of multiple neuronal classes in the cat lateral superior olivary nucleus. *J Comp Neurol*, 244, 533-549.

Helfert RH & Schwartz IR. (1987). Morphological features of five neuronal classes in the gerbil lateral superior olive. *Am J Anat*, 179, 55-69.

Helfert RH, Juiz JM, Bledsoe SC Jr, Bonneau JM, Wenthold RJ, & Altschuler RA. (1992). Patterns of glutamate, glycine, and GABA immunolabelling in four synaptic terminal classes in the lateral superior olive of the guinea pig. *J Comp Neurol*, 323, 305-325.

Hoffman, PM, Van Riswick JG, & Van Opstal AJ. (1998). Relearning sound localization with new ears. *Nat Neurosci*, 1, 417-421.

Hoopmann P, Punge A, Barysch SV, Westphal V, Buckers J, Opazo F, Bethani I, Lauterback MA, Hell SW, & Rizzoli SO. (2010). Endosomal sorting of readily releasable synaptic vesicles. *Proc Natl Acad Sci USA*, 107, 19055-19060.

Hui E, Bai J, Wang P, Sugimori M, Llinas RR, & Chapman ER. (2005) Three distinct kinetic groupings of the synaptotagmin family: candidate sensors for rapid and delayed exocytosis. *PNAS*, 102, 5210-5214.

Hunt DL & Castillo PE. (2012). Synaptic plasticity of NMDA receptors: mechanisms and functional implications. *Curr Opin Neurobiol*, 22, 496-508.

Kalmbach A, Kullmann PH, & Kandler K. (2010). NMDAR-mediated calcium transients elicited by glutamate co-release at developing inhibitory synapses. *Front Synaptic Neurosci*, 2: 27. doi 10.3389/fnsyn.2010.0027.

Kandler K, Clause A, & Noh J. (2009). Tonotopic reorganization of developing auditory brainstem circuits. *Nat Neurosci*, 12, 711-717.

Kapfer C, Seidl AH, Schweizer H, & Grothe B. (2002). Experience-dependent refinement of inhibitory inputs to auditory coincidence-detector neurons. *Nat Neurosci*, 5, 247-253.

Katz LC & Shatz CJ. (1996). Synaptic activity and the construction of cortical circuits. *Science*, 274, 1133-1138.

Kotak VC & Sanes DH. (2000). Long-lasting inhibitory synaptic depression is age- and calcium-dependent. *J Neurosci*, 20, 5820-5826.

Kotak VC, DiMattina C, & Sanes DH. (2001). GABA(B) and Trk receptor signaling mediates long-lasting inhibitory synaptic depression. *J Neurophysiol*, 86, 536-540.

Kotak VC & Sanes DH. (2002). Postsynaptic kinase signaling underlies inhibitory synaptic plasticity in the lateral superior olive. *J Neurobiol*, 53, 36-43.

Kullmann PH & Kandler K. (2008). Dendritic Ca2+ responses in neonatal lateral superior olive neurons elicited by glycinergic/GABAergic synapses and action potentials. *Neuroscience*, 154, 338-45.

Kuwabara N & Zook JM. (1992). Projections to the medial superior olive from the medial and lateral nuclei of the trapezoid body in rodents and bats. *J Comp Neurol*, 324, 522-538.

Leao KE, Leao, RN, & Walmsley B. (2011). Modulation of dendritic synaptic processing in the lateral superior olive by hyperpolarization-activated currents. *Eur J Neurosci*, 33, 1462-1470.

Lippe WR. (1994). Rhythmic spontaneous activity in the developing avian auditory system. *J Neurosci*, 14, 1486-1495.

Lorteije JA, Rusu SI, Kushmerick C, & Borst JG. (2009). Reliability and precision of the mouse calyx of Held synapse. *Journal of Neuroscience, 29*, 13770–13784.

Manis PB, Xie R, Wang Y, Marrs, GS, & Spirou GA. (2011). "The Endbulbs of Held." *Synaptic mechanisms in the auditory system*. Eds Trussell LO, Popper AN, & Fay RR. New York, Springer, 61-93.

Marek KW & Davis GW. (2002). Transgenically encoded protein photoinactivation (FlAsH-FALI): acute inactivation of synaptotagmin I. *Neuron*, 36, 805-813.

Matteoli M, Takei, K, Perin, MS, Sudhof TC, & De Camilli P. (1992) Exo-endocytic recycling of synaptic vesicles in developing processes of cultured hippocampal neurons. *J Cell Biol*, 117, 849-861,

Meier J, Vannier C, Serge, A, Triller A, & Choquet D. (2001). Fast and reversible trapping of surface glycine receptors by gephyrin. *Nat Neurosci*, 4, 253-260.

Meister M, Wong, RO, Baylor DA, & Shatz CJ. (1991) Synchronous bursts of action potentials in ganglion cells of the developing mammalian retina. *Science*, 252, 939-943.

Moreau AW and Kullmann DM. (2013). NMDA receptor-dependent function and plasticity in inhibitory circuits. *Neuropharmacology*, 74, 23-31.

Mutch SA, Kensel-Hammes P, Gadd JC, Fujimoto BS, Allen RWm Schiro PG, Lorenz RM, Kuyper CL, Kuo JS, Bajjalieh SM, & Chiu DT. (2011). Protein quantification at the single vesicle level reveals that a subset of synaptic vesicle proteins are trafficked with high precision. *J Neurosci*, 31, 1461-1470.

Okada Y, Yamakazi H, Sekinealy Y, & Hirokawa N. (1995). The neuron-specific kinesin superfamily protein KIF1A is a unique monomeric motor for anterograde axonal transport of synaptic vesicle precursors. *Cell*, 81, 769-780.

Ollo C and Schwartz IR. (1979). The superior olivary complex in C57BL/6 mice. *Am J Anat*, 155, 349-373.

Pawley JB. (1995). *Handbook of Biological Confocal Microscopy*, 2 Edn. Plenum Press, New York.

Penn AA, Riquelme PA, Feller MB, & Shatz CJ. (1998). Competition in retinogeniculate patterning driven by spontaneous activity. *Science*, 279, 2108-2112.

Perin MS, Brose, N, Jahn R, & Sudhof TC. (1991). Domain structure of synaptotagmin (p65). *J Biol Chem*, 266, 623-629.

Prado, VF & Prado, M. (2002). Signals involved in targeting membrane proteins to synaptic vesicles. *Cell mol neurobiol*, 22, 565-577.

Preibisch S, Saalfeld S, & Tomancak P. (2009). Globally optimal stitching of tiled 3D microscopic image acquisitions. *Bioformatics*, 25, 1463-5

Quinlan EM, Philpot BD, Huganir RL, & Bear MF. (1999). Rapid, experience-dependent expression of synaptic NMDA receptors in visual cortex in vivo. *Nat Neurosci*. 2, 352-357.

Rall W, Burke RE, Holmes WR, Jack JJ, Redman SJ, & Segev I. (1992). Matching dendritic neuron models to experimental data. *Physiol Rev*, 72, S159-S186.

Ramon y Cajal S. (1909). Histologie du systeme nerveux de l'homme et des vertebres. Ed. Maloine A. Paris. Retrieved from http://www.biodiversitylibrary.org/bibliography/48637

Rautenberg PL, Grothe B, and Felmy F. (2009). Quantification of the three-dimensional morphology of coincidence detector neurons in the medial superior olive of gerbils during late postnatal development. *J Comp Neurol*, 517, 385-396.

Rietzel HJ & Friauf E. (1998). Neuron types in the rat lateral superior olive and developmental changes in the complexity of their dendritic arbors. *J Comp Neurol*, 390, 20-40.

Roberts MT, Seeman SC, & Golding NL. (2013). A mechanistic understanding of the role of feedforward inhibition in the mammalian sound localization circuitry. *Neuron*, 78, 923-935.

Rogowski BA & Feng AS. (1981). Normal Postnatal development of medial superior olivary neurons in the albino rat: a Golgi and Nissl study. *J Comp Neurol*, 196, 85-97.

Rizzoli SO & Betz WJ. (2005). Synaptic Vesicle Pools. *Nat Rev Neurosci*, 6, 57-69.

Rusakov DA, Kullmann DM, & Stewart MG. (1999). Hippocampal synapses: do they talk to their neighbours? *Trends Neurosci*, 22, 382-388.

Ruthazer ES, Li J, & Cline HT. (2006) Stabilization of axon branch dynamics by synapse maturation. *J Neurosci*, 26, 3594-3603.

Sanes DH & Siverls V. (1991). Development and specificity of inhibitory terminal arborizations in the central nervous system. *J Neurobiol*, 8, 837-854.

Sanes DH, Song J, & Tyson J. (1992a). Refinement of dendritic arbors along the tonotopic axis of the gerbil lateral superior olive. *Brain Res*, 67, 47-55.

Sanes, DH, Markowitz, S, Berstein J, & Wardlow, J. (1992b) The influence of inhibitory afferents on the development of postsynaptic dendritic arbors. *J Comp Neurol*, 321, 637-644.

Santos, MS, Li H, & Voglmaier SM. (2009). Synaptic vesicle protein trafficking at the glutamate synapse. *Neuroscience*, 158, 189–203.

Santos MS, Park CK, Foss SM, Li H, & Voglmaier, SM. (2013). Sorting of the vesicular GABA transporter to functional vesicle pools by an atypical dileucine-like motif. *J Neurosci*, *33*, 10634–10646.

Scheibel, ME & Scheibel AB. (1974). Neuropil organization in the superior olive of the cat. *Exp Neurol*, *43*, 339–348.

Schindelin J, Arganda-Carreras I, Frise E, Kaynig V, Longair M, Pietzsch T, Preibisch S, Rueden C, Saalfeld S, Schmid B, Tinevez JY, White DJ, Hartenstein V, Eliceiri K, Tomancak P, & Cardona A. (2012). Fiji: an open-source platform for biological-image analysis. *Nat Methods*, 9, 676-82.

Scott LL, Mathews PJ, & Golding NL. (2005). Posthearing developmental refinement of temporal processing in principal neurons of the medial superior olive. *J Neurosci*, 25, 7887-7895.

Segev, I & London, M. (1999) "A theoretical view of passive and active dendrites." Dendrites. Eds. Stuart G, Spruston N, & Hausser M. New York, Oxford University Press, 205-230.

Sheng M, Cummings J, & Roldan LA, Jan YN, & Jan LY. (1994). Changing subunit composition of heteromeric NMDA receptors during development of rat cortex. *Nature*, 368,144-147.

Singh E. (2011). Postnatal developmental distribution of NMDA receptor subunit mRNA in auditory brainstem of rat. Open Access Dissertations and Theses. Paper 6329. http://digitalcommons.mcmaster.ca/opendissertations/6329

Spruston, N, Stuart G, & Hausser M. (1999) "Dendritic Integration." Dendrites. Eds. Stuart G, Spruston N, & Hausser M. New York, Oxford University Press, 231-270.

Staudt T, Lang MC, Medda R, Engelhardt J, & Hell SW. (2007). 2,2'-thiodiethanol: a new water soluble mounting medium for high resolution optical microscopy. *Microsc Res Tech*, 70, 1-9.

Stensrud MJ, Chaudry FA, Leergaard TB, Bjaalie JG, & Gundersen V. (2013). Vesicular glutamate transporter-3 in the rodent brain: Vesicular colocalization with vesicular γ-Aminobutyric acid transporter. *J Comp Neurol*, *521*, 3042-3056.

Stotler WA. (1953). An experimental study of the cells and connections of the superior olivary complex of the cat. *J Comp Neurol*, 98, 401-431.

Stuart GJ and Sakmann B. (1995) Amplification of EPSPs by axosomatic sodium channels in neocortical pyramidal neurons. *Neuron*, 15, 1065-1077.

Stuart GJ & Hausser M. (1998). Determinants of voltage attenuation in neocortical pyramidal neuron dendrites. *J Neurosci*, 18, 3501-3510.

Sudhof TC. (2013). Neurotransmitter release: the last millisecond in the life of a synaptic vesicle. *Neuron*, 80, 675-690.

Tessier-Lavigne M & Goodman CS. (1996). The molecular biology of axon guidance. *Science*, 274, 1123-1133.

Tollin DJ. (2003). The lateral superior olive: a functional role in sound source localization. *Neuroscientist*, 9, 127-143.

Tritsch NX, Rodriguez-Contreras A. Crins TT, Wang HC, Borst, JG, & Bergles DE. (2010). Calcium action potentials in hair cells pattern auditory neuron activity before hearing onset. *Nat Neurosci*, 13, 1050-1052.

van der Heijden M, Lorteije JA, Plauska A, Roberts MT, Golding NL, & Borst JG. Directional hearing by linear summation of binaural inputs at the medial superior olive. *Neuron*, 78, 936-948.

Voglmaier SM, Kam K, Yang H, Fortin DL, Hua Z, Nicoll RA, & Edwards RH. (2006). Distinct endocytic pathways control the rate and extent of synaptic vesicle protein recycling. *Neuron*, 51, 71-84.

Voglmaier SM & Edwards RH. (2007). Do different endocytic pathways make different synaptic vesicles? *Current Opin Neurobiol*, *17*, 374–380.

Von Bekesy, G. (1956). Current status of theories of hearing. *Science*, 123, 779-783).

Webster DB. (1991). "An overview of mammalian auditory pathways with an emphasis on humans." *The mammalian auditory pathway: Neuroanatomy*.

Eds. Webster DB, Popper AN, & Fay RR. New York, Springer-Verlag, 4-22.

Werthat F, Alexandra O, Grothe B, & Koch U. (2008). Experience-dependent refinement of the inhibitory axons projecting to the medial superior olive. *Dev Neurobiol*, 68, 1454-1462.

Westphal V, Rizzoli SO, Lauterback MA, Kamin, D, Jahn R, & Hell SW. (2008). Video-rate far-field optical nanoscopy dissects synaptic vesicle movement. *Science*, 320, 246-249.

Willig KI, Rizzoli SO, Westphal V, Jahn R, & Hell SW. (2006). STED microcopy reveals that synaptotagmin remains clustered after synaptic vesicle exocytosis. *Nature*, 440, 935-939.

Yao, J, Nowack, A, Kensel-Hammes, P, Gardner, RG, & Bajjalieh, SM. (2010). Cotrafficking of SV2 and synaptotagmin at the ynapse. *Journal of Neuroscience*, *30*, 5569–5578.

Yashiro K & Philpot BD. (2008). Regulation of NMDA receptor subunit expression and its implications for LTD, LTP, and metaplasticity. *Neuropharmacology*, 55, 1081-1094.

Zacksenhouse M, Johnson DH, Williams J, & Tsuchitani C. (1998). Single-neuron modeling of LSO unit responses. *J Neurophysiol*, 79, 3098-311.